



---

Publicly Accessible Penn Dissertations

---


1-1-2015

# Fighting HIV Infection by Defining Mechanisms to Remodel Semen-Derived Amyloid Fibrils

Laura Castellano

University of Pennsylvania, laurastong@gmail.com

Follow this and additional works at: <http://repository.upenn.edu/edissertations>

 Part of the [Biochemistry Commons](#), [Pharmacology Commons](#), and the [Virology Commons](#)

---

## Recommended Citation

Castellano, Laura, "Fighting HIV Infection by Defining Mechanisms to Remodel Semen-Derived Amyloid Fibrils" (2015). *Publicly Accessible Penn Dissertations*. 1024.

<http://repository.upenn.edu/edissertations/1024>

This paper is posted at ScholarlyCommons. <http://repository.upenn.edu/edissertations/1024>

For more information, please contact [libraryrepository@pobox.upenn.edu](mailto:libraryrepository@pobox.upenn.edu).

---

# Fighting HIV Infection by Defining Mechanisms to Remodel Semen-Derived Amyloid Fibrils

## **Abstract**

Human immunodeficiency virus (HIV) is a major public health threat worldwide, with 80% of infections acquired through sexual transmission. Semen is the principal vector for the transmission of HIV and several endogenous peptides in semen, including fragments of prostatic acid phosphatase (PAP248-286 and PAP85-120) and semenogelins (SEM1 and SEM2), assemble into amyloid fibrils that promote HIV infection. Semen-derived amyloid fibrils enhance infectivity by capturing HIV virions and facilitating their attachment and fusion to target cells. Deciphering methods to dissolve seminal amyloid fibrils would provide a novel preventative strategy for reducing HIV infection via sexual transmission.

Three previously described anti-amyloid agents were used to disassemble and/or counteract seminal amyloid fibrils: 1) Hsp104, an amyloid-remodeling factor from yeast, 2) CLR01, a lysine-specific molecular tweezer, and 3) EGCG, a small molecule polyphenol from green tea. Each strategy was found to antagonize seminal amyloid activity through diverse mechanisms. For instance, Hsp104 and a potentiated Hsp104 variant, Hsp104A503V, remodeled seminal amyloid fibrils into non-fibrillar aggregates and catalytically inactive Hsp104 scaffolds clustered fibrils into larger assemblies. Additionally, Hsp104 was modified to interact with the chambered protease ClpP, to enable coupled remodeling and degradation of seminal amyloid. CLR01 remodeled pre-formed amyloid fibrils through disruption of critical lysine residues, neutralized the cationic fibril surface charge, and exhibited a direct anti-viral effect via disruption of the viral membrane. Finally, epigallocatechin gallate (EGCG) is the first small molecule that can eradicate all four classes of seminal amyloid. Thus, all three strategies were highly effective at antagonizing seminal amyloid fibrils and could have therapeutic utility. Altogether, these findings provide insight into developing microbicidal agents that can abolish the infection-enhancing capabilities of seminal amyloid and counter HIV transmission.

## **Degree Type**

Dissertation

## **Degree Name**

Doctor of Philosophy (PhD)

## **Graduate Group**

Pharmacology

## **First Advisor**

James Shorter

## **Keywords**

amyloid fibrils, HIV, Hsp104, SEVI, small molecules

## **Subject Categories**

Biochemistry | Pharmacology | Virology

---

FIGHTING HIV INFECTION BY DEFINING MECHANISMS TO REMODEL SEMEN-DERIVED

AMYLOID FIBRILS

Laura M. Castellano

A DISSERTATION

in

Pharmacology

Presented to the Faculties of the University of Pennsylvania

in

Partial Fulfillment of the Requirements for the

Degree of Doctor of Philosophy

2015

Supervisor of Dissertation

---

James Shorter, Ph.D., Associate Professor of Biochemistry and Biophysics

Graduate Group Chairperson

---

Julie Blendy, Ph.D. Professor of Pharmacology

Dissertation Committee

Rahul Kohli, M.D., Ph.D., Assistant Professor of Medicine

Mark Lemmon, Ph.D., Professor of Biochemistry and Biophysics

Michael Marks, Ph.D., Professor of Pathology and Laboratory Medicine

Kelly Jordan-Sciutto, Ph.D., Professor of Pathology

FIGHTING HIV INFECTION BY DEFINING MECHANISMS TO REMODEL SEMEN-DERIVED  
AMYLOID FIBRILS

COPYRIGHT

2015

Laura M. Castellano

This work is licensed under the  
Creative Commons Attribution-  
NonCommercial-ShareAlike 3.0  
License

To view a copy of this license, visit

<http://creativecommons.org/licenses/by-nc-sa/3.0/>.

## ACKNOWLEDGMENT

I have many people to thank for their guidance and support throughout the course of my graduate work. First, I need to thank all Shorter Lab members, past and present, for providing a great work environment: Jim – for providing me with mentorship and direction throughout my project and helping me grow as a scientist; Morgan and Liz – for teaching me a great deal about designing experiments and learning new techniques in the lab; Mariana – for always lending an ear and providing advice on science and life; Alice – for her constant reassurance and friendship; and Mike (my “lab husband”) – for being a great colleague and a close friend through good times and bad. I also need to thank Weissman Lab members, especially Veronica, for their help setting up HIV infectivity assays and allowing me to use their lab space and our collaborators in the Munch lab that contributed many useful virological experiments in this thesis. I also need to recognize the National Science Foundation Graduate Research Fellowship for funding my graduate work.

I would also like to acknowledge my family for their constant support. I met my (real) husband, Nick, during my first year at Penn, and I cannot imagine what it would have been like to go through the challenges of graduate school without him. I also need to thank my parents for shaping me to be the person I am today and for their continual encouragement throughout my life.

## ABSTRACT

### FIGHTING HIV INFECTION BY DEFINING MECHANISMS TO REMODEL SEMEN-DERIVED AMYLOID FIBRILS

Laura M. Castellano

Dr. James Shorter

Human immunodeficiency virus (HIV) is a major public health threat worldwide, with 80% of infections acquired through sexual transmission. Semen is the principal vector for the transmission of HIV and several endogenous peptides in semen, including fragments of prostatic acid phosphatase (PAP248-286 and PAP85-120) and semenogelins (SEM1 and SEM2), assemble into amyloid fibrils that promote HIV infection. Semen-derived amyloid fibrils enhance infectivity by capturing HIV virions and facilitating their attachment and fusion to target cells. Deciphering methods to dissolve seminal amyloid fibrils would provide a novel preventative strategy for reducing HIV infection via sexual transmission.

Three previously described anti-amyloid agents were used to disassemble and/or counteract seminal amyloid fibrils: 1) Hsp104, an amyloid-remodeling factor from yeast, 2) CLR01, a lysine-specific molecular tweezer, and 3) EGCG, a small molecule polyphenol from green tea. Each strategy was found to antagonize seminal amyloid activity through diverse mechanisms. For instance, Hsp104 and a potentiated Hsp104 variant, Hsp104<sup>A503V</sup>, remodeled seminal amyloid fibrils into non-fibrillar aggregates and catalytically inactive Hsp104 scaffolds clustered fibrils into larger assemblies. Additionally, Hsp104 was modified to interact with the chambered protease ClpP, to enable coupled remodeling and degradation of seminal amyloid. CLR01 remodeled pre-formed amyloid fibrils through disruption of critical lysine residues, neutralized the cationic fibril surface charge, and exhibited a direct anti-viral effect via disruption of the viral membrane. Finally, epigallocatechin gallate (EGCG) is the first small molecule that can eradicate all four

classes of seminal amyloid. Thus, all three strategies were highly effective at antagonizing seminal amyloid fibrils and could have therapeutic utility. Altogether, these findings provide insight into developing microbicidal agents that can abolish the infection-enhancing capabilities of seminal amyloid and counter HIV transmission.



## TABLE OF CONTENTS

<b>ACKNOWLEDGMENT .....</b>	<b>III</b>
<b>ABSTRACT.....</b>	<b>IV</b>
<b>LIST OF TABLES .....</b>	<b>IX</b>
<b>LIST OF ILLUSTRATIONS .....</b>	<b>X</b>
<b>CHAPTER 1: BACKGROUND AND SIGNIFICANCE .....</b>	<b>1</b>
1.1 Discovery of natural agents involved in HIV transmission.....	1
1.2 How does SEVI augment HIV infection?.....	3
1.3 PAP85 and SEM amyloid fibrils .....	6
1.4 A physiological role for semen-derived amyloid fibrils? .....	8
1.5 Current strategies to counteract amyloid-mediated enhancement of HIV infection .....	10
1.6 Amyloid strains .....	14
1.7 Established amyloid-remodeling factors.....	17
1.7.1 Hsp104 .....	17
1.7.2 CLR01.....	19
1.7.3 EGCG.....	21
1.8 Research aims.....	22
<b>CHAPTER 2: REPURPOSING HSP104 TO ANTAGONIZE SEMINAL AMYLOID AND COUNTER HIV INFECTION .....</b>	<b>24</b>
2.1 Introduction .....	24
2.2 Results .....	26
2.2.1 Hsp104 remodels SEVI amyloid fibrils .....	26
2.2.2 A potentiated Hsp104 variant remodels SEVI at nanomolar concentrations .....	30
2.2.3 Hyperactive ClpB variants are unable to eliminate SEVI fibrils.....	30
2.2.4 Hsp104 and Hsp104 <sup>A503V</sup> remodel PAP85-120 fibrils.....	32
2.2.5 Hsp104 and Hsp104 <sup>A503V</sup> do not remodel SEM1(45-107) fibrils .....	33
2.2.6 Hsp104 promotes clustering of seminal amyloid into larger aggregates.....	34
2.2.7 HAP plus ClpP degrade SEVI fibrils and PAP85-120 fibrils .....	39
2.2.8 Fibril remodeling, clustering, and degradation reduce stimulation of HIV infection. ....	42

2.3 Discussion.....	45
<b>CHAPTER 3: A MOLECULAR TWEEZER ANTAGONIZES SEMINAL AMYLOIDS AND HIV INFECTION .....</b>	<b>50</b>
3.1 Introduction.....	50
3.2 Results.....	52
3.2.1 CLR01 inhibits spontaneous assembly of seminal amyloid fibrils .....	52
3.2.2 CLR01 inhibits assembly of PAP248-286 seeded by preformed SEVI fibrils .....	55
3.2.3 CLR01 inhibition depends on lysine and arginine residues in PAP248-286 .....	56
3.2.4 CLR01 remodels preformed SEVI and PAP85-120 fibrils .....	57
3.2.5 CLR01-driven disaggregation depends on lysine and arginine residues in PAP248-286 and PAP85-120 .....	60
3.2.6 CLR01 abrogates the interaction of seminal amyloids with viral particles and diminishes their infection enhancing property.....	62
3.2.7 CLR01 exhibits direct anti-HIV activity .....	65
3.2.8 CLR01 exhibits broad antiviral activity against enveloped viruses .....	68
3.2.9 CLR01 disrupts membranes enriched in lipid-raft domains .....	69
3.2.10 CLR01 antagonizes the infection enhancing property of human semen .....	70
3.3 Discussion.....	72
<b>CHAPTER 4: EPIGALLOCATECHIN-3-GALLATE RAPIDLY ERADICATES PAP85-120, SEM1(45-107), AND SEM2(49-107) SEMINAL AMYLOID FIBRILS.....</b>	<b>76</b>
4.1 Introduction.....	76
4.2 Results.....	77
4.2.1 EGCG slowly disassembles SEVI fibrils .....	77
4.2.2 EGCG rapidly eliminates PAP85-120 fibrils.....	78
4.2.3 EGCG rapidly eliminates SEM1(45-107) and SEM2(49-107) fibrils .....	80
4.2.4 EGCG inhibits HIV infectivity in cell culture.....	81
4.3 Discussion.....	82
<b>CHAPTER 5: CONCLUSIONS AND FUTURE DIRECTIONS .....</b>	<b>85</b>
5.1 Conclusions .....	85
5.2 Future Directions .....	86
<b>CHAPTER 6: MATERIALS AND METHODS .....</b>	<b>89</b>
6.1 Small molecules and seminal plasma.....	89
6.2 Peptides and amyloid formation .....	89
6.3 Protein expression and purification.....	90

<b>6.4 Inhibition of amyloid fibrillization with CLR01 .....</b>	<b>92</b>
<b>6.5 Sedimentation analysis .....</b>	<b>92</b>
<b>6.6 Fibril disaggregation assays .....</b>	<b>93</b>
<b>6.7 Fibril degradation assays.....</b>	<b>93</b>
<b>6.8 Transmission electron microscopy .....</b>	<b>94</b>
<b>6.9 Filter trap assays .....</b>	<b>94</b>
<b>6.10 Turbidity assays.....</b>	<b>94</b>
<b>6.11 Dynamic light scattering .....</b>	<b>95</b>
<b>6.12 Zeta potential (Work from collaborators in the Münch lab).....</b>	<b>95</b>
<b>6.13 Confocal microscopy (Work from collaborators in the Münch lab).....</b>	<b>95</b>
<b>6.14 Circular dichroism spectroscopy.....</b>	<b>95</b>
<b>6.15 Cell culture and HIV infectivity experiments using Hsp104.....</b>	<b>96</b>
<b>6.16 Effect of tweezer on amyloid and semen-mediated enhancement of HIV infection (Work from collaborators in the Münch lab) .....</b>	<b>97</b>
<b>6.17 Antiviral activity of CLR01 on HIV-1, HCMV, HSV-2, HCV and adenovirus infection (Work from collaborators in the Münch lab) .....</b>	<b>98</b>
<b>6.18 p24 release assay (Work from collaborators in the Münch lab).....</b>	<b>100</b>
<b>6.19 Atomic force microscopy of virions (Work from members of the Münch lab).....</b>	<b>100</b>
<b>6.20 Analysis of cellular toxicity.....</b>	<b>101</b>
<b>6.21 Dosing the anti-viral effect of EGCG.....</b>	<b>101</b>
<b>CHAPTER 7: BIBLIOGRAPHY .....</b>	<b>103</b>

## LIST OF TABLES

Table 1: Expression, induction, and storage conditions for purification of his-tagged proteins .....	92
--	----

## LIST OF ILLUSTRATIONS

Figure 1.1 Seminal amyloid fibrils are derived from proteolytic fragments of abundant semen proteins and form amyloid fibrils that enhance HIV infection .....	5
Figure 1.2 Semen-derived peptides have several regions of high amyloidogenic propensity. ....	15
Figure 1.3 Amyloid fibrils can form diverse conformational strains .....	16
Figure 1.4 Hsp104 and HAP-ClpP disaggregate and degrade aggregated substrates .....	18
Figure 1.5 Chemical structures of anti-amyloidogenic small molecules .....	21
Figure 2.1 Hsp104 rapidly remodels SEVI fibrils to non-templating forms.....	29
Figure 2.2 Hsp104 <sup>A503V</sup> rapidly remodels SEVI fibrils, whereas hyperactive ClpB variants are inactive .....	31
Figure 2.3 Hsp104 and Hsp104 <sup>A503V</sup> rapidly remodel PAP85- fibrils .....	33
Figure 2.4 Hsp104 and Hsp104 <sup>A503V</sup> do not remodel SEM1(45-107) fibrils .....	34
Figure 2.5 Hsp104 and ClpB promote the clustering of seminal amyloid fibrils into larger aggregates .....	36
Figure 2.6 Hsp104 stimulates the assembly of SEVI and SEM1(45-107) fibrils into larger particles .....	38
Figure 2.7 Monomeric Hsp104 <sup>1-548</sup> promotes the clustering of seminal amyloid fibrils .....	39
Figure 2.8 HAP plus ClpP degrade SEVI fibrils and PAP85-120 fibrils. ....	41
Figure 2.9 Hsp104 reduces the ability of seminal amyloid to enhance HIV infection .....	44
Figure 2.10 Hsp104-based treatments that remodel, degrade, or cluster seminal amyloid reduce their ability to stimulate HIV infection .....	47
Figure 3.1 Molecular structures of CLR01 and CLR03. (a) Chemical structures of CLR01 and CLR03. (b) Stick representation showing CLR01 engaging lysine, while CLR03 is unable to interact with lysine.....	51
Figure 3.2 CLR01 inhibits the formation of seminal amyloid fibrils. ....	54
Figure 3.3 CLR01 inhibits both the nucleation and elongation steps of amyloid assembly .....	56
Figure 3.4 CLR01 cannot block the amyloidogenesis of polypeptides devoid of lysine and arginine residues .....	57
Figure 3.5 CLR01 partially disassembles preformed SEVI and PAP85-120 fibrils.....	60
Figure 3.6 CLR01-mediated disaggregation of seminal amyloid depends on contacts with lysine and arginine residues.....	61

Figure 3.7 CLR01 neutralizes the positive surface charge of seminal amyloids and abrogates their ability to bind virions and enhance HIV infection .....	64
Figure 3.8 CLR01 has direct anti-HIV-1 activity and destroys retroviral particles.....	67
Figure 3.9 CLR01 is a broad-spectrum inhibitor of enveloped viruses .....	68
Figure 3.10 CLR01 diminishes the infection enhancing property of semen .....	72
Figure 3.11 Schematic overview of the anti-amyloid and anti-viral effects of CLR01 .....	73
Figure 4.1 EGCG slowly remodels SEVI fibrils into non-amyloid structures.....	78
Figure 4.2 EGCG rapidly disassembles PAP85-120 amyloid fibrils.....	79
Figure 4.3 EGCG rapidly eliminates SEM1(45-107) and SEM2(49-107) fibrils .....	81
Figure 4.4 EGCG inhibits HIV infectivity in cell culture .....	82

## CHAPTER 1: BACKGROUND AND SIGNIFICANCE

### 1.1 Discovery of natural agents involved in HIV transmission

Human immunodeficiency virus (HIV) causes acquired immune deficiency syndrome (AIDS), a condition characterized by progressive failure of the immune system [1-4]. Over three decades after its initial identification, HIV endures as a global epidemic and aggressive public health threat: ~39 million people have died of AIDS-related illnesses since the start of the epidemic, and ~35 million adults and children are living with HIV worldwide [5]. This problem is most acute in the developing world: ~68% of all adults and 90% of all children with HIV are in sub-Saharan Africa, and ~76% of all AIDS deaths occur in this locale [6]. The vast majority of these infections are acquired by heterosexual transmission [7-9]. Several factors dictate the efficiency of HIV transmission via the sexual route including the viral load, type of sexual practice, and susceptibility of the host [8, 9].

Despite the growth and prevalence of the AIDS pandemic, HIV is an unexpectedly weak pathogen with low infectivity [10, 11]. In fact, it is estimated that less than 0.1% of viral particles are infectious *in vitro*, since infectivity is limited by low viral attachment rates to host cells [12-14]. *In vivo*, HIV transmission is also inefficient, occurring as infrequently as 1 in every 200 to 2000 acts of sexual intercourse [8, 15]. However, high viral titers that occur during acute infection can enhance this rate ~10-fold [9], and further enhancements accrue with sexual practices connected with bleeding and lesions of the mucosal barrier as well as the presence of other sexually transmitted diseases [15]. Semen is the principal vehicle for the sexual transmission of HIV, and *in vitro* semen can enhance the infection of physiologically relevant cell types, including primary macrophages and CD4+ T cells [16-20]. Thus, it was hypothesized that natural cofactors in seminal fluid could play a key role in HIV transmission by enhancing the efficiency of viral infectivity [17].

To isolate natural agents involved in the sexual transmission of HIV, Münch and colleagues created a library comprising all peptides and small proteins derived from human seminal fluid and screened this library for enhancers and inhibitors of HIV infection [17, 19]. One fraction significantly enhanced HIV infection, and further analysis by mass spectrometry and sequencing revealed that the active fraction contained several peptides, each of which was a proteolytic fragment of prostatic acid phosphatase (PAP) [17], a protein highly abundant (1-2 mg/mL) in seminal fluid [21]. While these peptides differed in length, each mapped to the same region of PAP. The predominant peptide in the enhancing fraction corresponded to residues 248-286 of PAP and was isolated at a concentration of ~35 µg/mL (7.7µM) (Figure 1.1a) [17].

Unexpectedly, Münch *et al* discovered that freshly dissolved solutions of chemically synthesized PAP248-286 were unable to augment HIV infection [17]. However, once the solutions became turbid after short-term storage or agitation, activity was restored, and in fact, the insoluble precipitate contained the active form [17]. Further biophysical analysis revealed that PAP248-286 fragments formed amyloid fibrils as indicated by increases in Thioflavin-T fluorescence, Congo red binding, and  $\beta$ -sheet content (Figure 1.1a) [17]. These amyloid fibrils were termed SEVI (**S**emen-derived **E**nhancer of **V**iral **I**nfection) and were found to augment HIV infection by  $\sim 10^5$  fold under conditions of limiting virus, whereas soluble PAP248-286 had no effect [17]. The presence of SEVI reduced the number of virions required for productive infection from between 1,000-100,000 to between 1-3 [17]. Indeed, the stimulatory effect of SEVI fibrils is greatest at low virus concentration, similar to the conditions observed in mucosal transmission of HIV, where relatively few virions traverse the mucosal barrier [17, 20]. Further, semen and SEVI were shown to increase the risk of vaginal virus transmission in an SIV/rhesus macaque model after exposure to low viral doses [22]. This remarkable effect is independent of viral coreceptor tropism [17], and the potency of individual human semen samples to boost infection correlates with levels of SEVI [16]. Moreover, SEVI also boosts the efficiency of retroviral transduction for viruses with diverse



envelope proteins [23] and strongly enhances human cytomegalovirus infection in cell culture by greater than 10-fold [24].

## **1.2 How does SEVI augment HIV infection?**

The misfolding of proteins into a generic amyloid structure is a recurring facet of diverse neurodegenerative diseases [25-28]. Yet, in isolation many proteins can form amyloid fibrils, suggesting that amyloidogenesis is an integral part of polypeptide chemistry [28-30]. Indeed, amyloid fibrils have been exploited during evolution for various adaptive modalities including prion-based transmission of advantageous phenotypes, long-term memory formation, melanosome biogenesis, drug resistance and biofilm formation [31-39].

SEVI, like other generic amyloids, adopts a classic 'cross- $\beta$ ' amyloid structure [17] in which  $\beta$ -sheets run orthogonal to the fibril axis [40-42]. However, PAP248-286 is unusual in that it contains a wealth of positively charged basic residues (8 of its 39 residues are either lysine or arginine; theoretical  $pI=10.21$ ). Thus, SEVI fibrils likely serve as a cationic bridge that simultaneously precipitates the virus onto the cell surface and decreases the electrostatic repulsion between the negatively charged surfaces of the virus and host cell (Figure 1.1c) [20, 43]. SEVI binds directly to both HIV virions and target cells [20], and this facilitates virion fusion much in the same way that synthetic cationic polymers promote retrovirus-mediated gene transfer [44, 45]. Importantly, a mutant PAP248-286, in which all basic residues were replaced with alanine, was still capable of assembling into amyloid fibrils, but the activity of these fibrils to augment HIV infection was greatly reduced compared to SEVI [20].

NMR spectroscopy revealed that PAP248-286 is highly disordered when bound to membrane-mimicking micelles [46, 47], whereas the majority of amyloidogenic peptides adopt an alpha-helical conformation upon micelle binding. It is predicted that some disordered regions present in monomeric PAP248-286 will be retained in mature SEVI amyloid fibrils [46-48]. Indeed,

disordered segments that emanate from the surface of SEVI fibrils may increase fibril 'capture radius' and could explain the enhanced ability of SEVI to promote HIV infection [46, 47, 49]. Furthermore, SEVI fibrils are non-toxic to CACO-2 epithelial cells, implying that SEVI is unlikely to augment HIV transmission by comprising the integrity of the mucosal epithelial layer that acts as a barrier to HIV [50].

Additional amyloid fibrils have also been shown to boost the infectivity of HIV, and thus it is clear that the amyloid structure plays a key role in this process. For instance,  $\alpha$ -synuclein fibrils, which are involved in the pathogenesis of Parkinson's disease, promote HIV infectivity in Tzm-BI cells albeit with reduced efficiency as compared to SEVI [51]. Additionally, peptides derived from the HIV gp120 co-receptor binding domain [52] and from the membrane-proximal external region of the HIV gp41 transmembrane protein [53] both form amyloid fibrils that potently enhance HIV infectivity. In fact, a synthetic 12-amino acid peptide derived from the gp120 glycoprotein, termed EF-C, instantaneously self-assembles into amyloid fibrils that boost virus infection four times more potently than naturally occurring SEVI fibrils and is now marketed as a retroviral transduction reagent [54, 55]. Finally, A $\beta$ 40 and A $\beta$ 42 amyloid fibrils, which are involved in the pathogenesis of Alzheimer's disease [28], stimulate HIV infection of microglia by ~5-20-fold and could contribute to HIV infection in the central nervous system of patients with HIV-associated dementia [56].

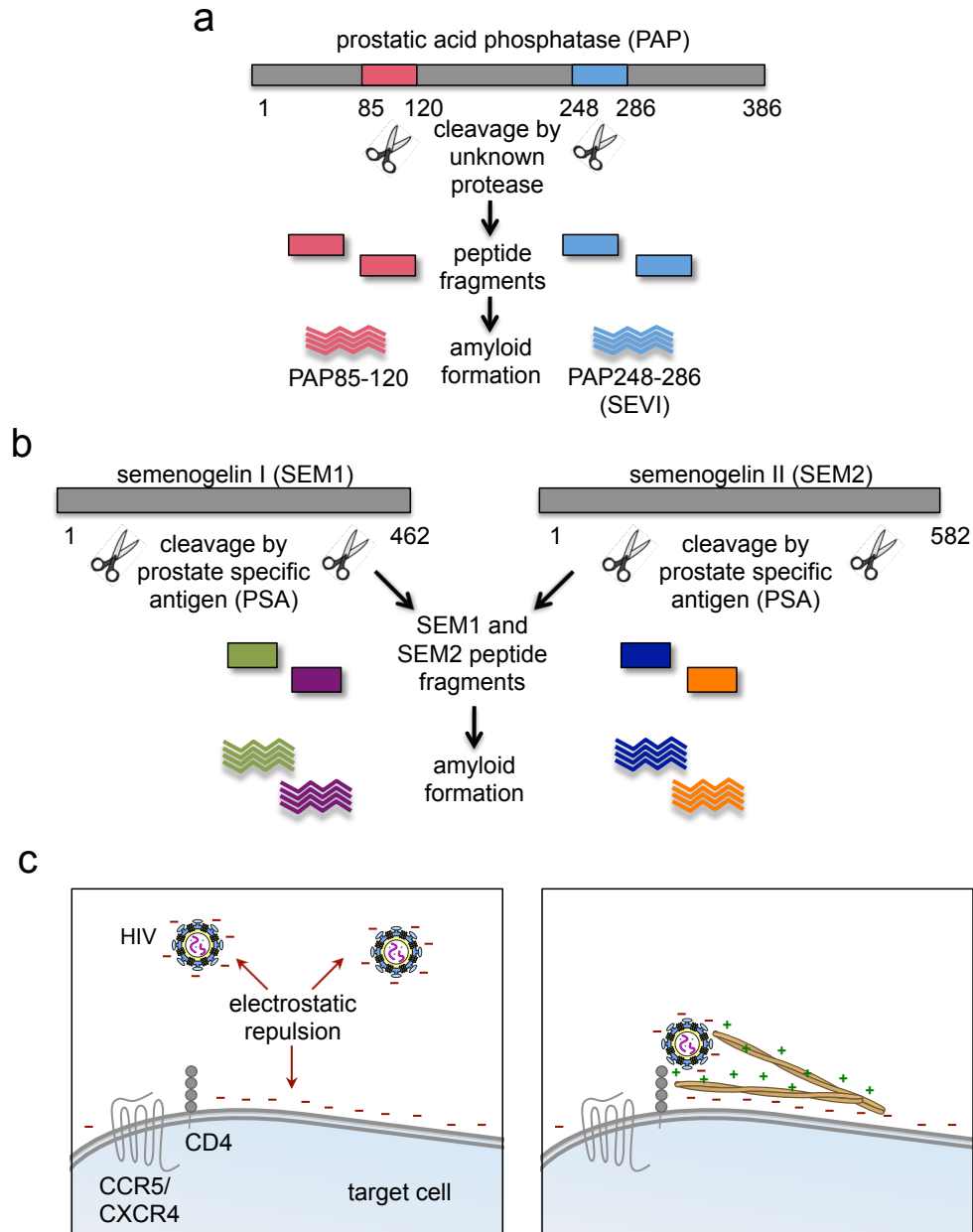


**Figure 1.1 Seminal amyloid fibrils are derived from proteolytic fragments of abundant semen proteins and form amyloid fibrils that enhance HIV infection. (a)** Full-length prostatic acid phosphatase (PAP) undergoes proteolysis to form peptide fragments PAP85-120 and PAP248-286, which readily aggregate and assemble into amyloid fibrils in semen. Amyloid fibrils formed from PAP248-286 are termed SEVI (Semen-derived Enhancer of Viral Infection). **(b)** Full-length semenogelin1 and semenogelin2 (SEM1 and SEM2) are proteolytically cleaved by prostate specific antigen (PSA) to yield several peptide fragments, which readily aggregate and assemble into amyloid fibrils in semen. **(c)** Left: In the absence of seminal amyloid, HIV infectivity is limited by electrostatic repulsion between the negatively charged surfaces of the viral and target cell membranes. Right: Cationic seminal amyloid fibrils shield this electrostatic repulsion and facilitate HIV infectivity by bringing virions in closer proximity to the cell surface.

### 1.3 PAP85 and SEM amyloid fibrils

After identifying SEVI, Münch and colleagues continued analysis of their semen-derived peptide library [57]. In particular, they noted an additional fraction that promoted HIV infection.

Remarkably, this fraction was identified to be an N-proximal fragment of PAP that comprised residues 85-120 (PAP85-120), and this peptide was isolated at a concentration of  $\sim 39 \mu\text{g/mL}$  ( $8.7 \mu\text{M}$ ) (Figure 1.1a) [57]. The discovery of a second peptide fragment that corresponded to the same precursor protein was unanticipated, especially since the library contained several thousand species. Like SEVI, PAP85-120 exists as amyloid fibrils in seminal fluid, and these fibrils promote HIV infection but are slightly less efficient [57]. Also like PAP248-286, PAP85-120 is highly cationic (8 of its 36 residues are either lysine or arginine; theoretical  $\text{pI}=9.99$ ) implying that PAP85-120 and SEVI act through a similar mechanism to boost HIV transmission. Notably, SEVI and PAP85-120 fibrils cooperate to exert additive HIV enhancing effects in cell culture [57].

The discovery of two positively charged fibrillar structures that augment virion fusion and infection led to the hypothesis that other positively charged factors might exist in semen that could also enhance HIV transmission. To test this hypothesis, pooled seminal fluid was depleted of positively charged factors and this resulted in a complete loss of its ability to augment HIV infection [58]. When the identity of these depleted cationic factors was subsequently determined, SEVI was surprisingly not detected. Rather, proteolytic fragments from two homologous semenogelin proteins, SEM1 and SEM2, were identified (Figure 1.1b) [58]. Semenogelins (SEMs) are proteins originating from the seminal vesicles that together with fibronectin comprise the major components of the semen coagulum [59, 60]. SEM proteins are rapidly cleaved after ejaculation by the chymotrypsin-like serine protease, prostate specific antigen (PSA), at highly specific sites [61, 62]. This cleavage event is associated with liquefaction of the semen coagulum, which is important for the release of motile spermatozoa and thus male fertility [59, 60]. The SEM1 and SEM2 peptides detected from this experiment corresponded to PSA-generated proteolytic fragments, and remarkably, these peptide fragments all formed amyloid fibrils capable

of promoting HIV infection to varying extents (Figure 1.1b) [58]. Like SEVI and PAP85-120, the SEM peptides are rich in lysine and arginine residues and carry a net positive charge at neutral pH (pIs of SEM peptides studied range from 8.16 to 10.12).

Interestingly, semen samples from patients with ejaculatory duct obstruction (EDO) were also analyzed. EDO patients are naturally deficient in SEMs, since duct obstruction prevents contents of the seminal vesicles from reaching the ejaculate. As expected, these semen samples lacked viral infection-enhancing activity [58]. Unexpectedly, however, levels of full-length PAP were elevated in EDO samples, while levels of the SEVI precursor peptide PAP248-286 were diminished [58]. Because semen from EDO patients lacks secretions from the seminal vesicles, these data suggest that the proteolytic activity responsible for generating the SEVI peptide from full-length PAP is diminished in semen from EDO patients. The identity of the protease that releases PAP248-286 from its full-length precursor is undetermined, but these data indicate that the protease may reside in the seminal vesicles. The identification of this protease will be valuable, since a protease inhibitor could be a useful tool to prevent the release of PAP248-286 and PAP85-120 peptides from their full-length precursor. Such a strategy could also be employed to inhibit PSA, thus blocking the cleavage of amyloidogenic SEM peptides from full-length SEM1 and SEM2.

The identification of numerous amyloidogenic peptides in seminal fluid is somewhat surprising. The presence of multiple peptides assembled into amyloid fibrils in semen suggests that they are potentially functional rather than disease-associated. Does the make-up of seminal fluid favor the formation of amyloid fibrils? Studies of SEVI, PAP85-120, and SEM amyloid fibrils have indicated that high peptide concentrations and extensive, non-physiological levels of agitation are required to induce amyloid formation *in vitro*. However, when the SEVI precursor peptide PAP248-286 was assembled into amyloid fibrils in the presence of seminal plasma, fibrillization was significantly enhanced and accelerated [63]. Seminal plasma drastically reduced the lag time for SEVI

fibrillization and eradicated the requirement for agitation. This finding indicates that the diversity of molecules in seminal plasma, especially anionic buffer components, have a drastic impact on fibrillization and can potentially explain the strong presence of amyloid fibrils in seminal fluid. Furthermore, semen contains high concentrations of  $Zn^{2+}$  cations (low mM concentrations), which can inactivate seminal proteases and protect amyloid fibrils from proteolytic degradation [63]. In fact, a positive correlation exists between HIV-infection enhancement and zinc concentration in semen, indicating that  $Zn^{2+}$  cations likely stabilize semen-derived amyloid fibrils, thus increasing their capacity to augment infection [64].

Despite the wealth of evidence illustrating the role of semen-derived amyloid fibrils in HIV transmission, the actual presence and proviral activity of these fibrils has been questioned. One study reported that the infection enhancing activity of SEVI fibrils formed *in vitro* was neutralized in the presence of 1% seminal plasma [65]. This effect was attributed to the natural degradation of the PAP248-286 peptide by seminal proteases [65], thus calling into question whether such fibrils could actually form naturally in seminal fluid. However, amyloid fibrils have been readily identified in fresh human seminal fluid using fluorescent amyloid-binding dyes, fibril-specific antibodies, and both confocal and transmission electron microscopy [66-68]. Semen does progressively lose its HIV-enhancing activity during prolonged periods of liquefaction, and this decline in activity correlates with levels of SEM peptide fragments, which are subjected to proteolysis by seminal serine proteases over time [69]. Nevertheless, seminal fluid retains its proviral activity for over 8h post-emission [69]. Simian immunodeficiency virus can infect cells in the vaginal mucosa within 30 to 60min of inoculation [70], and so seminal fluid likely maintains its virus-enhancing activity long enough to boost viral transmission in an *in vivo* setting.

#### **1.4 A physiological role for semen-derived amyloid fibrils?**

While the role of these naturally occurring semen-derived amyloidogenic peptides in HIV infection has been well defined, one crucial question is still unanswered: what is the adaptive role of these

amyloid species? It has been postulated that these amyloid fibrils may play a physiological role in promoting fertilization, especially since numerous commonalities exist between virion-target cell fusion and sperm-egg fusion [71]. Thus, semen-derived amyloid fibrils may facilitate the attachment and fusion of sperm with an oocyte much in the same way that SEVI and other semen-derived amyloid fibrils promote HIV virion binding and fusion with target cells. The most obvious commonality between the two processes is that they occur in the same anatomical context, and semen is utilized as a vehicle to transport both sperm and HIV. Another striking parallel between the two processes is that the HIV viral envelope and sperm share the same basic plasma membrane structure consisting of a phospholipid bilayer embedded with vital glycoproteins and lipids [71]. Furthermore, both processes proceed by an identical series of steps involving cell binding, fusion, and penetration. First, sperm and HIV must attach and bind to their target cells, and both carbohydrates and electrochemical interactions are crucially involved in this step [71]. Just as polyanions have been shown to block SEVI-mediated enhancement of HIV infection by inhibiting HIV cell entry [20, 72], several polyanions have also been shown to obstruct sperm-oocyte interactions [73, 74], further illustrating the similarities between these processes. Following cell attachment, membrane fusion must occur in both fertilization and HIV infection. The fusion of sperm and oocyte membranes, as well as HIV and target cell membranes, is an energetically unfavorable process that requires cooperative protein-protein interactions [73, 75, 76]. Finally, overlapping signal transduction pathways are essential for both sperm capacitation (a process through which sperm acquire fertilization capacity) and the post-entry stages of HIV replication and maturation [71, 77, 78].

Because of the apparent parallels between mammalian fertilization and HIV infection, it is certainly plausible that SEVI and other amyloids may play a role in the fertilization process. Further evidence stems from the fact that spermatozoa can be stained with the amyloid-binding dye Congo Red, indicating that amyloid fibrils may be bound to these motile sperm cells [79]. Additionally, immunostaining for SEM1 and SEM2 has revealed that SEM fragments bind to the

posterior head, midpiece, and tail of ejaculated spermatozoa [59, 80, 81]. However, it is unclear whether or not this result involves SEM amyloid fibrils or non-amyloid SEM fragments. If semen-derived amyloid fibrils are indeed bound to spermatozoa, this will further suggest a mechanism by which amyloid fibrils are involved in fertilization.

Further studies investigating the physiologic function of seminal amyloid have demonstrated that SEVI has indirect antimicrobial activity that is dependent on its cationic, fibrillar nature. Indeed, SEVI bound to both Gram-positive and Gram-negative bacteria in a charge-dependent manner, promoted bacterial aggregation, and facilitated phagocytosis of bacteria by primary human monocyte-derived macrophages [82]. In addition, mice exposed to *N. gonorrhoeae* in the presence of SEVI had reduced bacterial load [82]. Furthermore, peptides derived proteolytically from SEM1 and SEM2 have intrinsic bactericidal activity as a mechanism for protecting spermatozoa in the female reproductive tract [83, 84], however, whether this activity is attributed to the amyloid forms of these peptides is unclear.

### **1.5 Current strategies to counteract amyloid-mediated enhancement of HIV infection**

The highly unanticipated role of seminal amyloid in viral infection has opened a new window of opportunity. If we can inhibit the formation of seminal amyloid fibrils, block their infection promoting properties, or even rapidly dissolve these fibrils, then we can drastically reduce HIV infection via the sexual route. Thus far, several agents have been identified that fall into each of these classes of anti-seminal amyloid compounds. While this section focuses on agents that counteract SEVI's effects, it should be noted a truly effective agent should antagonize the stimulatory effects of all semen-derived amyloid fibrils.

Ultimately, agents that effectively block the ability of semen-derived amyloid to promote HIV infection might be developed into a microbicide, thus offering a preventative means to combat HIV transmission. A microbicide is an agent that reduces the infectivity of a pathogen. In this



case, an anti-amyloid topical formulation might be developed for application either vaginally or rectally to prevent the very earliest stage of sexual HIV transmission [85, 86]. Alternatively, methods to reduce initial amyloid formation in the seminal fluid of the male might also be explored. Ideally, the microbicide would be effective, safe, user-friendly and affordable to promote use in the developing world. The development of topical microbicides has proven challenging, and the vast majority of microbicidal compounds explored to date target the virus itself. However, mutations can rapidly arise that alter viral proteins and confer resistance to antiretroviral drugs [87]. Combinations of antiretroviral drugs tend to exhibit improved efficacy by functioning through multiple mechanisms of action [88]. By targeting host-encoded amyloid fibrils instead of the viral machinery, this issue of drug-resistant HIV variants could be circumvented, making amyloid fibrils a valuable and novel target for future microbicide development.

The most common class of anti-SEVI agents identified to date, shield the charged surface of the fibrils to block their infection boosting properties. Anionic polymers, which interfere with the binding of SEVI to HIV virions by shielding the intrinsic positive charges of SEVI, diminish SEVI-mediated enhancement of infection [20]. These polyanions, including heparin and various other glycosaminoglycans, have been investigated as HIV microbicides for decades, as they are also thought to exert direct anti-HIV activity by inhibiting the binding of the viral envelope glycoprotein, gp120, to its major cell surface receptor CD4 [89-91]. Unfortunately, such anionic polymers have proven unsuccessful in past clinical trials due to their poor bioavailability and induction of inflammatory responses in the genital tract, which instead augment HIV transmission by recruiting HIV-susceptible target cells to the genital mucosa [92, 93]. Additionally, polyanionic candidate microbicides were found to have considerably reduced HIV inhibitory activity in the presence of seminal plasma [94] and even efficiently promote SEVI fibrillization to enhance HIV infection [95]. Thus, more favorable options, which act through related mechanisms, are needed.

Aminoquinoline surfen, a small molecule heparan sulfate proteoglycan (HSPG) antagonist, exerts anti-SEVI effects through a slightly different mechanism [43]. It was initially hypothesized that SEVI bound to target cells through interactions with cell surface HSPGs [43]. Surfen antagonizes this interaction, and additional studies indicated that surfen also antagonized the interaction between SEVI and HIV virions [43]. Further, surfen possesses anti-inflammatory properties as an anaphylatoxin C5a receptor antagonist [96, 97], making it a promising microbicide candidate.

BTA-EG<sub>6</sub> (a hexa(ethylene glycol) derivative of benzothiazole aniline) is a small molecule capable of abrogating SEVI's effects by binding to its 'cross-β' structure [18]. BTA-EG<sub>6</sub> is an amyloid-binding small molecule akin to the amyloid-diagnostic dye, Thioflavin-T, that intercalates between β-strands, and by doing so, inhibits the interactions of SEVI with both target cells and HIV virions and thus prevents SEVI-mediated enhancement of HIV infection [18]. Importantly, oligovalent derivatives of BTA exhibited an improved capability to attenuate SEVI-enhanced infection of HIV as compared to the corresponding monomer [98]. It is likely that these amyloid-binding agents form a bio-resistive coating on SEVI to hinder interactions with virions and target cells [18, 98].

Another approach to target SEVI's deleterious effects is through inhibition of amyloid fibril formation. Structure-based design of peptides comprised of non-natural amino acids has yielded a highly specific peptide inhibitor of PAP248-286 fibrillization [48]. This approach focused on the characteristic steric-zipper motif, common to amyloid-forming proteins, in which β-sheets pack together through interdigitation of their peptide side chains to form a highly self-complementary interface [41, 99]. The G260 to N265 hexapeptide segment of PAP248-286, GGVLVN, is one of seven hexapeptides in PAP248-286 that is predicted by Zipper DB [100] to have high amyloid propensity (Figure 1.2a) [48]. The steric-zipper structure of GGVLVN was solved and used as a template to computationally design a peptide-based inhibitor termed WW61 that would cap the growing ends of fibrils to inhibit amyloid assembly [48]. WW61 is a hexapeptide, Trp-His-Lys-chAla-Trp-hydroxyTic, which contains an Ala derivative, β-cyclohexyl-L-alanine (chAla) and a

Tyr/Pro derivative, 7-hydroxy-(S)-1,2,3,4-tetrahydroisoquinoline-3-carboxylic acid (hydroxyTic), both of which are designed to increase contact area with the growing ends of SEVI fibrils. Remarkably, WW61 prevented full-length PAP248-286 from assembling into functional SEVI fibrils capable of promoting HIV infection [48]. While this breakthrough represents the first compelling example of a structure-based design of an amyloid inhibitor, there is no evidence that the WW61 peptide is active in blocking semen-mediated enhancement of HIV infection [48]. Indeed, WW61 is unlikely to inhibit the amyloidogenesis of PAP85-120, SEM1 and SEM2.

While this is a novel strategy to prevent SEVI assembly, SEVI fibrils are already formed and abundant in seminal fluid. Thus, inhibiting their initial formation would seem impractical in the male and futile in the female. Similarly, SEVI fibrils will persist in strategies that aim to coat the amyloid surface and prevent interactions with the virus or the cell surface or both. Thus, fibrils might still gain opportunities to promote viral infection. We suggest that a more desirable strategy would be to isolate agents that rapidly deconstruct SEVI fibrils and thereby eradicate structures that promote HIV infection. However, great difficulty lies in the unusual stability of the amyloid form, which resists proteases, protein denaturants, temperatures up to 98°C, and 2% SDS [41, 101, 102]. Indeed, because of their exceptional stability, amyloid fibrils are difficult to degrade and are widely perceived to be intractable [103].

Despite their exceptional stability, a few, very select agents can reverse amyloid formation. EGCG (epigallocatechin-3-gallate), a potent antioxidant found in green tea, has shown widespread antifibrillogenic effects [104-107]. EGCG can inhibit formation of SEVI amyloid fibrils, and more importantly, it slowly remodels preformed SEVI fibrils over 1-2 days at non-toxic concentrations [108]. By targeting and remodeling these fibrils, EGCG strongly antagonizes the activity of SEVI. In contrast to the initially proposed mechanism of action [105], EGCG was found to interact with the side chains of monomeric PAP248-286 (particularly lysine residues), leading to the formation of a covalently bound complex (Schiff base links with a lysine residues) [109].

Notably, EGCG is extremely stable in acidic solutions, a condition resembling the vaginal environment [110]. These data, taken together, suggest that EGCG may be a favorable option for use as a topical microbicide component, however the ability of EGCG to antagonize PAP85-120 and SEM amyloid fibrils remains to be elucidated.

### **1.6 Amyloid strains**

A phenomenon that further adds to the complexity of searching for anti-SEVI and anti-amyloid agents is that amyloid fibrils can exist as polymorphs and form diverse conformational strains. Conformational variation among amyloid fibrils of a given protein can give rise to fibrils with distinct properties [111-113]. The biochemical basis for amyloid polymorphism likely stems, at least in part, from the diversity of steric-zipper amyloid spines that a single protein can adopt [114]. For example, PAP248-286 is predicted to contain seven different hexapeptide segments that are capable of forming steric zippers (Figure 1.2a). Thus, each of these segments could drive the assembly of amyloid structures that are distinct at the atomic level, resulting in a segmental polymorphism (Figure 1.3) [114]. Moreover, six hexapeptides within PAP85-120 are predicted by Zipper DB [115] to be amyloidogenic, and the SEM1(45-107) and SEM2(45-107) peptides also contain multiple predicted regions of high fibrillization propensity (Figure 1.2b-d), implying that different amyloid strains may exist for these peptides as well.

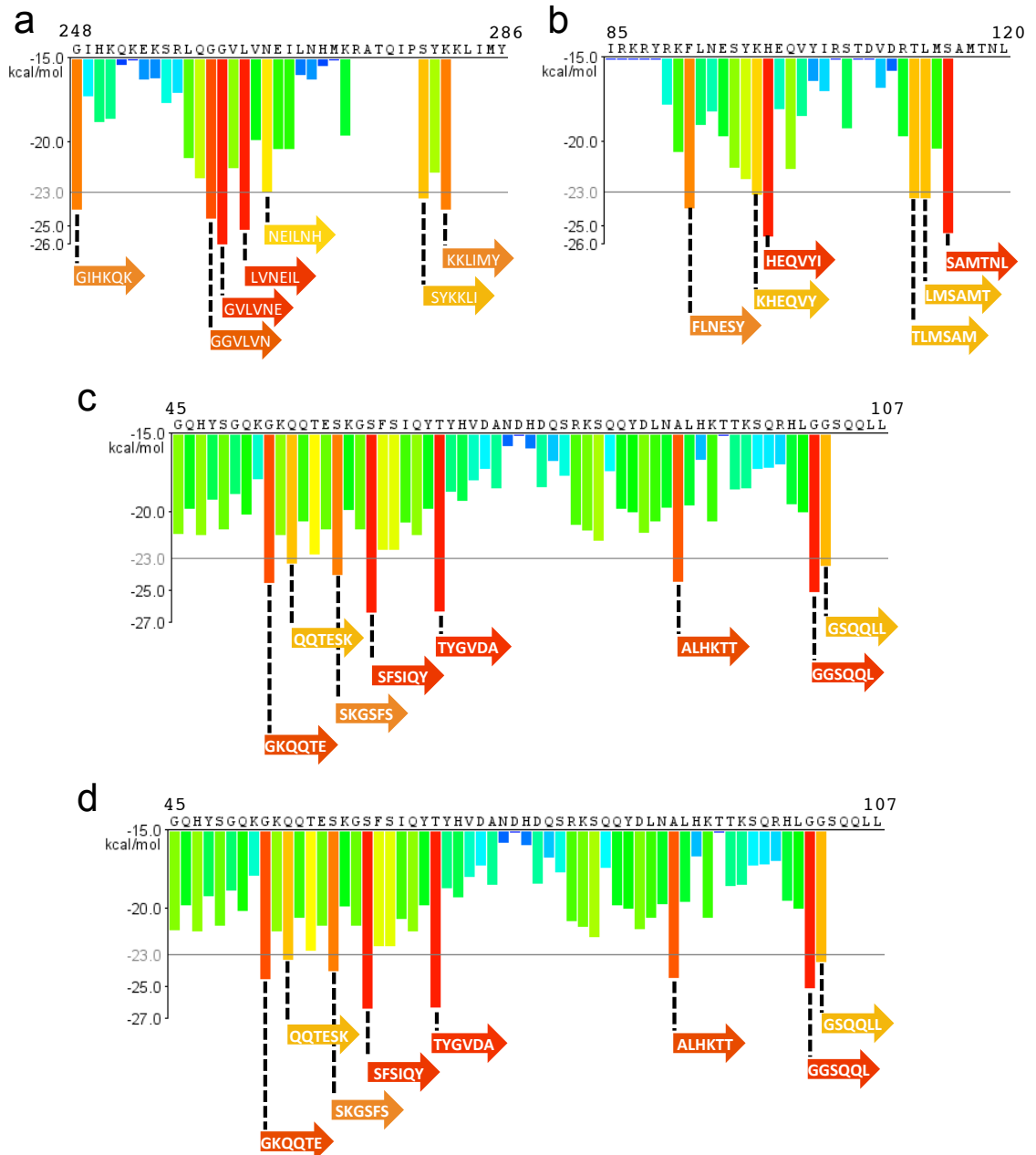


**Figure 1.2 Semen-derived peptides have several regions of high amyloidogenic propensity. (a-d)** Zipper DB [100] prediction of fibril-forming segments of PAP248-286 (a), PAP85-120 (b), SEM1(45-107) (c), and SEM2(45-107) (d). The propensity profile graph predicts hexapeptide segments (beginning at the indicated residue) that are highly likely to assemble into amyloid fibrils. Orange-red segments with energy values below the indicated threshold of -23kcal/mol (gray line) are expected to form steric-zipper spines of fibrils. Each semen-derived peptide contains 6-8 hexapeptide segments of high amyloidogenic propensity.

It is unclear whether each of the predicted hexapeptides present within PAP248-286 does indeed form a steric zipper. However, it is probable that SEVI fibrils can exist as multiple strains within seminal fluid. The presence of several SEVI strains could complicate the development of anti-SEVI inhibitors. For instance, WW61, the non-natural peptide inhibitor of SEVI assembly, was rationally designed to bind to the  $^{260}\text{GGVLVN}^{265}$  steric-zipper interface [48]. WW61 effectively inhibited PAP248-286 fibril formation, indicating that the  $^{260}\text{GGVLVN}^{265}$  motif plays a key role in driving SEVI formation under the specific assembly conditions employed [48]. However, this inhibitor might be ineffective against alternative segmental polymorphs (Figure 1.3), which could assemble under different assembly conditions. Indeed, different assembly conditions can shift the relative populations of amyloid strains and generate distinct strain ensembles [113, 114, 116, 117]. At present, the nature of the SEVI strain ensemble in seminal fluid is uncertain, and is likely to vary from individual to individual.

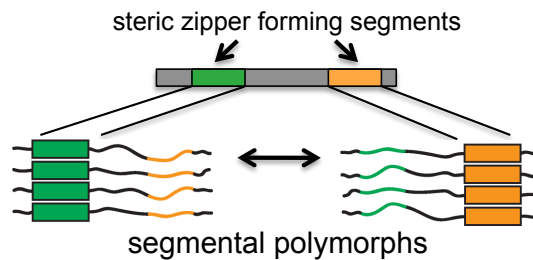


**Figure 1.3 Amyloid fibrils can form diverse conformational strains.** An amyloid forming protein with two segments (green and orange) capable of forming steric zippers can exist as segmental polymorphs, in which each segment can form the amyloid core.

This concern also extends to EGCG, which is a strain-selective inhibitor of Sup35 fibrillization [116]. Such strain-selectivity could impact the ability of EGCG to exert antifibrillogenic effects against SEVI. In a study examining the efficacy of EGCG at reducing SEVI-mediated enhancement of HIV infection in a cohort of 47 individual semen samples, EGCG was only efficacious in 41 out of 47 samples, and substantial heterogeneity was observed within the results [118]. This heterogeneity might indicate that EGCG is a strain-selective antagonist of SEVI as

well. Perhaps the most effective way to combat strain phenomena is to utilize combinations of inhibitors designed to target the entire spectrum of polymorphic strains [116, 117, 119-121].

## **1.7 Established amyloid-remodeling factors**

### **1.7.1 Hsp104**

Despite the exceptionally stable structure of amyloids, a few, very select agents can reverse amyloid formation. Moreover, only one agent, Hsp104, is known to catalytically take apart the amyloid form. No other candidate has emerged that can eliminate amyloid fibrils with such unprecedented alacrity. Hsp104 is a AAA<sup>+</sup> protein (**A**TPases **A**ssociated with various cellular **A**ctivities) from yeast that protects cells against stresses including heat shock, by renaturing and reactivating damaged proteins (Figure 1.4a) [122]. Hsp104 is also involved in induced thermotolerance, as yeast cells given a mild heat pre-treatment (37°C) were subsequently able to survive extreme heat shock (50°C), while  $\Delta hsp104$  mutant cells exhibited 1000-fold reduced survival rate [123, 124]. Unlike classical molecular chaperones, Hsp104 is less able to protect chemically or thermally denatured substrates from aggregation and instead mediates the resolubilization of these amorphous aggregates in concert with its obligate co-chaperones Hsp40 and Hsp70 [122, 125, 126]. In contrast, Hsp104 deconstruction of ordered amyloid fibrils does not always necessitate Hsp40 and Hsp70 [127-130]

Hsp104 is a three-tiered, hexameric, ring-shaped ATPase consisting of two stacked nucleotide binding domains (NBD1 and NBD2) separated by a coiled-coil middle domain and capped at either end by N- and C-terminal domains [131, 132]. ATP binding by Hsp104 is essential for substrate interaction; substrate cannot be released until the bound ATP is hydrolyzed, thus ensuring that all the energy generated by ATP hydrolysis is translated into mechanical work, i.e. substrate remodeling [133, 134]. It is hypothesized that ATP hydrolysis generates a 'power

stroke' to result in conformational changes within the protein that allow threading of substrate through the axial channel to promote refolding [135-137].

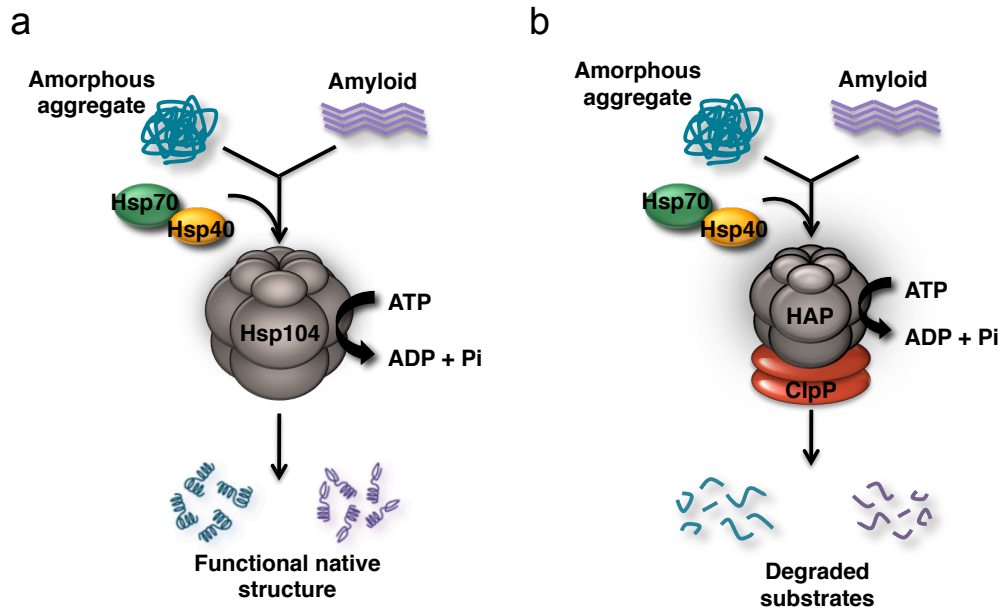


**Figure 1.4 Hsp104 and HAP-ClpP disaggregate and degrade aggregated substrates. (a)** Hsp104 couples ATP binding and hydrolysis to remodel protein aggregates and amyloid fibrils. **(b)** HAP, an Hsp104 variant, physically interacts with the bacterial peptidase ClpP. Substrate is translocated through the central pore of HAP and into ClpP for degradation.

Because amyloids share a common 'cross- $\beta$ ' structure, it is likely that agents capable of antagonizing amyloid fibers of one protein will prove useful against other amyloid fibers as well. Moreover, Sup35, a natural substrate of Hsp104, has a highly basic, lysine-rich stretch, and several lines of evidence suggest that lysine-rich regions provide an important component of substrate recognition by Hsp104 [138, 139]. The primary sequences of seminal amyloidogenic peptides are also alkaline and lysine-rich, further supporting the notion that seminal amyloids will be easily recognized substrates for Hsp104. However, the product of Hsp104 remodeling will likely be soluble peptide that may be free to reform amyloid fibrils. To combat this issue, Hsp104 disaggregation activity can be coupled to degradation to remove remodeled products [140, 141].



To achieve this functionality, an Hsp104 variant, termed HAP, has been engineered (G739, S740, K741 of Hsp104 to IGF) that physically interacts with the chambered bacterial protease ClpP [142], a highly conserved cylindrical serine protease [143]. In this proteolytic system, individual monomers are extracted from the amyloid substrate by HAP and translocated into the ClpP chamber where they are degraded into small peptides of ~7-8 residues (Figure 1.4b) [144]. These small peptides may be too short to reform stable amyloid structures and could also be degraded by extracellular proteases.

While Hsp104 is conserved across plants, bacteria, and fungi, there is surprisingly no homologue present in metazoans [130]. However, the introduction of Hsp104 into metazoan systems to reverse protein aggregation is not unprecedented, and in fact, Hsp104 is tolerated extremely well [128, 145-147]. Importantly, Hsp104 cooperates with the mammalian Hsp70 chaperone system to promote protein disaggregation [125, 148, 149]. In mammalian cell models of Huntington's disease, Hsp104 reduced both polyglutamine aggregate formation and toxicity [150] and these results were replicated in mouse models [146]. The introduction of Hsp104 into a rat model of Parkinson's disease reduced formation of  $\alpha$ -synuclein inclusions and prevented  $\alpha$ -synuclein induced neurodegeneration [128]. Thus, we hypothesize that both Hsp104 and the HAP-ClpP proteolytic system will remodel and/or degrade seminal amyloid fibrils, thus eliminating their ability to enhance HIV infectivity.

### **1.7.2 CLR01**

Lysine and arginine residues play a key role in many biological processes, and therefore artificial receptors for these residues could be interesting candidates for pharmaceuticals or molecular probes. Klärner *et al* sought to design a synthetic, water-soluble receptor that was selective for lysine residues in polypeptides and developed a compound called CLR01, which has a rigid torus-shaped nonpolar cavity featuring two anionic phosphate groups at the bridgehead (Figure 1.5a) [151]. CLR01 achieves lysine specificity by inclusion of the butylene moiety of the lysine

side chain within the nonpolar cavity and electrostatic interaction of the lysine ammonium group with one of the anionic phosphates, and this binding occurs with micromolar affinity [151].

Amyloid self-assembly is a complex process mediated by a combination of hydrophobic and electrostatic interactions, and lysine residues have been shown to play a vital role in the assembly and toxicity of many amyloidogenic peptides [152]. Thus, Sinha *et al* hypothesized that compounds that interfere with lysine residues with moderate affinity would have sufficient power to disrupt the relatively weak interactions involved in amyloid nucleation, oligomerization, and elongation while having little to no effect on disruption of structurally stable proteins or normal protein function [152]. In fact, the lysine specific “molecular tweezer” CLR01 was found to inhibit the aggregation of several amyloidogenic peptides including A $\beta$ , tau, islet amyloid polypeptide, calcitonin, transthyretin, and  $\alpha$ -synuclein and it also dose-dependently inhibited their toxicity [152-154]. In addition, CLR01 gradually disaggregated mature A $\beta$  and  $\alpha$ -synuclein fibrils into nonfibrillar aggregates over a period of days to months [152, 154].

The “molecular tweezer” CLR01 has also shown neuroprotective effects in animal models of neurodegenerative diseases. For instance, in a mouse model of Alzheimer’s disease, CLR01 reduced A $\beta$  and tau aggregate loads and ameliorated microgliosis with no apparent signs of toxicity [155]. In a zebrafish model of  $\alpha$ -synuclein toxicity, CLR01 treatment dose-dependently reduced toxicity and improved survival [154]. Finally, CLR01 reduced transthyretin burden in the gastrointestinal tract and peripheral nervous system in a mouse model of familial amyloidotic polyneuropathy [156].

While CLR01 has shown efficacy in numerous cell and animal models of amyloidoses without any signs of toxicity, obvious concerns have been raised about a mode of action targeting exposed lysine residues in virtually any protein. Attar *et al* compared the concentration of CLR01 needed to interfere with aberrant protein aggregation to the controlled physiologic self-assembly of tubulin

polymerization. They found that a substantially higher CLR01 concentration (~50 fold) was required to disrupt tubulin polymerization, supporting the specificity of CLR01 for inhibition of aberrant protein aggregation [157]. In addition, when CLR01 was tested for enzyme inhibition of alcohol dehydrogenase *in vitro*, a 865-fold excess of CLR01 was needed for inhibition [158], further supporting the process-specific mechanism of CLR01.

Because seminal amyloid fibrils are rich in lysine and arginine residues, we hypothesized that CLR01 would disrupt their initial formation and remodel preformed fibrils, thus inhibiting seminal amyloid-mediated enhancement of HIV infection.

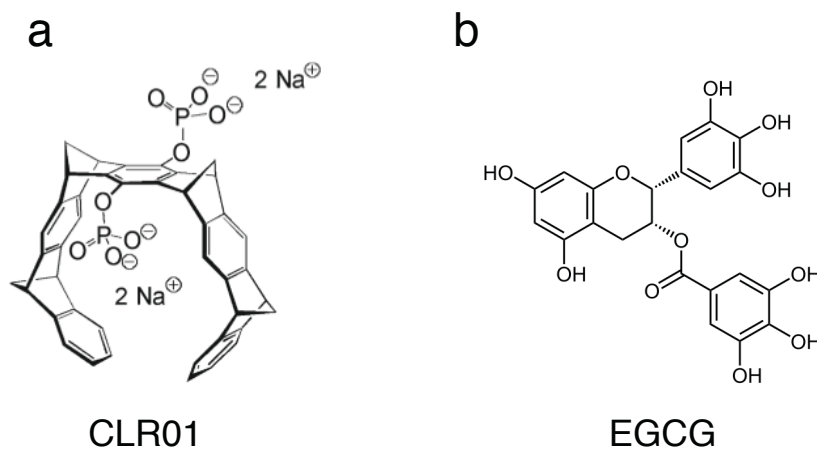


**Figure 1.5 Chemical structures of anti-amyloidogenic small molecules. (a)** The lysine-specific “molecular tweezer”, CLR01. **(b)** The major green tea polyphenol epigallocatechin-3-gallate (EGCG).

### 1.7.3 EGCG

As previously discussed, EGCG (epigallocatechin-3-gallate), the most abundant and powerful polyphenol found in green tea, is the most well studied anti-amyloidogenic compound (Figure 1.5b). In addition to this property, EGCG is associated with numerous health benefits including cardioprotective, neuroprotective, anti-carcinogenic, anti-inflammatory, and weight loss effects [159]. In terms of its anti-aggregation effects, EGCG can modulate assembly and even

disassemble amyloid forms of several disease associated amyloidogenic polypeptides including islet amyloid polypeptide (type II diabetes) [160],  $\alpha$ -synuclein (Parkinson's disease) [161], A $\beta$  (Alzheimer's disease) [161], TTR (transthyretin amyloidoses) [162], and the yeast prion protein Sup35 [116]. Furthermore, in cell culture models of A $\beta$ -,  $\alpha$ -synuclein-, and huntingtin-induced neurotoxicity, EGCG treatment was neuroprotective and reduced cytotoxicity [161, 163, 164]

The mechanisms of action for EGCG-mediated inhibition of amyloid assembly and amyloid remodeling have been studied using various biochemical and biophysical techniques. To inhibit amyloid fibrillization, EGCG is proposed to bind to exposed backbone sites in the unfolded regions of monomeric proteins and divert aggregation pathways to instead favor the formation of off-pathway aggregates [105]. An additional study investigated the mechanisms by which EGCG remodels mature amyloid fibrils. It was found that EGCG-mediated remodeling of A $\beta$ , islet amyloid polypeptide, and Sup35 was dependent on auto-oxidation of EGCG into a mixture of monomeric and polymeric EGCG-based quinones [165]. EGCG is proposed to engage hydrophobic binding sites within amyloid fibrils, and oxidized EGCG products react with free amino groups of lysine side chains within fibrils to covalently modify the amyloidogenic proteins through Schiff base formation [165].

As discussed earlier, EGCG inhibits the formation of SEVI amyloid fibrils and remodels preformed SEVI fibrils [108]. However, the ability of EGCG to remodel additional semen-derived amyloid fibrils, namely PAP85-120, SEM1, and SEM2 remained to be further elucidated.

### **1.8 Research aims**

Seminal amyloid fibrils represent a novel microbicide target, as the idea of targeting host protein conformers is fundamentally different from traditional microbicidal approaches that target HIV itself. This strategy might be less susceptible to HIV escape variants, which can rapidly evolve and evade therapies that directly target components of the viral machinery [166-168]. Thus,

deciphering a method to dissolve semen-derived fibrils would offer a preventative strategy to combat HIV infection via sexual transmission. However, the relative contributions of SEVI, PAP85-120 and SEM amyloid fibrils, as well as amyloid strain phenomena, in semen-mediated enhancement of HIV infection have yet to be determined. Therefore, we reasoned that the utility of general amyloid-remodeling factors would be greater than agents with specialized activity against individual amyloid conformers.

The goals of this thesis were to investigate the efficacy of three established anti-amyloid agents to counteract amyloid-mediated enhancement of HIV infection. First, I set out to study the utility of Hsp104, a protein-remodeling machine from *Saccharomyces cerevisiae*. Here, we show that Hsp104 remodels SEVI and PAP85-120 fibrils, the engineered HAP-ClpP proteolytic system optimizes amyloid clearance, and enzymatically inactive Hsp104 scaffolds cluster fibrils into larger conglomerates. Importantly, each effect resulted in a reduction in amyloid-mediated HIV infectivity enhancement. Secondly, we analyzed the lysine-specific “molecular tweezer” CLR01, which was previously shown to interfere with the aggregation of numerous amyloidogenic proteins. We found that CLR01 interferes with the amyloidogenesis of seminal amyloid, partially dissolves pre-formed SEVI and PAP85-120 fibrils, and directly inhibits infection of multiple enveloped viruses, including HIV. Through a combination of these anti-amyloid and anti-viral effects, CLR01 antagonizes the infection-enhancing properties of both seminal amyloid and human semen. Finally, epigallocatechin gallate (EGCG), the principal polyphenol in green tea, has broad-spectrum anti-amyloidogenic properties. Here, we describe EGCG as the first agent to eradicate all four classes of seminal amyloid (SEVI, PAP85-120, SEM1, and SEM2). This, in combination with its well-studied anti-viral properties, makes EGCG a promising microbicide candidate.

## **CHAPTER 2: REPURPOSING HSP104 TO ANTAGONIZE SEMINAL AMYLOID AND COUNTER HIV INFECTION**

### **2.1 Introduction**

Human immunodeficiency virus (HIV) is a global epidemic that has claimed the lives of nearly 30 million people since its discovery [6]. The HIV pandemic is most severe in the developing world. In Sub-Saharan Africa, ~5% of the adult population is infected with the virus [169]. Nearly 80% of HIV infections are acquired through heterosexual transmission [7, 170, 171], and endogenous peptides in semen play a critical role in the spread of this retrovirus [51, 172, 173].

Naturally occurring fragments of proteins abundant in semen form amyloid fibrils [68], and the unique composition of semen drives the fibrillization process [174]. Specifically, proteolytic fragments of prostatic acid phosphatase (PAP248-286 (SEVI) and PAP85-120), semenogelin 1 (SEM1), and semenogelin 2 (SEM2) form fibrils that enhance HIV infectivity by several orders of magnitude under conditions of limiting viral inoculum, whereas the soluble, non-amyloid peptides have no effect [51, 172, 173]. Semen-derived fibrils are highly basic and contain a large proportion of lysine and arginine residues. These charged fibrils promote HIV infection by neutralizing the inherent electrostatic repulsion between the negatively charged surfaces of HIV virions and target cells, and through direct binding to virions, fibrils simultaneously promote viral binding to the cell surface [175]. Amyloid fibrils are implicated in the pathogenesis of numerous neurodegenerative and systemic diseases [28, 176, 177], and they are notoriously difficult to clear due to their self-templating character and extraordinary stability, which lies at the extremes of protein-based structures [178]. Nonetheless, deciphering a method to eliminate semen-derived fibrils could massively reduce viral transmission [179]. This approach could be advantageous as it targets host-encoded viral-enhancing factors rather than the viral machinery itself. However, because of the plethora of different polypeptides that form fibrils in semen and promote viral

infection, we explored remodeling factors with activity against amyloids formed by diverse proteins, rather than agents with specialized activity against any single peptide [48, 179].

With this design principle in mind, we turned to Hsp104, an amyloid-remodeling factor and protein disaggregase from yeast, which belongs to the AAA+ family of proteins (ATPases associated with various cellular activities) [103, 180]. In addition to resolving and renaturing amorphous protein aggregates generated following thermal or chemical stress [122, 125], Hsp104 also catalytically deconstructs amyloid fibrils formed by a variety of polypeptides [127, 128, 181-184]. Hsp104 is a generalist and has been optimized during evolution to remodel diverse prion conformers and remodel a large proportion of the yeast proteome in response to environmental stress [147, 185]. Despite being highly conserved in eubacteria and eukaryotes, Hsp104 homologues are surprisingly absent in metazoa [103]. However, Hsp104 has previously been utilized in metazoan systems to counteract disease-associated protein aggregates and amyloid fibrils [103, 128, 146, 150, 183, 186-188].

Here, we exploit the broad spectrum, amyloid-remodeling activity of Hsp104 to antagonize semen-derived amyloid fibrils as a means to reduce HIV transmission. We devise three strategies to antagonize seminal amyloid based on Hsp104. First, we describe that Hsp104 and a potentiated Hsp104 variant, Hsp104<sup>A503V</sup> [183], efficaciously remodel SEVI and PAP85-120 fibrils into non-amyloid forms. Second, we elucidate catalytically inactive Hsp104 scaffolds that do not remodel amyloid structure, but cluster SEVI, PAP85-120, and SEM1 fibrils into larger assemblies. Third, we modify Hsp104 to interact with the chambered protease ClpP [142], which enables the coupled remodeling and degradation of SEVI and PAP85-120 fibrils. Each strategy diminishes the ability of seminal amyloid to promote HIV infection and could have therapeutic utility. Altogether, our findings provide insight into developing agents that can abolish the infection-enhancing capabilities of seminal amyloid and complement microbicidal approaches.

## 2.2 Results

### 2.2.1 Hsp104 remodels SEVI amyloid fibrils

To begin, we tested Hsp104 for its ability to remodel SEVI amyloid fibrils. We assessed fibril disassembly using the amyloid-binding dye Thioflavin-T (ThT) and by transmission electron microscopy (TEM). Incubation of SEVI fibrils with a substoichiometric concentration of Hsp104 (PAP248-286:Hsp104 of 6.67:1) reduced ThT fluorescence intensity to ~37% of the initial value after 2h, and a further decrease to ~27% was observed after 6h of treatment (Figure 2.1a). The only other agent known to remodel SEVI fibrils is the green tea polyphenol, epigallocatechin-3-gallate, which slowly eradicates SEVI fibrils over the course of 24-48h [108]. Thus, Hsp104 remodels SEVI fibrils more rapidly than any other factor identified to date. The ThT fluorescence intensity plateaued after 6h, indicating that under these conditions amyloid fibrils cannot reform rapidly after Hsp104-mediated remodeling. TEM revealed that the products of Hsp104 remodeling were structures resembling amorphous protein aggregates (Figure 2.1b). After 2h, SEVI fibrils were completely converted into these non-amyloid aggregates by Hsp104, and no further alteration in morphology was observed after a longer 24h treatment. Dose-response analysis of Hsp104 disassembly of SEVI fibrils indicates a half maximal effective concentration ( $EC_{50}$ ) value of ~0.72 $\mu$ M, suggesting that Hsp104 is an efficacious SEVI-remodeling factor (Figure 2.1c).

We obtained a similar result when SEVI fibrils were incubated with Hsp104 plus Hsp70 and Hsp40. Hsp70 and Hsp40 are usually required for the disaggregation of amorphous protein aggregates by Hsp104 [125], whereas amyloid remodeling by Hsp104 does not always necessitate Hsp70 and Hsp40 [182]. However, in some instances Hsp104 mediated disassembly of amyloid can be enhanced by Hsp70 and Hsp40 [128, 182, 189, 190]. Hsp70 and Hsp40 alone had no effect on SEVI fibrils (Figure 2.1d). By contrast, the ThT fluorescence intensity of SEVI fibrils incubated with Hsp104, Hsp70, and Hsp40 decreased to ~36% of the initial value after 2h, and a larger reduction to ~16% was observed after 24h (Figure 2.1d). Thus, there is a slight



enhancement in disaggregation in the presence of Hsp70 and Hsp40, particularly after extended incubation times.

Next, we explored the effects of inactive Hsp104 variants on SEVI fibril integrity. Hsp104<sup>DWB</sup> is an ATPase deficient Hsp104 variant that contains E285Q and E687Q substitutions at Walker B sites that are critical for ATP hydrolysis [133]. Hsp104<sup>DWB</sup> can bind but not hydrolyze ATP, which renders the protein inactive in amyloid remodeling and disaggregation [182]. Hsp104<sup>DWB</sup> is also a “trap” mutant, which binds to substrates without releasing them [133]. SEVI fibrils incubated with Hsp104<sup>DWB</sup> for 24h exhibited no change in ThT fluorescence (Figure 2.1a). Hsp104<sup>DWB</sup> had no effect on fibril integrity (Figure 2.1e). Thus, Hsp104 actively remodels SEVI amyloid fibrils through cycles of ATP binding and hydrolysis and not merely through passive binding events.

Next, we tested the efficacy of ClpB, the *E. coli* homologue of Hsp104, which can renature and remodel amorphous protein aggregates but has limited ability to disassemble amyloid fibrils due to differences in inter-subunit collaboration [181, 182, 191]. ClpB did not reduce ThT fluorescence intensity when incubated with SEVI fibrils (Figure 2.1a). TEM confirmed that intact SEVI amyloid fibrils were still present after incubation with ClpB (Figure 2.1e). Thus, ClpB is unable to remodel SEVI fibrils.

To determine whether Hsp104 dissolved SEVI fibrils, we passaged reactions through a 10-kDa filter. The resulting filtrate and retentate were analyzed by SDS-PAGE. Because the PAP248-286 peptide is ~4.5kDa, only PAP248-286 monomers and dimers pass through the filter while any larger aggregates and fibrillar species are retained. Hsp104-remodeled SEVI products were predominately retained by the filter, suggesting that Hsp104 does not dissolve SEVI fibrils into PAP248-286 monomers (Figure 2.1f). Rather, as suggested by TEM (Figure 2.1b), the products are likely larger non-fibrillar aggregates. Thus, Hsp104 does not dissolve SEVI fibrils unlike several other amyloids [182]. Hsp104 has reduced ability to dissolve specific Sup35 prions

strains, but instead converts them to a mixture of soluble protein and non-templating aggregated forms [184, 189]. Hsp104 transforms SEVI fibrils into another aggregated form, which likely lacks cross- $\beta$  structure as indicated by reduced ThT fluorescence (Figure 2.1a), but can these aggregated species template the assembly of SEVI fibrils?

To assess whether Hsp104 eliminated the self-templating activity of SEVI fibrils we tested the ability of Hsp104-remodeled SEVI products to seed fibrillization of PAP248-286. Assembly of PAP248-286 into SEVI fibrils can be accelerated by the addition of a small amount of pre-formed SEVI fibril seed, which eliminates the lag phase for nucleation [192]. In the presence of 0.1% untreated SEVI fibril seed, the lag phase for assembly was abolished, and monomeric PAP248-286 polymerized into fibrils, with ThT fluorescence intensity plateauing around 24h (Figure 2.1g). At this time, unseeded reactions remained in lag phase (Figure 2.1g). Importantly, SEVI fibrils pre-treated with Hsp104 for 6h were no longer capable of seeding PAP248-286 fibrillization (Figure 2.1g). Thus, Hsp104 converts SEVI fibrils into altered non-amyloid conformers that lack seeding activity.

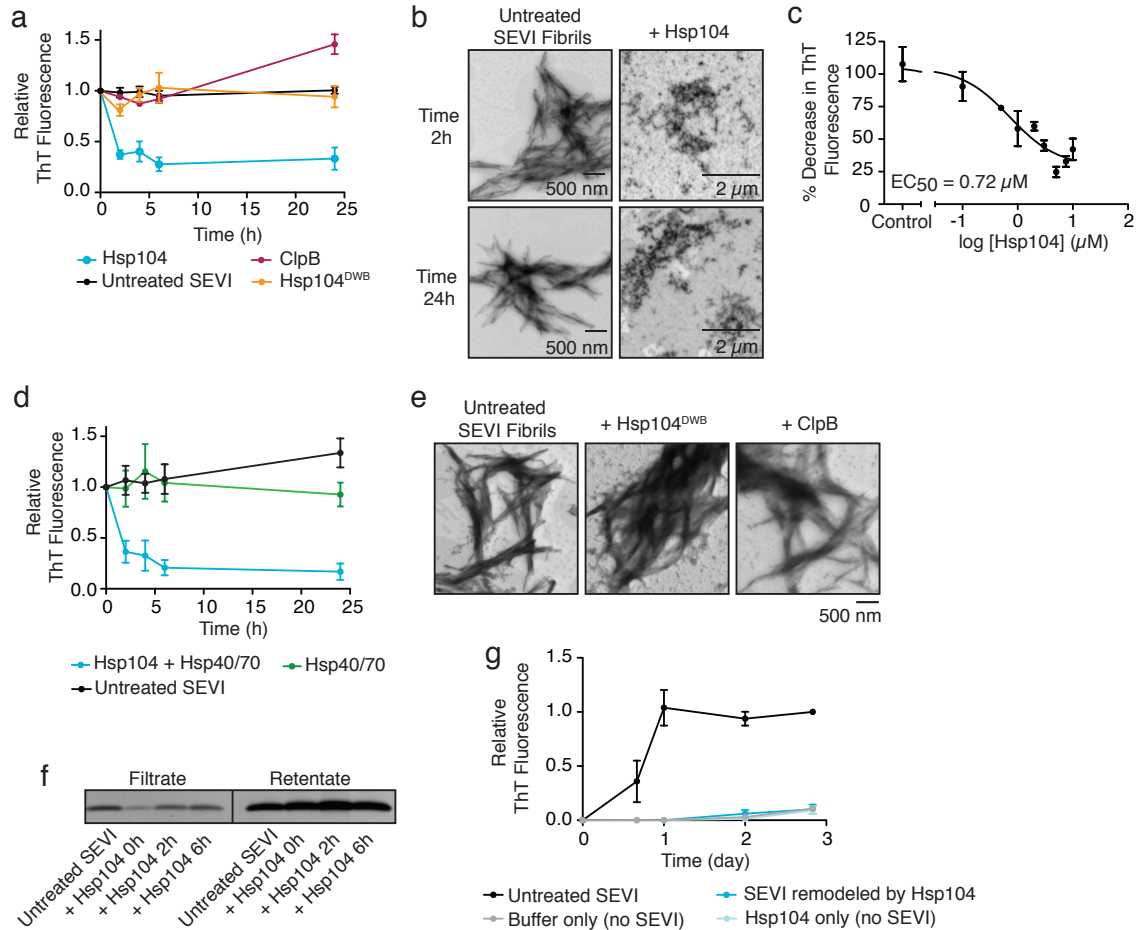


**Figure 2.1 Hsp104 rapidly remodels SEVI fibrils to non-templating forms.** (a) Preformed SEVI fibrils (20μM monomer) were incubated with buffer (untreated), Hsp104 (3μM), Hsp104<sup>DWB</sup> (3μM) or ClpB (3μM; DnaK (3μM), DnaJ (0.6μM), and GrpE (0.3μM)) for 0-24h. Fibril integrity was assessed via ThT fluorescence. Values represent means ± SEM (n=3-4). (b) TEM of SEVI fibrils incubated with buffer (untreated) or Hsp104 (3μM) for either 2h or 24h. The scale bar is indicated. (c) Dose-response analysis of SEVI fibrils (20μM monomer) treated with various concentrations of Hsp104 for 6h. Fibril integrity was assessed via ThT fluorescence and the EC<sub>50</sub> was calculated. Values represent means ± SEM (n=3). (d) Preformed SEVI fibrils (20μM monomer) were incubated with buffer (untreated) or the indicated combinations of Hsp104 (3μM), Hsp70 (1μM) and Hsp40 (1μM). Fibril integrity was assessed via ThT fluorescence. Values represent means ± SEM (n=4). (e) TEM of SEVI fibrils incubated with buffer (untreated), Hsp104<sup>DWB</sup>, or ClpB (3μM) for 3h. The scale bar is indicated. (f) Preformed SEVI fibrils (20μM monomer) were incubated with buffer (untreated) or Hsp104 (3μM) for 0-6h. The resulting products were passed over a 10-kDa molecular weight cut off filter. Filtrate and retentate fractions were then processed for SDS-PAGE and silver stain. (g) SEVI fibrils (20μM monomer) were incubated with buffer (untreated) or Hsp104 (3μM) for 6h, and the resulting products were used to seed soluble PAP248-286 (1mM, 0.1% fibril seed) fibrillization. Buffer conditions lacking fibril seed were included. Fibril assembly was monitored by ThT fluorescence. Values represent means ± SEM (n=4).

### 2.2.2 A potentiated Hsp104 variant remodels SEVI at nanomolar concentrations

Next, we assessed whether a potentiated Hsp104 variant had improved ability to disassemble SEVI fibrils. A missense mutation in the coiled-coil middle domain region of Hsp104, Hsp104<sup>A503V</sup>, yields a potentiated variant with elevated basal ATPase activity, an accelerated substrate translocation rate, and enhanced disaggregase activity [183]. Hsp104<sup>A503V</sup> also suppresses TDP-43 and  $\alpha$ -synuclein proteotoxicity by dissolution of protein aggregates and restoration of proper protein localization [183].

When tested against SEVI fibrils in vitro, Hsp104<sup>A503V</sup> caused a reduction in ThT fluorescence that was of similar magnitude to that observed with Hsp104 (Figure 2.1a, 2.2a). After 2h of incubation with Hsp104<sup>A503V</sup>, ThT fluorescence intensity decreased to ~49% of the initial value, with a further decrease to ~35% after 24h (Figure 2.2a). TEM revealed that non-fibrillar aggregates accumulated after Hsp104<sup>A503V</sup> treatment, comparable to those observed after incubation with Hsp104 (Figure 2.2b). Indeed, Hsp104<sup>A503V</sup> did not dissolve SEVI fibrils as a 10-kDa filter retained remodeled products (Figure 2.2c). Remarkably, dose-response studies of Hsp104<sup>A503V</sup>-catalyzed remodeling of SEVI fibrils established an EC<sub>50</sub> of only ~36nM (Figure 2.2d), which is ~20-fold lower than the EC<sub>50</sub> determined for Hsp104 (Figure 2.1c). This nanomolar EC<sub>50</sub> for SEVI remodeling by Hsp104<sup>A503V</sup> is unprecedented and could have therapeutic potential.

### 2.2.3 Hyperactive ClpB variants are unable to eliminate SEVI fibrils

Next, we assessed whether ClpB activity might also be enhanced against SEVI fibrils by specific mutations in the middle domain that enhance ClpB activity against disordered protein aggregates [193]. Thus, we assessed the activity of three hyperactive ClpB variants: ClpB<sup>R356C</sup>, ClpB<sup>K476C</sup>, and ClpB<sup>Y503D</sup> [193]. Remarkably, none of the hyperactive ClpB variants reduced ThT fluorescence of SEVI fibrils in the presence or absence of the Hsp70 chaperone system: DnaK, DnaJ, and GrpE (Figure 2e). In fact, in the absence of DnaK, DnaJ, and GrpE, ClpB and the hyperactive variants increased ThT fluorescence of SEVI fibrils (Figure 2.2e), which might

indicate a ClpB activity that exposes further ThT binding sites on SEVI fibrils. DnaK, DnaJ, and GrpE had no effect on SEVI fibrils alone and prevented the increase in ThT fluorescence caused by ClpB or ClpB<sup>Y503D</sup>, but not ClpB<sup>R356C</sup> or ClpB<sup>K476C</sup> (Figure 2.2e). Thus, ClpB is unable to eliminate amyloid structure even when its activity is enhanced by hyperactivating mutations in the middle domain. This finding likely reflects profound differences in how Hsp104 and ClpB subunits process substrates for disaggregation [182].

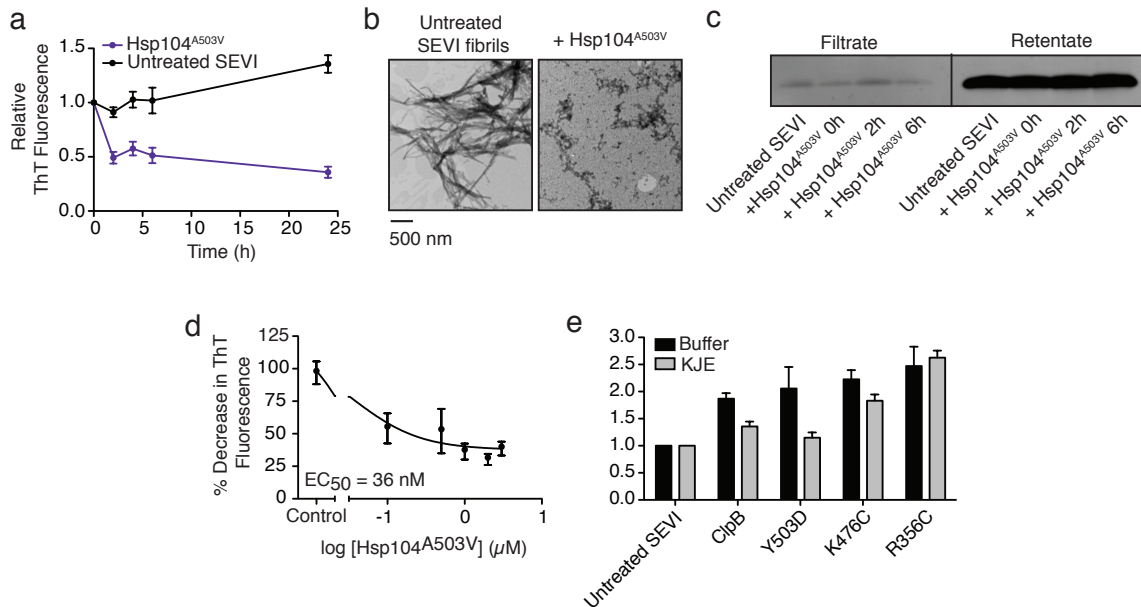


**Figure 2.2 Hsp104<sup>A503V</sup> rapidly remodels SEVI fibrils, whereas hyperactive ClpB variants are inactive.** (a) Preformed SEVI fibrils (20μM monomer) were incubated with buffer (untreated) or Hsp104<sup>A503V</sup> (3μM) for 0-24h and fibril integrity was assessed by ThT fluorescence. Values represent means ± SEM (n=4). (b) TEM of SEVI fibrils incubated with buffer (untreated) or Hsp104<sup>A503V</sup> (3μM) for 3h. The scale bar is indicated. (c) SEVI fibrils (20μM monomer) were incubated with Hsp104<sup>A503V</sup> (3μM) for 0-6h, and the resulting products were then passed over a 10kDa molecular weight cut off filter. Filtrate and retentate fractions were then processed for SDS-PAGE and silver stain. (d) Dose-response analysis of Hsp104<sup>A503V</sup> disassembly of SEVI fibrils (20μM monomer) after 6h of treatment. The EC<sub>50</sub> is based on ThT fluorescence. Values represent means ± SEM (n=6). (e) Preformed SEVI fibrils (20μM monomer) were incubated with buffer (untreated) or the indicated ClpB variant (3μM) in the absence (black bars) or presence (grey bars) of DnaK (3μM), DnaJ (0.6μM), and GrpE (0.3μM) for 6h and fibril integrity was assessed by ThT fluorescence. Values represent means ± SEM (n=3-4). (Work of Stephen Bart, Shorter lab)

#### **2.2.4 Hsp104 and Hsp104<sup>A503V</sup> remodel PAP85-120 fibrils**

The relative contribution of each seminal amyloid to the observed enhancement of HIV infection by human semen is uncertain, and thus, it is important to search for amyloid-remodeling factors that can deconstruct a range of substrates [179]. Thus, we examined whether Hsp104 and Hsp104<sup>A503V</sup> could remodel additional amyloid fibrils endogenous to seminal fluid, including those formed by another PAP fragment, PAP85-120 [172, 179]. Hsp104 remodeled PAP85-120 fibrils, whereas ClpB and Hsp104<sup>DWB</sup> were inactive (Figure 2.3a). After 2h, Hsp104 reduced ThT fluorescence to ~63% of the initial value, and a further decrease to ~39% was observed after 6h, indicating rapid fibril remodeling (Figure 2.3a). TEM revealed that Hsp104 remodels PAP85-120 fibrils into non-fibrillar aggregates (Figure 2.3b). Similar results were obtained with Hsp104<sup>A503V</sup>. Under these conditions, the ThT fluorescence intensity decreased more slowly than with Hsp104, and a reduction to only 67% was observed after 2h (Figure 2.3c). However, after 24h of incubation with Hsp104<sup>A503V</sup>, the ThT fluorescence intensity decreased markedly to ~28% of the initial value (Figure 2.3c). TEM analysis also revealed non-amyloid aggregates after treatment with Hsp104<sup>A503V</sup> (Figure 2.3d). Thus, Hsp104 and Hsp104<sup>A503V</sup> can rapidly remodel SEVI and PAP85-120 fibrils.

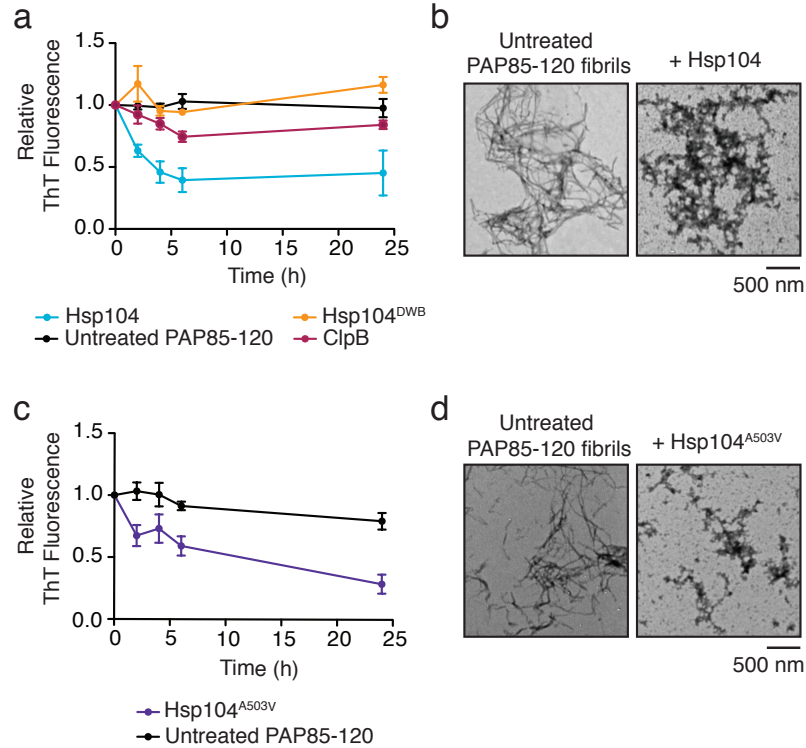


**Figure 2.3 Hsp104 and Hsp104<sup>A503V</sup> rapidly remodel PAP85- fibrils.** (a) Preformed PAP85-120 fibrils (20 $\mu$ M monomer) were incubated with buffer (untreated), Hsp104, Hsp104<sup>DWB</sup>, or ClpB (3 $\mu$ M) for 0-24h. Fibril integrity was assessed via ThT fluorescence. Values represent means  $\pm$  SEM (n=3-7). (b) TEM of PAP85-120 fibrils incubated with buffer (untreated) or Hsp104 (3 $\mu$ M) for 6h. The scale bar is indicated. (c) Preformed PAP85-120 fibrils (20 $\mu$ M monomer) were incubated with buffer (untreated) or Hsp104<sup>A503V</sup> (3 $\mu$ M) for 0-24h. Fibril integrity was assessed via ThT fluorescence. Values represent means  $\pm$  SEM (n=4). (d) TEM of PAP85-120 fibrils incubated with buffer (untreated) or Hsp104<sup>A503V</sup> (3 $\mu$ M) for 6h. The scale bar is indicated.

### 2.2.5 Hsp104 and Hsp104<sup>A503V</sup> do not remodel SEM1(45-107) fibrils

Numerous peptide fragments of SEM1 and SEM2 can assemble into amyloid and enhance HIV infection [173]. We focused on the SEM1(45-107) fragment as a representative sample. ThT fluorescence intensity remained unchanged when SEM1(45-107) fibrils were treated with Hsp104 or Hsp104<sup>A503V</sup> for 24h (Figure 2.4a, 2.4c). This result was verified by TEM, which showed abundant, dense clumps of SEM1(45-107) fibrils in samples incubated with Hsp104 or Hsp104<sup>A503V</sup> (Figure 2.4b, 2.4d). Thus, SEM1(45-107) fibrils are refractory to remodeling by

Hsp104 and Hsp104<sup>A503V</sup>, indicating that some feature of SEM1(45-107) fibrils antagonizes Hsp104 activity.

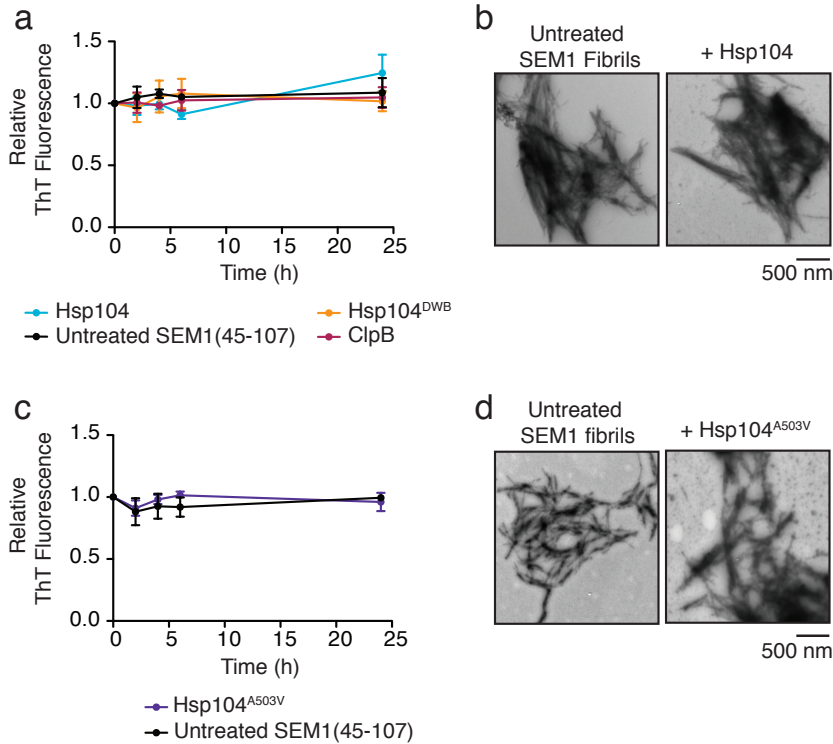


**Figure 2.4 Hsp104 and Hsp104<sup>A503V</sup> do not remodel SEM1(45-107) fibrils.** (a) Preformed SEM1(45-107) fibrils (20 $\mu$ M monomer) were incubated with buffer (untreated), Hsp104, Hsp104<sup>DWB</sup> or ClpB (3 $\mu$ M) for 0-24h. Fibril integrity was assessed via ThT fluorescence. Values represent means  $\pm$  SEM (n=3). (b) TEM of SEM1(45-107) fibrils incubated with buffer (untreated) or Hsp104 (3 $\mu$ M) for 6h. The scale bar is indicated. (c) Preformed SEM1(45-107) fibrils (20 $\mu$ M monomer) were incubated with buffer (untreated) or Hsp104<sup>A503V</sup> (3 $\mu$ M) for 0-24h. Fibril integrity was assessed via ThT fluorescence. Values represent means  $\pm$  SEM (n=3). (d) TEM of SEM1(45-107) fibrils incubated with buffer (untreated) or Hsp104<sup>A503V</sup> (3 $\mu$ M) for 6h. The scale bar is indicated.

### 2.2.6 Hsp104 promotes clustering of seminal amyloid into larger aggregates

We noticed that even though Hsp104<sup>DWB</sup> and ClpB failed to eliminate cross- $\beta$  structure of seminal amyloid as indicated by ThT fluorescence (Figure 2.1a, 2.3a, 2.4a), solutions became turbid, indicating a clustering of fibrils into higher order conglomerates. Sequestration of seminal amyloid into larger aggregated structures could be a valuable strategy, as it would shield the network of



positive charge presented by fibrils and reduce their ability to stimulate HIV infection. Indeed, molecular chaperones stimulate the clustering of toxic misfolded oligomers into larger species in the absence of any structural reorganization or disassembly of oligomers [194]. The larger aggregated species mask the reactive surfaces of oligomers and decrease their diffusional mobility, thereby neutralizing oligomer toxicity [194]. Importantly, this mechanism is extremely effective, as significant effects are observed at highly substoichiometric chaperone levels [194]. Moreover, several chaperones do not require ATP or ATPase activity to cluster oligomers [194]. By analogy, we wondered whether Hsp104-based scaffolds might cluster seminal amyloid into larger aggregates in an ATP-independent manner and neutralize their ability to promote HIV infection.

To assess formation of larger aggregates we employed turbidity (absorbance at 395nm). GFP was included as a protein control and did not affect the turbidity of any of the seminal amyloid fibrils analyzed (Figure 2.5a-c). By contrast, the turbidity of SEVI, PAP85-120, and SEM1(45-107) fibrils increased rapidly upon incubation with Hsp104, Hsp104<sup>DWB</sup>, or ClpB (Figure 2.5a-f). Thus, Hsp104 remodels the amyloid structure of SEVI and PAP85-120 fibrils (Figure 2.1a, 2.3a) and simultaneously transforms these conformers into large amorphous aggregates (Figure 2.1b, 2.3b, 2.5a, 2.5b). By contrast, Hsp104 does not remodel SEM1(45-107) fibrils but clusters them into large aggregates (Figure 2.4a, 2.5c). Hsp104<sup>DWB</sup> and ClpB fail to remodel the amyloid structure of SEVI, PAP85-120, and SEM1(45-107) fibrils (Figure 2.1a, 2.3a, 2.4a), but cluster them into larger species (Figure 2.5a-f). In all instances, a marginally larger increase in turbidity was observed when seminal amyloid fibrils were incubated with Hsp104<sup>DWB</sup> as compared to Hsp104 (Figure 2.5a-c). Thus, the seminal amyloid clustering activity does not require ATP hydrolysis and resembles the clustering of toxic oligomers into larger aggregates by various molecular chaperones [194].

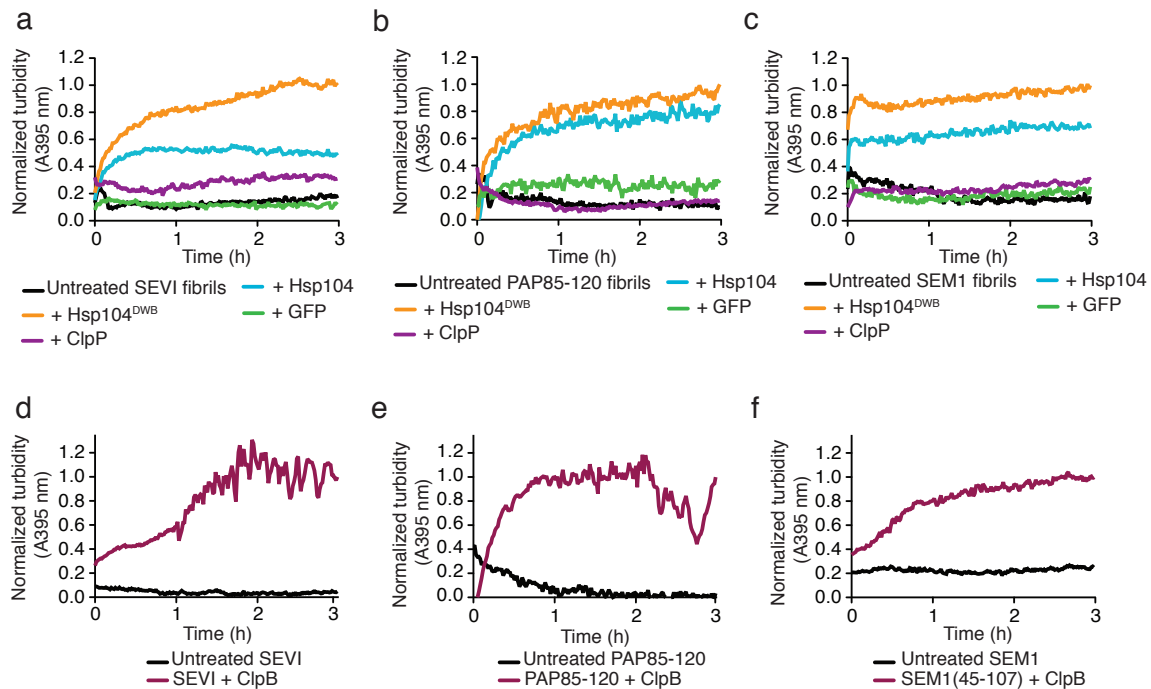


**Figure 2.5 Hsp104 and ClpB promote the clustering of seminal amyloid fibrils into larger aggregates.** (a-c) SEVI (a), PAP85-120 (b), and SEM1(45-107) (c) fibrils (20 $\mu$ M monomer) were incubated with buffer (untreated), Hsp104, Hsp104<sup>DWB</sup>, ClpP, or GFP (1.8 $\mu$ M monomer) and absorbance at 395nm was measured continuously for 3h. One representative trial is shown. (d-f) SEVI (d), PAP85-120 (e), and SEM1(45-107) (f) fibrils (20 $\mu$ M monomer) were incubated with buffer (untreated) or ClpB (1.8 $\mu$ M monomer) and absorbance at 395nm was measured continuously for 3h. One representative trial is shown.

To confirm this clustering effect, dynamic light scattering (DLS) was used to investigate the size distribution profile of seminal amyloid in the absence and presence of Hsp104, Hsp104<sup>DWB</sup>, or GFP. DLS of Hsp104 alone revealed species with a diffusion coefficient of  $\sim 2.7 \times 10^{-7} \text{ cm}^2/\text{s}$  and hydrodynamic radius ( $R_h$ ) of  $\sim 7\text{-}10\text{ nm}$  (Figure 2.6a), indicative of a hexamer and consistent with previous studies [133, 195]. The soluble PAP248-286 peptide had an  $R_h$  of  $\sim 1\text{-}2\text{ nm}$  (Figure 2.6b), which might indicate dimeric or trimeric forms or an extended, unstructured monomer [46]. By contrast, untreated SEVI fibrils contained an assortment of species with different  $R_h$  values (Figure 2.6c). The major species had  $R_h$ 's of  $\sim 1,000\text{-}3,000\text{ nm}$  (Figure 2.6c). The DLS profile shifted drastically upon addition of Hsp104 or Hsp104<sup>DWB</sup>, revealing a broad size distribution of larger particles ranging in  $R_h$  of  $\sim 100\text{-}10,000\text{ nm}$  (Figure 2.6d, 2.6e). In contrast, when SEVI fibrils

were incubated with GFP, the size distribution profile closely resembled the buffer (untreated) control (Figure 2.6f). Similarly, in the presence of Hsp104 and Hsp104<sup>DWB</sup>, the size distribution profile of SEM1(45-107) fibrils shifted toward larger species (Figure 2.6g-j). Indeed, aggregated species were now observed with  $R_n$  greater than 5,000nm (Figure 2.6h, 2.6i), which are not observed in the buffer (untreated) control (Figure 2.6g). Contrastingly, the particle sizes of SEM1(45-107) fibrils treated with GFP were more similar to the buffer (untreated) control (Figure 2.6j). These data suggest that Hsp104 and Hsp104<sup>DWB</sup> cluster PAP248-286 and SEM1(45-107) into larger aggregated species.

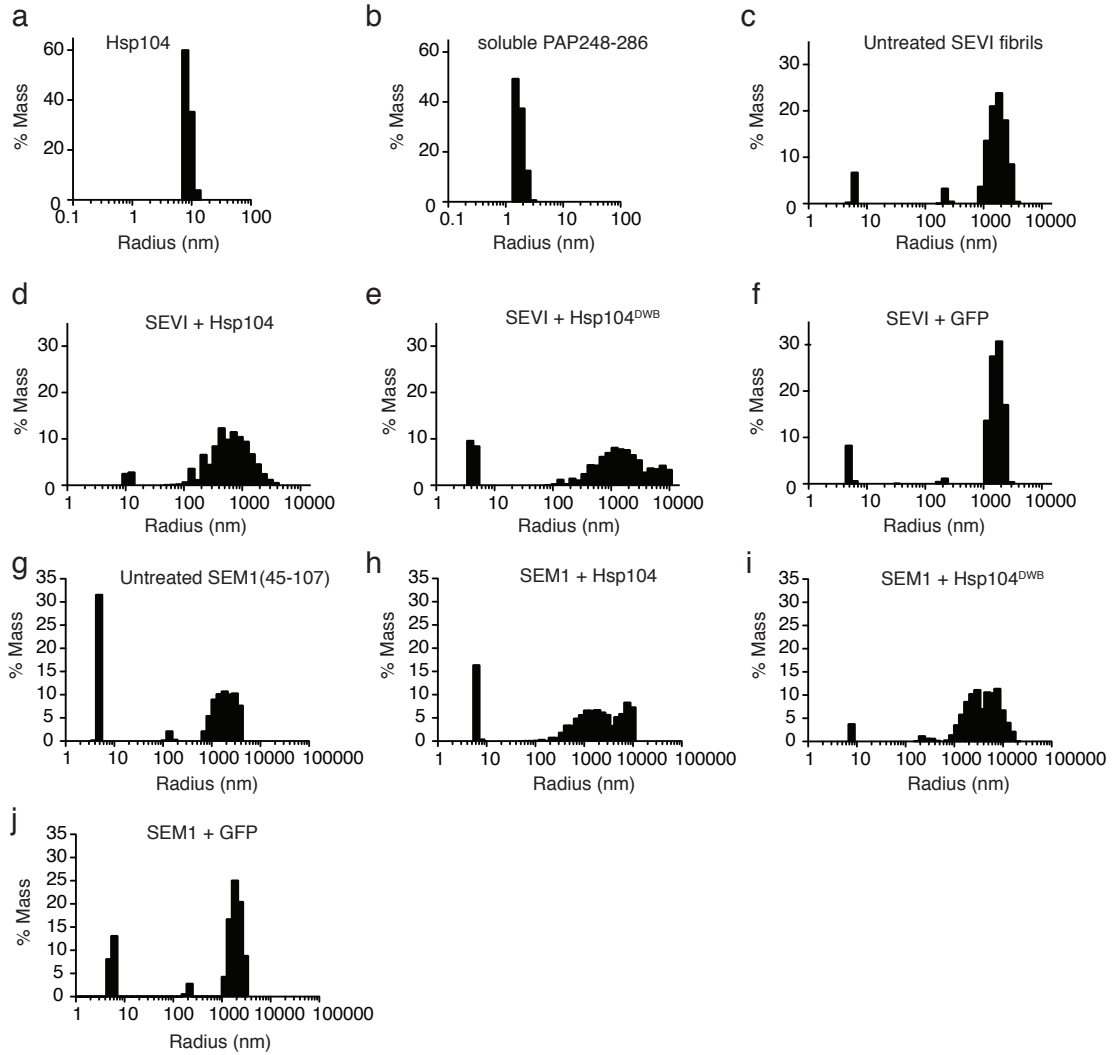


**Figure 2.6 Hsp104 stimulates the assembly of SEVI and SEM1(45-107) fibrils into larger particles.** (a,b) Dynamic light scattering was used to determine the hydrodynamic radius ( $R_h$ ) of Hsp104 (0.3 $\mu$ M hexamer) (a) and soluble PAP248-286 (20 $\mu$ M) (b). (c-f) Dynamic light scattering was used to determine the size distribution by mass of SEVI fibrils (20 $\mu$ M monomer) treated with buffer (c), Hsp104 (d), Hsp104<sup>DWB</sup> (e), or GFP (f) (1.8 $\mu$ M monomer) for ~5min at 25°C. (g-j) Dynamic light scattering was used to determine the size distribution by mass of SEM1(45-107) fibrils (20 $\mu$ M monomer) treated with buffer (g), Hsp104 (h), Hsp104<sup>DWB</sup> (i), or GFP (j) (1.8 $\mu$ M monomer) for ~5min at 25°C.

Next, we tested whether Hsp104 hexamers or ATP were required for the observed clustering activity. Thus, we explored two monomeric Hsp104 fragments: Hsp104<sup>1-548</sup>, comprising the N-terminal domain (NTD), nucleotide-binding domain 1 (NBD1), and middle domain (MD) of

Hsp104; and Hsp104<sup>773-908</sup> comprising the small domain of NBD2 and the C-terminal domain of Hsp104, which can engage basic substrates such as poly-lysine [138, 196]. Remarkably, incubation of SEVI, PAP85-120, and SEM1(45-107) fibrils with Hsp104<sup>1-548</sup> but not Hsp104<sup>773-908</sup> resulted in a substantial increase in turbidity (Figure 2.7a-c). Importantly, neither Hsp104<sup>1-548</sup> nor Hsp104<sup>773-908</sup> remodeled SEVI or PAP85 fibrils as indicated by ThT fluorescence (data not shown). Thus, neither Hsp104 hexamerization nor ATP hydrolysis is necessary for clustering activity. The clustering of seminal amyloid into larger conglomerates likely decreases availability of virion binding sites on fibrils via occlusion.

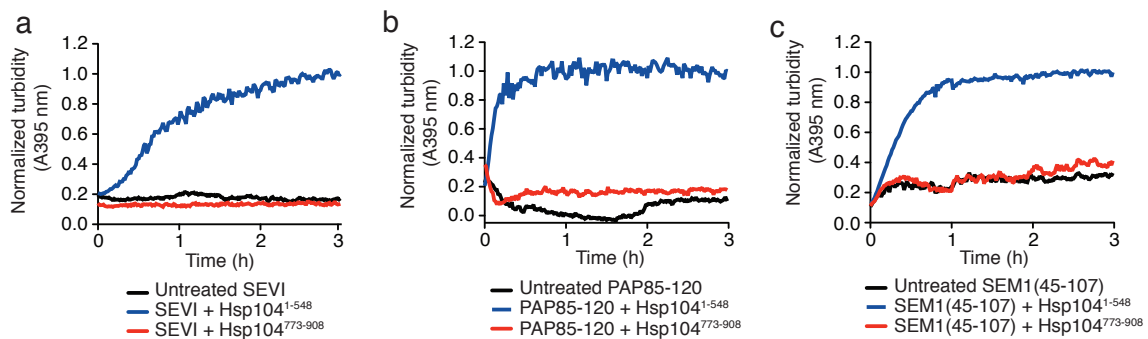


**Figure 2.7 Monomeric Hsp104<sup>1-548</sup> promotes the clustering of seminal amyloid fibrils (a-c)** SEVI (a), PAP85-120 (b), and SEM1(45-107) (c) fibrils (20 $\mu$ M monomer) were incubated with buffer (untreated), Hsp104<sup>1-548</sup>, or Hsp104<sup>773-908</sup> (1.8 $\mu$ M monomer) and absorbance at 395nm was measured continuously for 3h. One representative trial is shown.

### 2.2.7 HAP plus ClpP degrade SEVI fibrils and PAP85-120 fibrils

A potential problem with the seminal amyloid-remodeling activity of Hsp104 (Figure 2.1-2.3) is that peptides might eventually reform amyloid and promote HIV infection. Likewise, the clustering of seminal amyloid into larger aggregates by various Hsp104 scaffolds (Figure 2.5, 2.6) might also be reversed and enable fibrils to promote HIV infection. To irrevocably remove seminal amyloid, we coupled Hsp104 remodeling activity to proteolysis. Thus, we employed HAP, an Hsp104 variant carrying three missense mutations (G739I:S740G:K741F) in a critical helix-loop-helix motif that enables association with ClpP, a chambered peptidase from *E. coli* akin to the proteasome [142]. HAP maintains disaggregase activity and substrate recognition but threads

remodeled products through its central pore and into the proteolytic chamber of ClpP for degradation [142].

Like Hsp104 (Figure 2.1a), HAP or HAP plus ClpP effectively remodeled SEVI fibrils, whereas ClpP alone was ineffective (Figure 2.8a). After 24h, HAP or HAP plus ClpP reduced ThT fluorescence to ~22% (Figure 2.8a). Importantly, this large decrease in ThT fluorescence intensity occurred when SEVI fibrils were subjected to substoichiometric concentrations of HAP or HAP plus ClpP. In fact, the  $EC_{50}$  for SEVI fibril remodeling by HAP was ~0.36 $\mu$ M (Figure 2.8b), and a slightly higher  $EC_{50}$  of ~1.28  $\mu$ M was determined for HAP plus ClpP (Figure 2.8c), indicating that the presence of ClpP reduces HAP efficacy [141].

TEM revealed that HAP or HAP plus ClpP converted SEVI fibrils to amorphous aggregates, similar to those observed with Hsp104, whereas ClpP alone was ineffective (Figure 2.8d). The extreme stability of the amyloid cross- $\beta$  fold allows amyloid to resist disruption from proteases and other protein denaturants [147]. Thus, as expected, ClpP alone was unable to degrade SEVI fibrils (Figure 2.8e), although curiously it was able to rapidly degrade soluble PAP248-286 in the presence or absence of HAP (Figure 2.8e). Usually, ClpP alone cannot degrade folded proteins without a cognate AAA+ ATPase partner [143, 197]. Indeed, only small peptides typically shorter than 6 residues are able to enter the ClpP chamber for degradation [198]. Thus, soluble PAP248-286 is likely to be unfolded and must effectively access the proteolytic chamber of ClpP. Importantly, HAP plus ClpP degraded SEVI fibrils over the course of 24h (Figure 2.8e). Accordingly, HAP plus ClpP eliminated the ability of SEVI fibrils to seed the fibrillization of soluble PAP248-286, confirming a deconstruction of amyloid structure (Figure 2.8f). To the best of our knowledge, this is the first example of a proteolytic system that can effectively remodel and degrade amyloid.

We next examined whether SEM1(45-107) fibrils and PAP85-120 fibrils could be degraded using HAP plus ClpP. HAP plus ClpP rapidly degraded the soluble SEM1(45-107) and PAP85-120 peptides, whereas ClpP alone was ineffective (Figure 2.8g, 2.8h). HAP plus ClpP were unable to degrade SEM1(45-107) fibrils (Figure 2.8g), which is consistent with the inability of Hsp104 to remodel SEM1(45-107) fibrils (Figure 2.4a). By contrast, HAP plus ClpP degraded PAP85-120 fibrils, whereas ClpP alone was ineffective (Figure 2.8h). Thus, HAP plus ClpP degrade preformed SEVI and PAP85-120 fibrils.

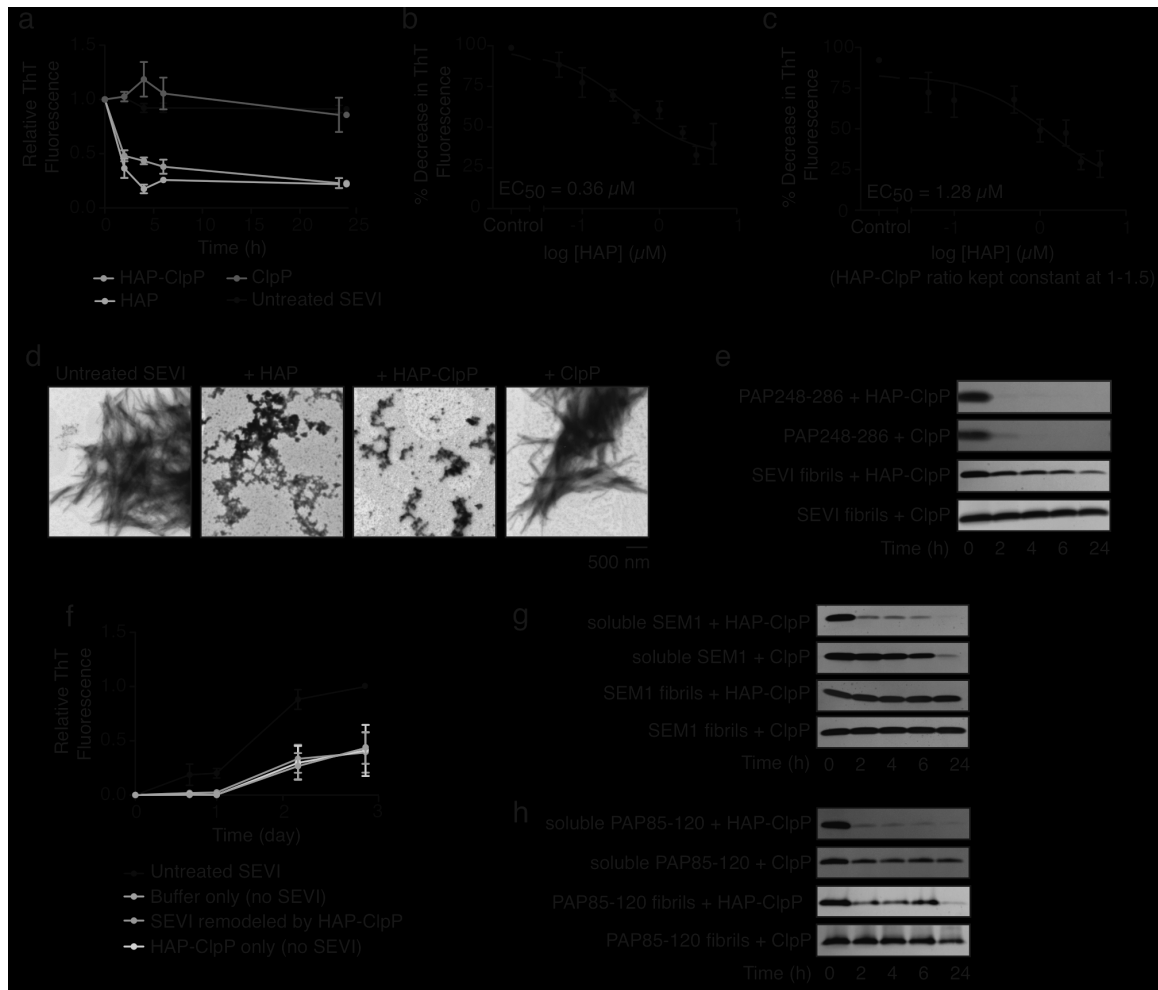


**Figure 2.8 HAP plus ClpP degrade SEVI fibrils and PAP85-120 fibrils.** (a) SEVI fibrils (20 $\mu\text{M}$  monomer) were incubated with buffer (untreated), HAP (3 $\mu\text{M}$ ), ClpP (4.5 $\mu\text{M}$ ), or HAP (3 $\mu\text{M}$ ) plus ClpP (4.5 $\mu\text{M}$ ) for 0-24h. Fibril integrity was assessed via ThT fluorescence. Values represent

means  $\pm$  SEM (n=3-4). **(b, c)** Dose-response analysis for HAP (b) and HAP plus ClpP (c) remodeling of SEVI fibrils (20 $\mu$ M monomer) after 6h. The EC<sub>50</sub> is based on ThT fluorescence. Values represent means  $\pm$  SEM (n=3-7). **(d)** TEM of SEVI fibrils (20 $\mu$ M monomer) incubated with buffer (untreated), HAP (3 $\mu$ M), ClpP (4.5 $\mu$ M), or HAP (3 $\mu$ M) plus ClpP (4.5 $\mu$ M) for 24h. The scale bar is indicated. **(e)** SEVI fibrils or soluble PAP248-286 (20 $\mu$ M monomer) were treated with HAP (3 $\mu$ M), ClpP (4.5 $\mu$ M), or HAP (3 $\mu$ M) plus ClpP (4.5 $\mu$ M) for 0-24h at 37°C. Reactions were then processed for SDS-PAGE and silver stain. **(f)** SEVI fibrils (20 $\mu$ M monomer) were incubated with HAP (3 $\mu$ M) and ClpP (4.5 $\mu$ M) for 6h, and the resulting products were used to seed soluble PAP248-286 (1mM, 0.1% fibril seed) fibrillization. Buffer conditions lacking fibril seed were included. Fibril assembly was monitored by ThT fluorescence. Values represent means  $\pm$  SEM (n=4). **(g, h)** PAP85-120 fibrils or soluble PAP85-120 (g) or SEM1(45-107 fibrils) or SEM1(45-107) (20 $\mu$ M monomer) (h) were treated with HAP (3 $\mu$ M), ClpP (4.5 $\mu$ M), or HAP (3 $\mu$ M) plus ClpP (4.5 $\mu$ M) for 0-24h at 37°C. Reactions were then processed for SDS-PAGE and silver stain.

### 2.2.8 Fibril remodeling, clustering, and degradation reduce stimulation of HIV infection

Finally, we assessed whether these Hsp104-based treatments affected the ability of the various seminal amyloids to promote HIV infection in cell culture. We employed TZM-bl cells containing a luciferase reporter construct under control of the HIV-1 long terminal repeat to assess the extent of infectivity. First, we determined that Hsp104, Hsp104<sup>A503V</sup>, Hsp104<sup>DWB</sup>, ClpB, Hsp104<sup>1-548</sup>, Hsp104<sup>773-908</sup>, HAP, ClpP, and GFP had no effect on HIV infection of TZM-bl cells in the absence of seminal amyloid (Figure 2.9a). Moreover, none of the Hsp104 conditions affected cell viability assessed via MTT reduction (not shown). Thus, any effects of Hsp104-based treatments were due to an effect on the fibrils rather than any direct effect on HIV or on cell viability.

Hsp104 and variants were unable to remodel or degrade SEM1(45-107) fibrils (Figure 2.4a, 2.4c, 2.8g), but Hsp104, Hsp104<sup>DWB</sup>, and ClpB could cluster them into larger conglomerates, whereas GFP was ineffective (Figure 2.5c, 2.5f). Remarkably, this clustering activity was sufficient to reduce the ability of SEM1(45-107) fibrils to promote HIV infection, whereas GFP and ClpP were ineffective (Figure 2.9b). Hsp104<sup>DWB</sup> converted SEM1(45-107) fibrils into the largest structures (Figure 2.5c, 2.6i) and accordingly caused the largest reduction in HIV infection (Figure 2.9b). The partitioning of SEM1(45-107) amyloid into larger aggregates likely decreases the availability of virion binding sites and thereby restricts the enhancement of infection (Figure 2.10b). Thus, seminal amyloid fibrils must be disseminated to counter electrostatic repulsion and promote HIV



infection. Clustering seminal amyloid into large conglomerates reduces their ability to enhance HIV infection.

Hsp104-based treatments that remodeled, clustered, or degraded SEVI fibrils or PAP85-120 fibrils reduced their ability to promote HIV infection (Figure 2.9c-e, 2.10). Thus, Hsp104<sup>773-908</sup>, ClpP, and GFP, which could neither remodel, cluster, nor degrade SEVI fibrils or PAP85-120 fibrils had no effect on their ability to enhance HIV infection (Figure 2.9c, 2.9d). By contrast, Hsp104, Hsp104<sup>A503V</sup>, or HAP remodeled SEVI fibrils (Figure 2.1a, 2.2a, 2.8a) and PAP85-120 fibrils (Figure 2.3a) and reduced their ability to enhance HIV infection (Figure 2.9c-e). Likewise, Hsp104<sup>DWB</sup>, ClpB, and Hsp104<sup>1-548</sup>, which clustered SEVI fibrils or PAP85-120 fibrils, also reduced enhancement of HIV infection (Figure 2.9c-e). Finally, HAP plus ClpP degraded SEVI and PAP85-120 fibrils (Figure 2.8e, 2.8h) and yielded a strong reduction of enhancement of HIV infection (Figure 2.9c, 2.9d). Thus, fibril remodeling, clustering, and degradation can all reduce the enhancement of HIV infection by seminal amyloid (Figure 2.10).

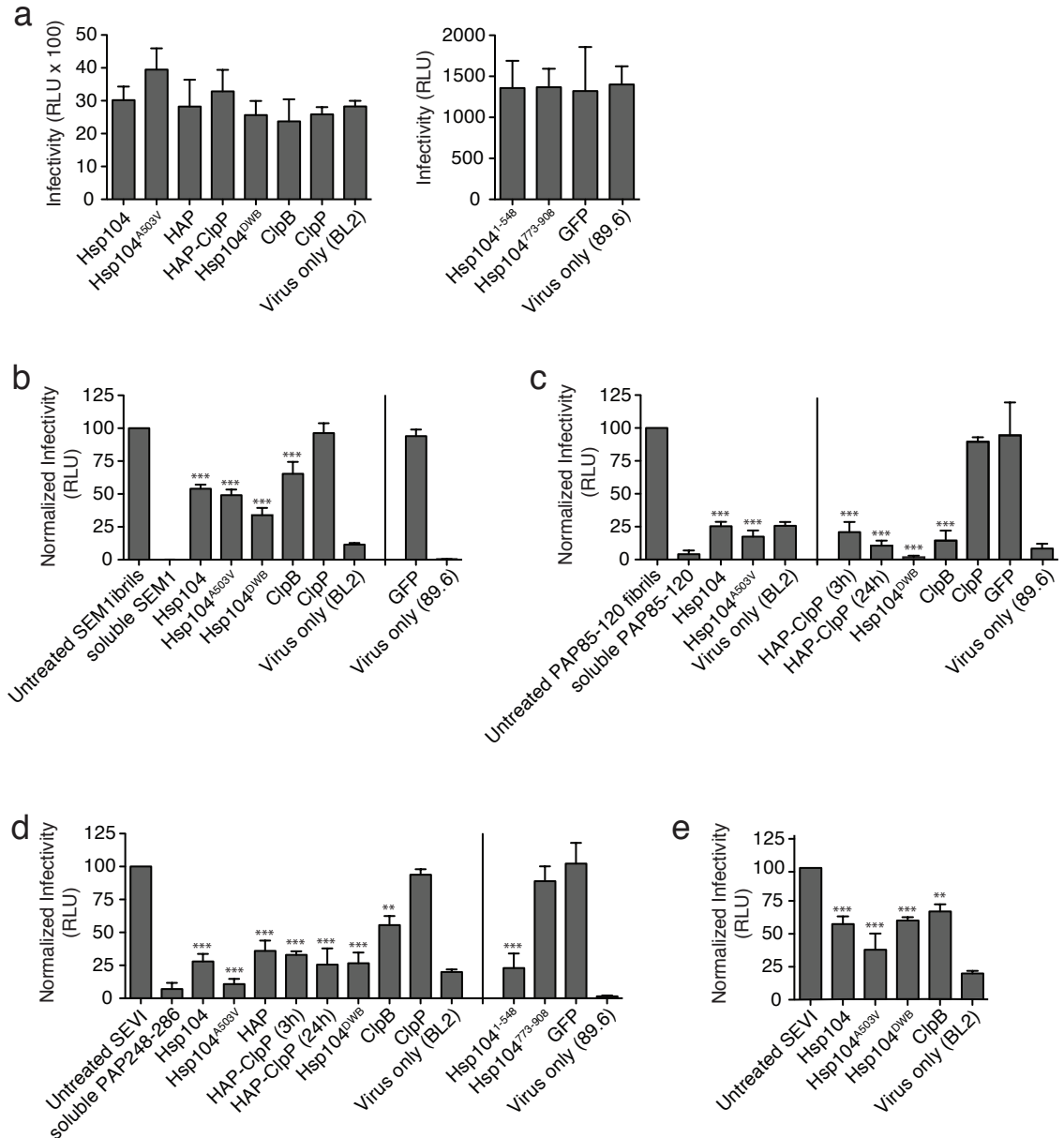


**Figure 2.9 Hsp104 reduces the ability of seminal amyloid to enhance HIV infection. (a)** Effect of Hsp104 variants and ClpP on viral infectivity (left panel: BL2 virions, right panel: 89.6 virions) in the absence of any enhancing seminal amyloid. Values represent means  $\pm$  SEM (n=3-6). **(b)** Preformed SEM1(45-107) fibrils (20 $\mu$ M monomer) were pretreated with buffer, Hsp104, Hsp104<sup>A503V</sup>, Hsp104<sup>DWB</sup>, ClpB, ClpP, or GFP and HIV infectivity was assessed in TZM-bl cells by measuring luciferase activity (in RLUs). The background luminescence from buffer control samples was subtracted and values were normalized to untreated fibril samples. Different viral strains were used for samples on either side of the solid line. Values represent means  $\pm$  SEM (n=3-6). **(c)** Preformed PAP85-120 fibrils (20 $\mu$ M) were pretreated with buffer, Hsp104, Hsp104<sup>A503V</sup>, Hsp104<sup>DWB</sup>, ClpB, ClpP, HAP plus ClpP, or GFP and HIV infectivity was assessed in TZM-bl cells and expressed as normalized infectivity to untreated fibril samples. Different viral

strains were used for samples on either side of the solid line. Values represent means  $\pm$  SEM (n=3-4). **(d)** SEVI fibrils (20 $\mu$ M) were pretreated with buffer, Hsp104, Hsp104<sup>A503V</sup>, Hsp104<sup>DWB</sup>, ClpB, Hsp104<sup>1-548</sup>, Hsp104<sup>773-908</sup>, HAP, ClpP, HAP plus ClpP, or GFP and HIV infectivity was assessed in TZM-bl cells and expressed as normalized infectivity to untreated fibril samples. Different viral strains were used for samples on either side of the solid line. Values represent means  $\pm$  SEM (n=3-7). For all experiments in (a-d), the protein concentrations used were as follows: Hsp104 (3 $\mu$ M), Hsp104<sup>A503V</sup> (3 $\mu$ M), HAP (3 $\mu$ M), HAP-ClpP (3 $\mu$ M and 4.5 $\mu$ M, respectively), Hsp104<sup>DWB</sup> (3 $\mu$ M), Hsp104<sup>1-548</sup> (18 $\mu$ M monomer), Hsp104<sup>773-908</sup> (18 $\mu$ M monomer), ClpB (3 $\mu$ M), ClpP (18 $\mu$ M monomer), and GFP (18 $\mu$ M monomer). **(e)** SEVI fibrils were treated as in (d) except Hsp104 variant concentration was 0.3 $\mu$ M. HIV infectivity was assessed in TZM-bl cells and expressed as normalized infectivity to untreated fibril samples. Values represent means  $\pm$  SEM (n=3-7).

## 2.3 Discussion

In this study, we repurpose an amyloid-remodeling factor from yeast, Hsp104, to antagonize seminal amyloid and reduce amyloid-mediated enhancement of HIV infection. Hsp104, as well as a potentiated Hsp104 variant, Hsp104<sup>A503V</sup> [183], were highly effective at rapidly remodeling SEVI and PAP85-120 fibrils into non-fibrillar structures. This remodeling activity required ATP hydrolysis, as Hsp104<sup>DWB</sup> was ineffective. The *E. coli* Hsp104 homolog, ClpB, was unable to remodel SEVI or PAP85-120 fibrils, even when it was activated by mutations in the middle domain that enhance activity [193]. The inability of ClpB variants to remodel amyloid likely reflects profound differences in how Hsp104 and ClpB subunits process substrates for disaggregation [182]. In stark contrast, Hsp104<sup>A503V</sup> remodeled SEVI fibrils (20 $\mu$ M monomer) at extremely low concentrations, with a calculated EC<sub>50</sub> value in the nanomolar range. An EC<sub>50</sub> this low relative to the quantity of fibrils has not been observed for Hsp104 with any amyloid, including its natural amyloid substrate: Sup35 prions [189]. Importantly, treatment of SEVI and PAP85-120 fibrils with Hsp104 or Hsp104<sup>A503V</sup> greatly reduced their ability to enhance HIV infection.

The heightened susceptibility of SEVI and PAP85-120 fibrils to remodeling by Hsp104 and Hsp104<sup>A503V</sup> might reflect the high lysine content of PAP248-286 (15.4%) and PAP85-120 (8.6%) [179]. Indeed, lysine-rich regions provide an important recognition feature for Hsp104, and poly-lysine stimulates ATP hydrolysis by Hsp104 [135, 138]. However, SEM1(45-107) contains a similar proportion of lysine residues (9.5%) and SEM1(45-107) fibrils were not remodeled by

Hsp104 or Hsp104<sup>A503V</sup>. Thus, some other feature of SEM1(45-107) fibrils likely prevents remodeling by Hsp104. One possibility is that SEM1(45-107) also contains a high proportion of residues that disfavor Hsp104 binding, including serine, glycine, and histidine [135], which are all less abundant in PAP248-286 and PAP85-120 [179]. Thus, Hsp104 may fail to gain sufficient traction to remodel SEM1(45-107) fibrils. Alternatively, SEM1(45-107) fibrils might access a specific amyloid strain, which is intractable for other reasons such as binding site inaccessibility or enhanced stability.

Remodeling amyloid structure by Hsp104 was not necessary, however, for specific Hsp104 variants to reduce the ability of seminal amyloid to enhance HIV infection. Thus, even though Hsp104 did not remodel SEM1(45-107) fibrils, it reduced their ability to enhance HIV infection. Indeed, Hsp104 clustered SEM1(45-107) fibrils into large, higher order aggregates. This activity did not require ATP hydrolysis as Hsp104<sup>DWB</sup> also promoted fibril clustering. Indeed, several Hsp104 variants unable to remodel amyloid structure, including ClpB, and even the monomeric Hsp104 fragment, Hsp104<sup>1-548</sup> encompassing the NTD, NBD1, and the MD [180], could cluster seminal amyloid fibrils (SEVI, PA85-120, and SEM1(45-107)) into larger conglomerates with reduced ability to promote HIV infection. Importantly, this effect was specific as not any protein could cluster seminal amyloid into higher order aggregates. Thus, the control protein GFP and another Hsp104 fragment, Hsp104<sup>773-908</sup> were unable to promote seminal amyloid clustering and consequently had no effect on the enhancement of HIV infection. We postulate three mechanisms to explain how the clustering of seminal amyloid into larger conglomerates reduces the enhancement of infection: first, the formation of larger fibril clusters could decrease the availability of virion binding sites on fibrils; second, these higher order assemblies may act as a physical barrier obstructing virion access to the target cell surface; and third, virions may bind to fibrils and become trapped inside large fibril conglomerates such that they can no longer navigate to the target cell surface. These findings indicate that seminal amyloid fibrils must be disseminated to counter electrostatic repulsion and promote HIV infection. If fibrils become too

clustered then their ability to promote HIV infection declines. Future studies will decipher the specific region within Hsp104 that is sufficient to cause seminal amyloid clustering, which could ultimately lead to the design of peptide-based inhibitors or small molecules that impede seminal amyloid functionality.

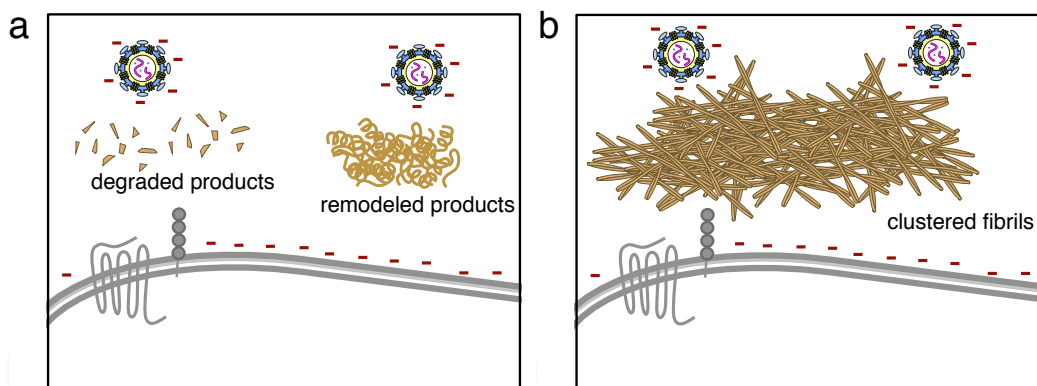


**Figure 2.10 Hsp104-based treatments that remodel, degrade, or cluster seminal amyloid reduce their ability to stimulate HIV infection. (a)** Hsp104-based treatments remodel (Hsp104 and Hsp104<sup>A503V</sup>) and degrade (HAP plus ClpP) SEVI and PAP85-120 fibrils such that their ability to boost infection is greatly reduced. **(b)** Hsp104-based treatments non-catalytically promote the assembly of seminal amyloid into higher order conglomerates, which not only results in fewer available sites within fibrils for virion binding, but also acts as a physical barrier for cell entry.

The clustering activity we observed is reminiscent of the ability of various molecular chaperones to stimulate the clustering of toxic misfolded oligomers into larger species in the absence of structural reorganization of the oligomers themselves [194]. The larger aggregated species mask the reactive surfaces of oligomers and consequently neutralize oligomer toxicity [194]. This activity does not require chaperone ATPase activity or even ATP and can be driven by substoichiometric quantities of chaperone [194]. Hsp104 is known to stimulate the prionogenesis of various yeast prion proteins, including Sup35 and Ure2, when acting at substoichiometric concentrations [129, 181, 184]. However, the clustering of preformed amyloid fibrils into large conglomerates is not an activity we have observed previously with other substrates. Nonetheless, this activity, which does not require Hsp104 ATPase activity or even hexameric structure, could

play an important role in vivo in the partitioning and concentration of aggregated proteins into higher order compartments, such as Q bodies (also called stress foci), JUNQ (JUxta Nuclear Quality control compartment) and IPOD (Insoluble Protein Deposit compartment) [199-202].

Therapeutically, Hsp104 and its analogs that we are studying could be used as a genital tract applied microbicide. A potential problem with remodeling seminal amyloid or clustering amyloid into higher order structures is that remodeled peptides might reform amyloid and clustered fibrils might disperse and be able to enhance HIV infection once again. To avoid this risk and irreversibly clear seminal amyloid, we developed a strategy that couples seminal amyloid remodeling to degradation. Thus, we engineered Hsp104 to interact with ClpP, a chambered protease from *E. coli* [142]. The modified Hsp104 variant, termed HAP, passes remodeled substrates into the ClpP chamber for degradation [142]. Although ineffective against SEM1(45-107) fibrils, HAP plus ClpP effectively remodeled and degraded SEVI fibrils and PAP85-120 fibrils. This ability to remodel and degrade exceptionally stable amyloid has not been previously reconstituted using pure components and could also prove useful in the removal of pathologic or disease-associated amyloid fibrils. Coupled fibril disaggregation and degradation could be especially advantageous in instances where reactivation of the protein sequestered in fibrils is not beneficial, as with amyloid-beta deposits in Alzheimer's disease [203].

There is a great need for microbicidal agents that interfere with HIV infectivity without inducing tissue inflammation [179]. Our studies suggest that seminal amyloid is likely a tractable target. We have demonstrated that various strategies based on Hsp104 interfere with the infectivity enhancing function of seminal amyloid. The most irreversible of these entails coupled remodeling and degradation of seminal amyloid. The ability to irrevocably clear seminal amyloid and block sexual transmission of HIV would provide a powerful and much needed weapon against the global HIV/AIDS pandemic. Our approach of targeting host protein conformers (seminal amyloid) is fundamentally different from traditional microbicidal approaches that target the virus.

Consequently, we anticipate that this strategy will synergize with direct anti-viral strategies, such that microbicides containing anti-viral agents and anti-amyloid agents could display enhanced efficacy.

## CHAPTER 3: A MOLECULAR TWEEZER ANTAGONIZES SEMINAL AMYLOIDS AND HIV INFECTION

### 3.1 Introduction

The majority of new HIV-1 infections are transmitted via sexual intercourse, and semen is the main vector for viral spread. Far from being a passive vehicle, semen massively enhances HIV infectivity [51, 204]. This HIV-enhancing activity can be attributed to seminal amyloid fibrils [51, 68, 173, 204] which form by self-assembly of proteolytic fragments of prostatic acid phosphatase (PAP248-286 and PAP85-120) and the homologous proteins semenogelin 1 (SEM1) and semenogelin 2 (SEM2) [51, 172, 173]. Seminal amyloid fibrils are highly cationic, and the positively charged fibrils capture HIV virions, increase viral attachment rates to target cells and augment fusion [68, 172, 175]. By doing so, fibrils promote HIV infection *in vitro* by several orders of magnitude, whereas the corresponding monomeric peptides have no effect [51, 172, 173]. Importantly, the stimulatory effect of seminal amyloid is greatest at low virus concentrations [51], and semen and SEVI fibrils may facilitate vaginal virus transmission after exposure to low viral doses [22]. HIV transmission rates are relatively low, occurring as infrequently as 1 in 200 to as low as 1 in 10,000 coital acts [170]. Thus, counteraction of infectivity promoting amyloids in semen should reduce or even prevent HIV transmission via the sexual route.

The lysine-specific molecular tweezer, CLR01 (Figure 3.1a), inhibits amyloid fibrillization by engaging specific lysine residues within a variety of disease-associated amyloidogenic proteins including amyloid- $\beta$  protein (A $\beta$ ), tau, islet amyloid polypeptide, and  $\alpha$ -synuclein [152, 154, 205]. Furthermore, CLR01 can even slowly disassemble preformed A $\beta$  and  $\alpha$ -synuclein fibrils over the course of several days [152, 154]. CLR01 binds lysine residues with a  $K_d$  of  $\sim 20$   $\mu$ M and also arginine residues albeit with  $\sim 10$ -fold lower affinity [151, 206]. Its unprecedented high specificity for basic amino acids relies on a unique binding mode in which the tweezer draws the cationic side chains into its torus-shaped cavity and locks the ammonium or guanidinium cation with its



anionic phosphate group in a tight ion pair (Figure 3.1b). No other amino acids fulfill the requirements for this threading mechanism. Moreover, on protein surfaces only readily accessible lysine or arginine residues are complexed, as evidenced by crystal structures and NMR experiments [207].

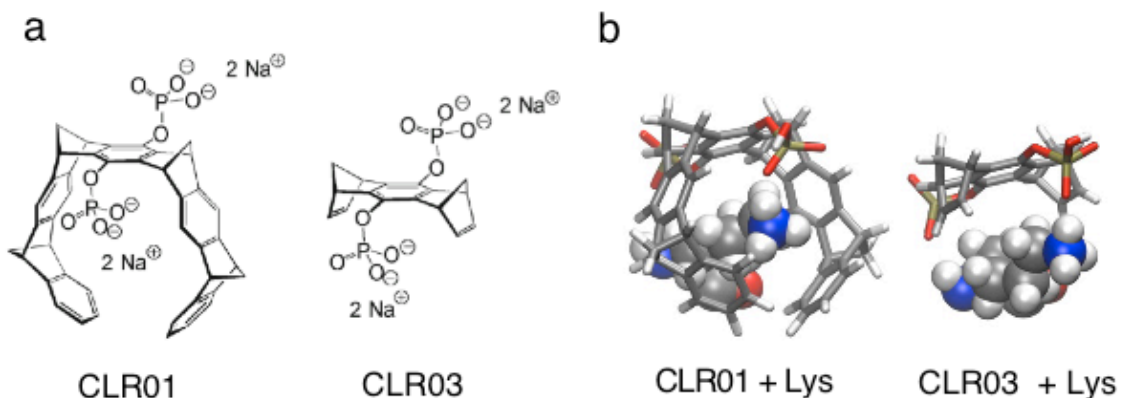


**Figure 3.1 Molecular structures of CLR01 and CLR03. (a)** Chemical structures of CLR01 and CLR03. **(b)** Stick representation showing CLR01 engaging lysine, while CLR03 is unable to interact with lysine.

Since amyloidogenic seminal peptides are particularly rich in lysine and arginine residues (Figure 3.2a-c, Lys and Arg residues are highlighted in red) [172, 175, 179], we hypothesized that CLR01 might interfere with their HIV-enhancing activity. Here, we establish that CLR01 inhibits amyloidogenesis of PAP and SEM peptides, neutralizes the cationic surface charge of seminal amyloid, and rapidly remodels preformed PAP248-286 fibrils (termed SEVI for Semen-derived Enhancer of Virus Infection) and PAP85-120 fibrils. Strikingly, CLR01 also exhibits a direct antiviral effect by selectively disrupting the membrane of enveloped viruses. Thus, the lysine tweezer CLR01 represents an unprecedented candidate for further development as a microbicide as it not only inactivates HIV and other viruses but also antagonizes host-encoded seminal amyloids that enhance viral infection.

## 3.2 Results

### 3.2.1 CLR01 inhibits spontaneous assembly of seminal amyloid fibrils

Lysine residues in PAP248-286, PAP85-120, SEM1, and SEM2 are often found within or immediately adjacent to hexapeptides predicted to form self-complementary  $\beta$ -strands (Figure 3.2a-c, underlined residues), termed steric zippers, which often comprise the spine of amyloid fibrils [100, 179, 208]. In fact, residues Lys271, Arg272, Lys280, and Lys281 within PAP248-286 are predicted to form part of the cross- $\beta$  SEVI fibril core as defined by hydrogen-deuterium exchange and protease protection experiments [209]. The wealth of basic residues in PAP248-286, PAP85-120, and SEM1(45-107) (Figure 3.2a-c) led us to hypothesize that the lysine-specific tweezer, CLR01, but not its truncated derivative CLR03, which lacks hydrophobic sidewalls and consequently cannot bind lysine residues (Figure 3.1) [152], might bind to these residues and interfere with fibril assembly. To test this hypothesis, CLR01 was assessed for its ability to inhibit the spontaneous amyloidogenesis (i.e. assembly in the absence of preformed fibril seeds) of PAP248-286. The truncated derivative CLR03 was used as a negative control in all assays. PAP248-286 was incubated in the presence or absence of equimolar concentrations of CLR01 or CLR03. Fibril assembly was assessed using the fluorescence of the diagnostic dye Thioflavin-T (ThT), which increases upon amyloid binding and by transmission electron microscopy (TEM). In the absence of tweezer molecules, PAP248-286 fibrillization proceeded slowly, with a lag phase of at least 24h, and gradually reached a fluorescence intensity maximum after 3 days. As expected, CLR03 had no effect on fibril assembly, and the ThT signal increased similarly to untreated PAP248-286. In the presence of CLR01 however, ThT fluorescence intensity remained unchanged for ~48h and only increased marginally after 3 days, indicating that the formation of cross- $\beta$  structures was inhibited (Figure 3.2a). At an assembly concentration of 1mM peptide, a half maximal inhibitory concentration ( $IC_{50}$ ) of 2.6 $\mu$ M CLR01 was determined (Figure 3.2d), indicating that CLR01 is a potent inhibitor of PAP248-286 assembly at substoichiometric concentrations. The morphology of fibrillization products was further assessed by TEM. PAP248-286 formed abundant fibrils in the absence of molecular tweezers, and consistent with ThT data,

fibrillization was unhindered upon incubation with CLR03. TEM confirmed the absence of amyloid fibrils in CLR01 treated samples and instead revealed small species (Figure 3.2a). Thus, CLR01 potentially inhibits spontaneous PAP248-286 fibrillization.

Next, the effects of CLR01 on PAP85-120 fibrillization were assessed. For PAP85-120, the ThT fluorescence signal began increasing immediately with no apparent lag phase and reached a plateau by ~24h. As expected, the fibrillization kinetics were unchanged in the presence of CLR03. Notably, fibril assembly in the presence of CLR01 appeared to be completely inhibited, as the ThT signal failed to increase (Figure 3.2b). Indeed, at an assembly concentration of 1mM PAP85-120, an  $IC_{50}$  of 970 $\mu$ M CLR01 was determined based on ThT fluorescence (Figure 3.2e). This high concentration of CLR01 needed to inhibit PAP85-120 fibrillization is likely due to the lower number of lysine/arginine residues in the PAP85-120 sequence located in hexapeptide segments that are predicted to have high amyloid propensity (Figure 3.2b) [179]. The effect of CLR01 on PAP85-120 assembly was less apparent by TEM (Figure 3.2b). However, the assemblies formed in the presence of CLR01 appeared more flexible and curvilinear, and differed from the rigid, straight fibrils formed in the presence of CLR03 or buffer (Figure 3.2b). Since the structures that formed in the presence of CLR01 were not ThT-reactive (Figure 3.2b) they most likely represent non-amyloid aggregates. Thus, CLR01 appears to impede the transition of PAP85-120 to mature amyloid fibrils

Finally, the ability of CLR01 to obstruct SEM1(45-107) fibrillization was evaluated. In the absence of CLR01, following a lag phase of at least 24h, ThT fluorescence intensity increased and began to plateau after ~40h. As predicted, the kinetics of SEM1 assembly were unchanged in the presence of CLR03. Remarkably, at an equimolar concentration of CLR01:SEM1, only a minimal increase in ThT fluorescence was observed, indicating that CLR01 inhibits the formation of SEM1 amyloid fibrils (Figure 3.2c). At an assembly concentration of 500 $\mu$ M SEM1, an  $IC_{50}$  of 18.8 $\mu$ M CLR01 was calculated (Figure 3.2f). Large clusters of fibrils were detected in samples incubated

with CLR03 or buffer by TEM, while only amorphous aggregates and sparse short fibrils were found in samples incubated with CLR01 (Figure 3.2c). Importantly, CLR01 is the first example of an agent that interferes with the fibrillization of three semen-derived amyloidogenic peptides involved in HIV transmission.

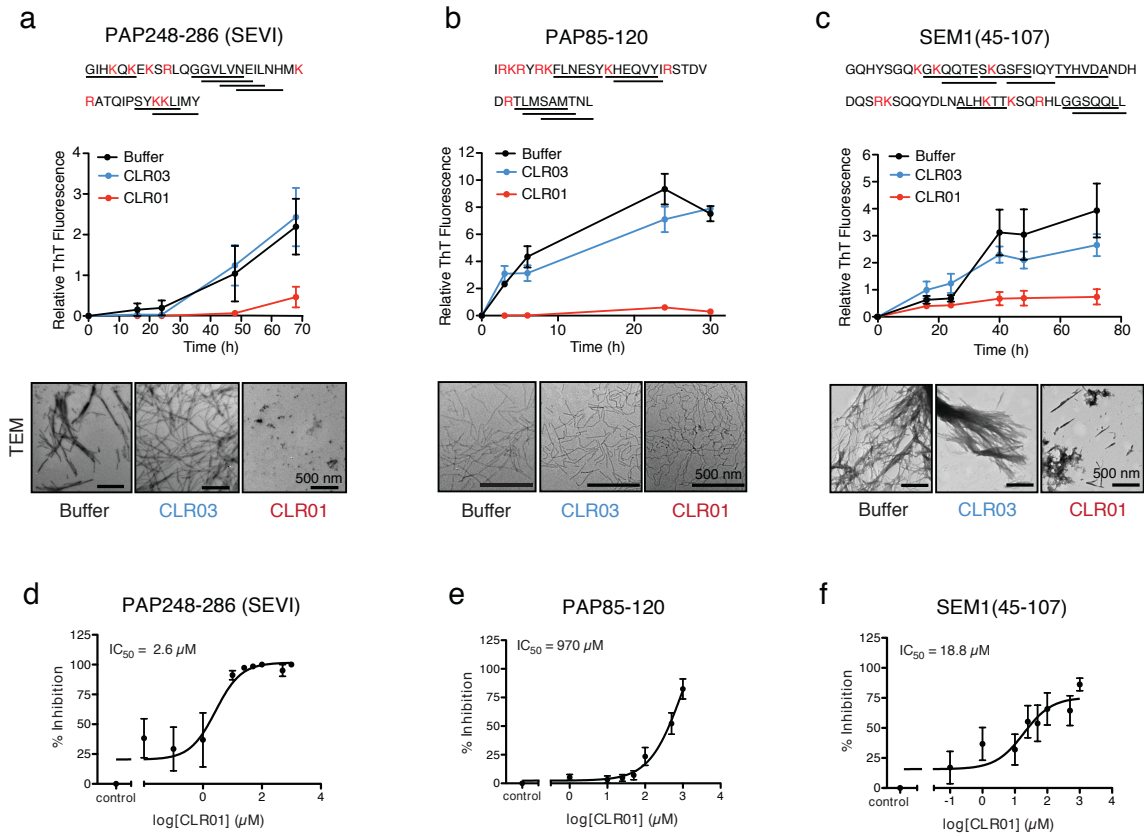


**Figure 3.2 CLR01 inhibits the formation of seminal amyloid fibrils.** (a-c) The primary sequences of PAP248-286 (a), PAP85-120 (b) and SEM1(45-107) (c) are provided. Lysine and arginine residues are in red and hexapeptides predicted to form steric zippers [100, 179] are underlined. CLR01 inhibits fibril formation by PAP248-286 (1mM) (a), PAP85-120 (1mM) (b) and SEM1(45-107) (500 $\mu$ M) (c). Peptides were incubated with equimolar CLR01, CLR03, or buffer and agitated at 1400rpm at 37°C. Aliquots were removed at various time points and fibrillization was assessed using the amyloid-binding dye, Thioflavin-T (ThT). Values represent means  $\pm$  SEM (n = 3 for PAP248-286; n = 4 for PAP85-120; n = 9 for SEM1(45-107)). Transmission electron microscopy (TEM) images of PAP248-286 (a), PAP85-120 (b), and SEM1(45-107) (c) agitated in the presence of CLR01, CLR03, or buffer. PAP248-286 and SEM1(45-107) samples were visualized after 72h of agitation, PAP85-120 after 2 h. Scale bar: 500nm. (d-f) Dose-response curves for CLR01 inhibition of PAP248-286 (1mM) fibrillization after 72h of agitation (d), PAP85-120 (1mM) fibrillization after 24h of agitation (e), and SEM1(45-107) (500 $\mu$ M) fibrillization after 72 h of agitation (f). The  $IC_{50}$  values are indicated. Values represent means  $\pm$  SEM (n = 3-5 for PAP248-286; n=4 for PAP85-120; n=7 for SEM1(45-107)).

### **3.2.2 CLR01 inhibits assembly of PAP248-286 seeded by preformed SEVI fibrils**

Next, we assessed whether CLR01 could also inhibit the assembly of PAP248-286 that was seeded by preformed SEVI fibrils. The addition of a small amount of preformed fibril seed to reconstituted PAP248-286 solutions induces polymerization and eliminates the lag phase for assembly [192]. In the presence of 2% fibril seed, the lag phase was indeed eliminated and PAP248-286 solutions assembled rapidly into fibrils, with ThT fluorescence intensity plateauing at ~24h. Remarkably, in addition to obstructing unseeded PAP248-286 assembly, CLR01 also completely inhibited seeded fibrillization as the ThT signal remained at baseline (Figure 3.3a). TEM images looked similar to unseeded experiments, with no fibrils present in CLR01 treated samples (Figure 3.3b). Dose-response analysis established an  $IC_{50}$  of 12.3 $\mu$ M for CLR01 inhibition of seeded PAP248-286 assembly at a peptide concentration of 1mM (Figure 3.3c). This substoichiometric effect is unprecedented and indicates a direct effect of CLR01 on fibril ends such that they can no longer recruit and convert monomeric peptide. Importantly, because CLR01 impedes both unseeded and seeded PAP248-286 assembly, it is likely acting at multiple stages of the fibrillization process including the initial nucleation and fibril elongation steps. These observations also indicate that lysine, arginine, or both residues play an important role in the nucleation and elongation of PAP248–286 fibrils.

To further confirm that CLR01 inhibits the nucleation process that is essential for amyloid assembly, we tested whether the products of CLR01 inhibition of PAP248-286 fibrillization could act as effective seeds for fresh assembly experiments. To do so, soluble PAP248-286 solutions were incubated with CLR01, CLR03, or buffer for 4 days. After this time, the reaction products were used as seeds for soluble PAP248-286 fibrillization. Buffer- and CLR03-treated products were able to seed fibrillization by eliminating the lag phase, while CLR01-treated products were significantly less efficient seeds (Figure 3.3d), indicating that CLR01 inhibits the formation of nuclei that are essential for amyloid fibrillization.

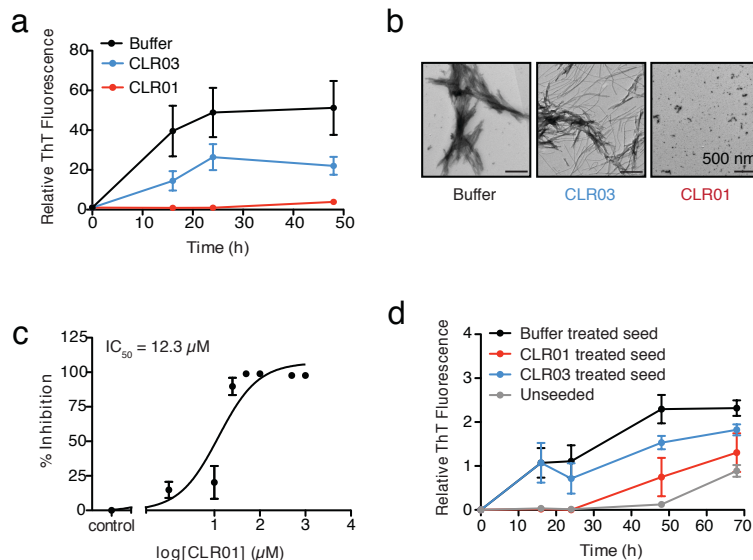


**Figure 3.3 CLR01 inhibits both the nucleation and elongation steps of amyloid assembly.** (a) Inhibition of seeded PAP248-286 fibrillization by CLR01. PAP248-286 (1mM) was incubated with CLR01 (1mM), CLR03 (1mM), or buffer. Preformed SEVI fibrils (2% seed) were added to each sample and agitated at 1400 rpm at 37°C. Fibrillization was assessed using ThT fluorescence. Values represent means  $\pm$  SEM (n = 6). (b) Electron microscopy visualization of CLR01 inhibition of seeded PAP248-286 fibrillization after 48h of agitation. Scale bar: 500nm. (c) Dose-response curve for CLR01 inhibition of seeded PAP248-286 (1mM; 2% seed) fibrillization after 48h of agitation. The  $IC_{50}$  value is indicated. Values represent means  $\pm$  SEM (n = 4). (d) CLR01 inhibits the formation of nuclei needed for fibril assembly. Soluble PAP248-286 solutions (1mM) were incubated with CLR01 (50 $\mu\text{M}$ ), CLR03 (50 $\mu\text{M}$ ), or buffer and agitated at 1400rpm at 37°C for 4 days. After 4 days, these inhibition products (5% volume) were used to seed soluble PAP248-286 (1mM) assembly. An unseeded control was included. Values represent means  $\pm$  SEM (n = 4).

### 3.2.3 CLR01 inhibition depends on lysine and arginine residues in PAP248-286

To investigate the role of lysine and arginine interactions with CLR01 in the inhibition of fibril assembly, we examined PAP248-286(Ala), an analogue in which all eight lysine and arginine residues are replaced by alanine [175]. PAP248-286(Ala) readily forms amyloid fibrils in the presence of CLR03 and buffer, and ThT fluorescence intensity also increases in the presence of CLR01, yet to a lesser extent (Figure 3.4a). To further analyze the effect of CLR01 on PAP248-286(Ala) assembly, we employed a sedimentation (or centrifugation) assay. This assay revealed that equal amounts of PAP248-286(Ala) entered the pellet fraction when the peptide was incubated with buffer or CLR01, indicating that the formation of PAP248-286(Ala) amyloid fibrils is

unaffected by CLR01 treatment (Figure 3.4b). Thus, it is likely that in the presence of CLR01, PAP248-286(Ala) assembles into a fibril strain that is less ThT-reactive. These findings confirm that CLR01-lysine contacts, CLR01-arginine contacts, or both are essential for inhibition, and CLR01 cannot block the amyloidogenesis of polypeptides devoid of lysine and arginine residues.

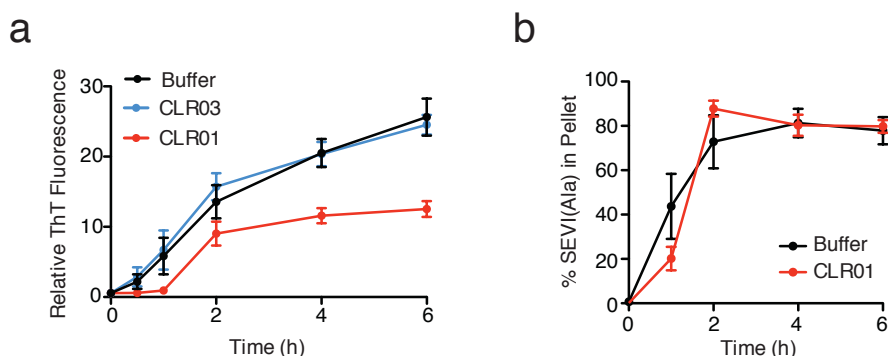


**Figure 3.4 CLR01 cannot block the amyloidogenesis of polypeptides devoid of lysine and arginine residues.** (a) PAP248-286(Ala) (100 $\mu$ M) was incubated with CLR01 (100 $\mu$ M), CLR03 (100 $\mu$ M) or buffer and agitated at 1400rpm and 37°C. Fibril assembly was assessed using ThT. Values represent means  $\pm$  SEM (n=9). (b) PAP248-286(Ala) (100 $\mu$ M) was incubated with CLR01 (100 $\mu$ M) or buffer and agitated at 1400rpm and 37°C. At each timepoint, samples were centrifuged and the amount of PAP248-286(Ala) in the pellet was assessed by SDS-PAGE. Values represent means  $\pm$  SEM (n=3).

### 3.2.4 CLR01 remodels preformed SEVI and PAP85-120 fibrils

Semen-derived fibrils are already formed and abundant in liquefied fresh ejaculates [68]. Thus, compounds that not only inhibit fibril formation but also disassemble preformed fibrils are advantageous for microbicide development [179]. To test whether CLR01 could remodel seminal amyloid, a ten-fold excess of CLR01 or CLR03 was incubated with preformed SEVI fibrils and ThT fluorescence intensity was monitored. After 2h, CLR01 treatment of SEVI fibrils resulted in a reduction in ThT fluorescence intensity to 45%, indicating rapid disassembly of amyloid fibrils, while CLR03 had no effect on fibril integrity (Figure 3.5a). No additional disaggregation was observed after 2h. Fibril disassembly was confirmed by TEM, which showed few intact fibrils and

predominately smaller nonfibrillar species (Figure 3.5a). Similar results were obtained by fluorescence microscopy of samples stained with Proteostat, a red fluorescent aggregate sensing dye (Figure 3.5a-c) [68]. A dose-response curve for CLR01 disassembly of SEVI fibrils (20 $\mu$ M) reveals a half maximal effective concentration ( $EC_{50}$ ) value of 0.12 $\mu$ M (Figure 3.5d), indicating that CLR01 acts efficiently at very low levels. These effects of CLR01 were remarkably rapid in comparison to the slow disassembly of A $\beta$  or  $\alpha$ -synuclein fibrils by CLR01, which required several weeks [152]. Thus, CLR01 can rapidly disassemble SEVI fibrils on a time scale that would be useful for prevention of HIV infection. Furthermore, SEVI fibrils remodeled by CLR01 were less effective seeds for polymerization of monomeric PAP248-286 than those treated with CLR03 or buffer, verifying that CLR01 actively remodels fibrils into alternative, non-templating conformers (Figure 3.5h).

We next performed circular dichroism experiments to examine the effect of CLR01 on the amyloid cross- $\beta$  structure. Untreated SEVI fibrils or SEVI fibrils treated with CLR03 exhibited a pronounced minimum indicative of a characteristic  $\beta$ -sheet rich structure (Figure 3.5f,g). However, SEVI fibrils incubated with CLR01 showed a loss in the  $\beta$ -sheet minimum (Figure 3.5f,g), confirming that CLR01 alters the cross- $\beta$  architecture of SEVI fibrils.

Next, CLR01 was tested for its ability to remodel preformed PAP85-120 fibrils. After 2h of incubation with CLR01, ThT fluorescence intensity decreased to 48% of its initial value, while remaining unchanged in the presence of CLR03 (Figure 3.5b). No additional drop in ThT signal was observed after 2h. TEM examination revealed few short fibrils as well as small oligomeric species (Figure 3.5b). Dose-response analysis indicated an  $EC_{50}$  value for remodeling of 1.54 $\mu$ M CLR01 (for 20 $\mu$ M PAP85-120 fibrils) (Figure 3.5e). This higher  $EC_{50}$  needed to remodel PAP85-120 fibrils is likely due to the lower abundance of lysine residues in the PAP85-120 sequence compared to PAP248-286. Importantly, CLR01 is the first agent capable of dissolving multiple semen-derived amyloid fibrils.



In contrast, CLR01 was unable to disassemble preformed SEM1(45-107) fibrils. There was no change in the ThT fluorescence signal after 6h of incubation of fibrils with CLR01 (Figure 3.5c). TEM visualization showed large, dense clusters of fibrils in samples treated with CLR01, CLR03, and buffer, verifying that CLR01 was incapable of dissolving SEM1 fibrils (Figure 3.5c).

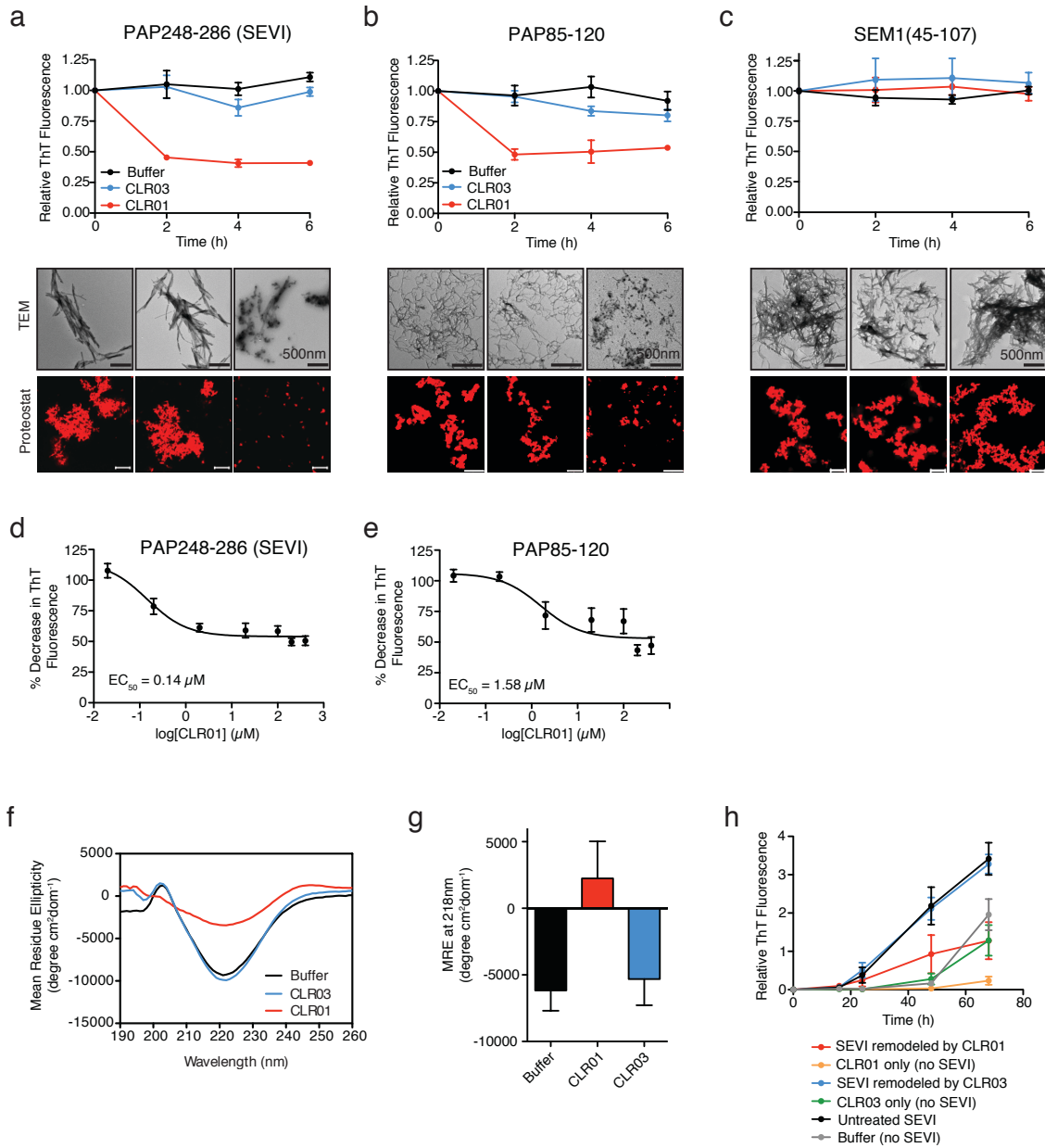


**Figure 3.5 CLR01 partially disassembles preformed SEVI and PAP85-120 fibrils. (a-c)** Preformed SEVI (a), PAP85-120 fibrils (b), and SEM1(45-107) (c) fibrils (20 $\mu$ M) were treated with a 10-fold excess of CLR01 or CLR03 or buffer for 0-6h. Fibril integrity was assessed using ThT. Values represent means  $\pm$  SEM (n = 3). TEM (middle panel) and confocal microscopy (bottom panel) of SEVI (a), PAP85-120 fibrils (b), and SEM1(45-107) fibrils (c) obtained after 2h treatment with CLR01, CLR03, or buffer. Scale bar for TEM images: 500nm. For confocal microscopy, samples were stained with Proteostat dye (Experiments performed by members of the Munch lab). Scale bar: 20 $\mu$ m. **(d,e)** Dose-response curve for CLR01 disaggregation of SEVI (d) or PAP85-120 (e) fibrils (20 $\mu$ M) after 2h of treatment. The EC<sub>50</sub> value is indicated. Values represent means  $\pm$  SEM (n = 7 for SEVI; n = 5-9 for PAP85-120). **(f)** CD spectrum of SEVI fibrils (50 $\mu$ M) incubated with CLR01 or CLR03 (50 $\mu$ M), or buffer. A representative spectrum is shown. **(g)** The mean residue ellipticity (MRE) at 218 nm was averaged from 3 independent experiments. Values represent means  $\pm$  SEM (n=3). **(h)** Seeding with CLR01-remodeled SEVI products. SEVI fibrils (20 $\mu$ M) were treated with CLR01 or CLR03 (200 $\mu$ M), or buffer for 3h and reaction products were used to seed PAP248-286 fibrillization (0.1% fibril seed, 1mM peptide). Buffer conditions with no fibril seed present were also included. Fibrillization was monitored by ThT fluorescence. Values represent means  $\pm$  SEM (n = 8).

### **3.2.5 CLR01-driven disaggregation depends on lysine and arginine residues in PAP248-286 and PAP85-120**

To elucidate the role of lysine- and arginine-tweezer interactions in CLR01-mediated disaggregation of SEVI and PAP85-120 fibrils, experiments were performed with PAP248-286(Ala) and PAP85-120(Ala) peptides. These mutant peptides have all lysine and arginine residues present in the original peptides exchanged for alanine. PAP248-286(Ala) and PAP85-120(Ala) were assembled into fibrils that were subsequently incubated with CLR01, CLR03 or buffer. ThT fluorescence intensity remained unchanged for all samples after 6h of incubation, indicating that CLR01 is unable to disrupt PAP248-286(Ala) or PAP85-120(Ala) fibrils (Figure 3.6a,d). Furthermore, CD experiments confirmed that the beta-sheet structure of SEVI(Ala) was unaffected by treatment with CLR01 (Figure 3.6b,c). Thus, CLR01-lysine contacts, CLR01-arginine contacts, or both are critical for the disassembly process.

To further confirm the importance of CLR01-lysine and CLR01-arginine contacts in seminal amyloid disaggregation, competitive binding experiments were conducted using poly-lysine. Increasing concentrations of poly-lysine (MW 4,000-15,000 corresponding to poly-lysine chain lengths of 27-102 residues) were added to solutions containing seminal amyloid fibrils and

CLR01, and the extent of disassembly was assessed by ThT. We observed that as poly-lysine concentration increased, the degree of disaggregation of both SEVI and PAP85-120 fibrils by CLR01 was lessened (Figure 3.6e,f). This finding suggests that poly-lysine can compete with seminal amyloid fibrils for CLR01 binding, and thus, CLR01 binding to lysine residues within fibrils is crucial for disassembly.

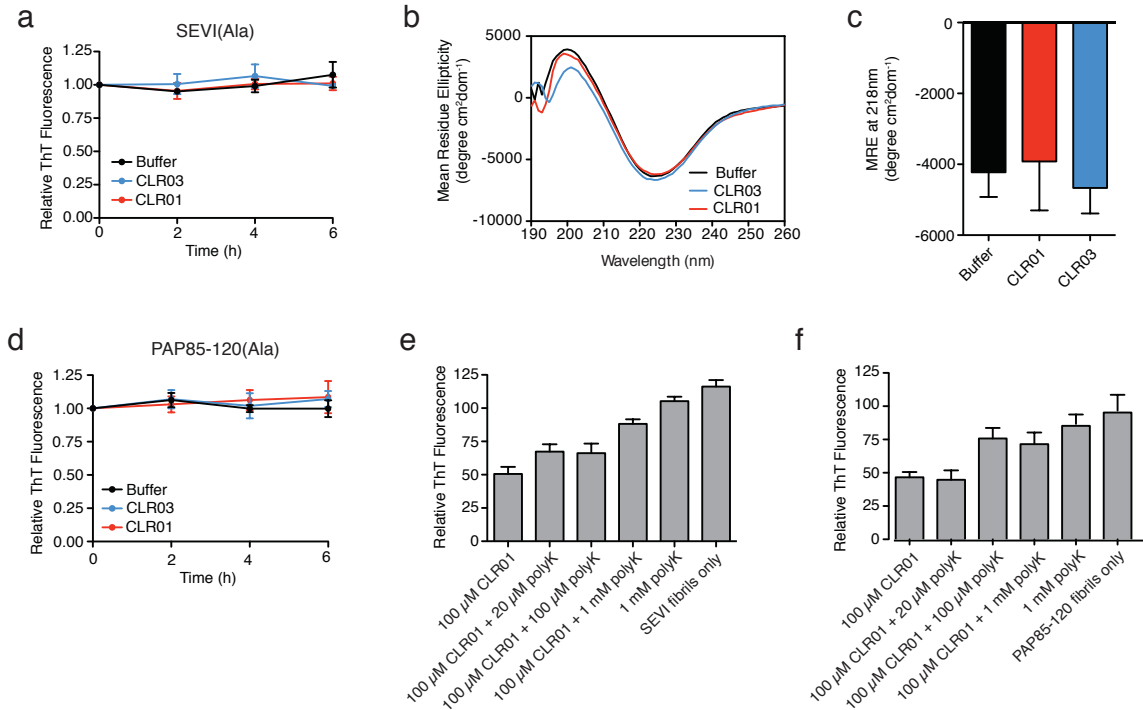


**Figure 3.6 CLR01-mediated disaggregation of seminal amyloid depends on contacts with lysine and arginine residues.** (a) Preformed SEVI(Ala) fibrils (20μM) were treated with CLR01 or CLR03 (200μM) or buffer for 0-6 h. Fibril integrity was assessed using ThT fluorescence. Values represent means ± SEM (n = 3). (b) CD spectrum of SEVI(Ala) fibrils (50μM) incubated with CLR01 or CLR03 (50μM) or buffer. One representative example is shown. (c) The mean residue ellipticity (MRE) at 218 nm was averaged from 3 independent experiments. Values represent means ± SEM (n=3). (d) Preformed PAP85-120(Ala) fibrils (20μM) were treated with CLR01 or CLR03 (200μM) or buffer for 0-6 h. Fibril integrity was assessed using ThT fluorescence. Values represent means ± SEM (n = 3). (e,f) SEVI (e) or PAP85-120 (f) fibrils (20μM) were incubated with CLR01 (100μM) and increasing concentrations of poly-lysine (polyK). Fibril integrity was assessed after 2h using ThT fluorescence. Values represent means ± SEM (n = 4-5).

### **3.2.6 CLR01 abrogates the interaction of seminal amyloids with viral particles and diminishes their infection enhancing property**

Since the infectivity-enhancing activity of seminal amyloid fibrils is due to their positive surface charge [172, 175], we sought to determine whether CLR01 affects this property. To prevent fibril disassembly from occurring in these experiments, fibrils were mixed with CLR01, CLR03, or buffer, and samples were immediately centrifuged to remove unbound CLR01 and CLR03 molecules. Subsequently, the surface charge of resuspended fibrils was determined by zeta potential measurements. We found that CLR01, but not CLR03, neutralized the positive surface charge of SEVI, PAP85-120 and SEM1 fibrils within minutes (Figure 3.7a). Next, confocal microscopy was used to assess whether this neutralization could abrogate fibril binding to YFP-tagged virions. As previously shown [55, 172, 173], buffer-treated fibrils efficiently sequestered virions, while in contrast, fibrils pretreated with CLR01, but not CLR03, were unable to form fibril-virion complexes (Figure 3.7b).

Since fibril-virion complexes are already present before ejaculation or form rapidly post emission [68], we next investigated whether CLR01 could displace virions from preformed fibril-virion complexes. Remarkably, CLR01 but not CLR03 substantially reduced the number of virions covering the surface of SEVI, PAP85-120, and SEM1(45-107) fibrils, however, the fluorescent virions did not appear as displaced individual particles in these images (Figure 3.7c). Thus, to exclude the possibility that CLR01 quenches the fluorescence of YFP-tagged virions, we analyzed virions treated with CLR01 or controls by confocal microscopy. We found that treatment of virions with CLR01 did not affect virion fluorescence or the number of fluorescent particles (not shown). However, this analysis also revealed that CLR01 prevented virion binding to the surface of the chamber slides, suggesting that CLR01 might also directly interact with viral particles thereby altering their biophysical properties (not shown). Our results demonstrate that the lysine-specific tweezer, CLR01, not only prevents the interaction of fibrils with virions but also displaces viral particles from preformed fibril-virion complexes.

The combined effects of CLR01 on fibril architecture and the formation of fibril-virion complexes led us to investigate whether the tweezer might diminish the infection-enhancing property of seminal amyloids. We first confirmed that the tweezer did not cause cytotoxic effects at concentrations of up to 500 $\mu$ M in TZM-bl cells (Figure 3.7d), a HIV reporter cell line commonly used to study virus infection [51, 68]. Next, preformed fibrils were treated for 5min with CLR01, CLR03, or buffer. After addition of a low dose of CCR5-tropic HIV, the resulting mixture was added to TZM-bl cells and infection was measured via  $\beta$ -galactosidase activity three days later. As previously reported [51, 172, 173], the three semen-derived amyloids augmented HIV infection in a dose-dependent manner with maximal enhancements between 33- to 64-fold (Figure 3.7e). Remarkably, pretreatment of SEVI, PAP85-120 and SEM1(49-107) amyloid with CLR01 eliminated the infection-enhancing property of the fibrils, while CLR03 had no effect (Figure 3.7e). Thus, CLR01 abrogates the infection enhancing activity of seminal amyloids.

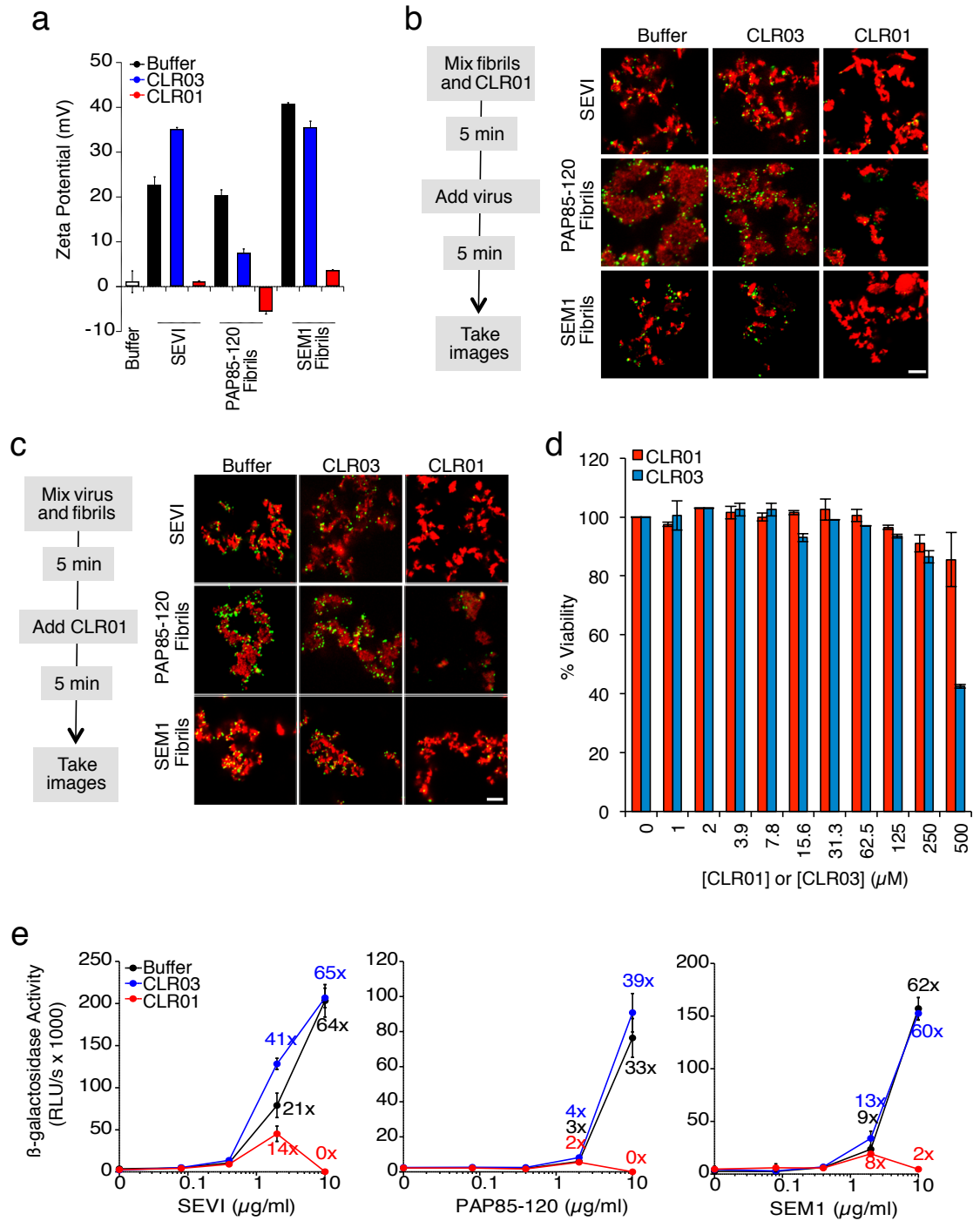


**Figure 3.7 CLR01 neutralizes the positive surface charge of seminal amyloids and abrogates their ability to bind virions and enhance HIV infection. (a)** Surface charge of seminal amyloids determined by zeta potential measurements. Fibrils were mixed with buffer, CLR01, or CLR03, and centrifuged for 10min at 20,000g. The pellets were resuspended in KCl and zeta potential was measured. Values represent means  $\pm$  SD ( $n = 3$ ). (Work from

collaborators in the Münch lab) **(b)** CLR01 inhibits binding of virus to semen-derived fibrils. Fibrils (200µg/ml) were pretreated with PBS, CLR01, or CLR03 in 20-fold excess for 5min and stained with Proteostat dye. MLV Gag-YFP particles were added 1:2 and allowed to incubate with pretreated fibrils for 5min. Samples were analyzed using confocal microscopy. Scale bar: 5µm. (Work from collaborators in the Münch lab.) **(c)** CLR01 displaces virions from fibrils (Work from collaborators in the Münch lab). MLV Gag-YFP particles (green) were incubated with Proteostat-stained seminal amyloids (red) for 5min. PBS, CLR01, or CLR03 were added at 20-fold excess, and after an additional 5min of incubation, samples were analyzed by confocal microscopy. Scale bar: 5µm. **(d)** CLR01 is not cytotoxic. TZM-bl cells were incubated for 3 days with the indicated concentrations of CLR01 or CLR03. Metabolic activity was measured in an MTT assay. Values shown are means ± SD (n = 3). (Work from collaborators in the Münch lab.) **(e)** CLR01 antagonizes the HIV-1 enhancing activity of seminal amyloids. SEVI, PAP85-120, and SEM1(49-107) fibrils were mixed with a 20-fold excess of CLR01 or CLR03. CCR5-tropic HIV-1 was added and samples were used to inoculate TZM-bl cells. Infection rates were determined 3 days post infection. Values represent mean β-galactosidase activities derived from triplicate infections ± SD (RLU/s: relative light units per second). Numbers above symbols indicate the n-fold enhancement of infection. (Work from collaborators in the Münch lab.)

### 3.2.7 CLR01 exhibits direct anti-HIV activity

In addition to engaging amyloid fibrils, our microscopy results (Figure 3.7b,c) led us to believe that CLR01 may be interacting directly with viral particles to alter their biophysical properties. To study the consequences of the latter interaction in more detail, two T-cell line-adapted CXCR4- and CCR5-tropic HIV-1 variants and two CCR5-tropic transmitted/founder viruses were pretreated with CLR01 or controls and then examined for infectivity. Remarkably, CLR01 but not CLR03 abrogated viral infectivity in a dose-dependent manner with IC<sub>50</sub> values ranging from 13.7 to 20.1µM (Figure 3.8a). This reduction in infectivity was only observed when virions were exposed to CLR01 and not when target cells were pretreated with the tweezer (Figure 3.8b). Thus, in addition to its anti-amyloid properties, CLR01 also has direct anti-HIV activity that appears to be independent of the viral coreceptor tropism or strain.

To define the underlying mechanism of this antiviral activity, we tested whether CLR01 disrupts the integrity of the viral membrane, leading to the release of the inner viral p24 capsid protein. HIV virions were exposed to buffer, CLR01 or CLR03 and then separated by centrifugation into a soluble fraction (containing free p24) and a sedimentable fraction (containing intact viral particles). ELISA measurements demonstrated that the amount of p24 was increased in the

soluble fraction of CLR01-treated samples as compared to samples treated with CLR03 or buffer (Figure 3.8c). Time course experiments revealed that a 5min incubation of virus with 10 $\mu$ M CLR01 resulted in a 62% decrease in HIV infectivity, while a 10min incubation achieved almost a 100% reduction (Figure 3.8d). Atomic force microscopy (AFM) of mouse leukemia virus particles (MLV) confirmed that treatment with CLR01 destroyed virion architecture (Figure 3.8e). This effect was independent of the presence of viral glycoproteins, since CLR01 also destroyed HIV-1 particles lacking gp120/41 ( $\Delta$ env) (Figure 3.8e), suggesting that CLR01 disrupts the integrity of the viral membrane.



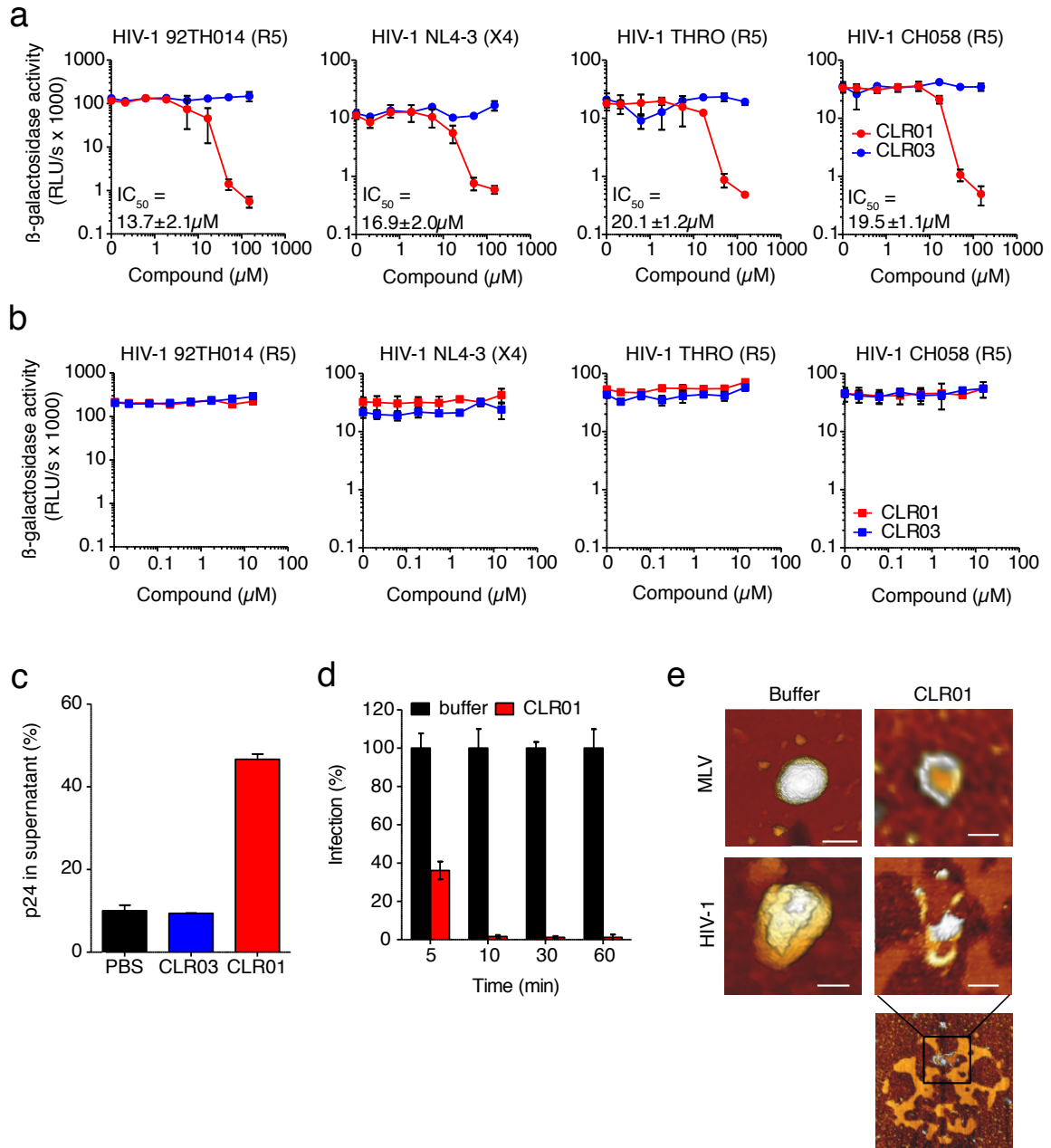


**Figure 3.8 CLR01 has direct anti-HIV-1 activity and destroys retroviral particles.** (a) CLR01 blocks HIV-1 infection by targeting virions. Two lab-adapted HIV-1 strains (92TH014 and NL4-3) and two transmitted/founder viruses (THRO and CH058) were incubated with CLR01 or CLR03 for 10min and then used to infect TZM-bl cells. Infection rates were determined 3 days post infection. Values represent mean  $\beta$ -galactosidase activities derived from triplicate infections  $\pm$  SD (RLU/s: relative light units per second). (Work from collaborators in the Münch lab.) (b) The antiviral activity of CLR01 is not directed against mammalian cells. TZM-bl cells were exposed to CLR01 or CLR03 for 1h. Thereafter, medium was removed and cells were infected with the indicated viruses. Infection rates were determined 3 days post infection. Values represent mean  $\beta$ -galactosidase activities derived from triplicate infections  $\pm$  SD (RLU/s: relative light units per

second). (Work from collaborators in the Münch lab.) **(c)** CLR01 releases p24 capsid antigen from HIV particles. HIV-1 was incubated with PBS, 100 $\mu$ M CLR03, or 100 $\mu$ M CLR01 and centrifuged at 20,000g and 4°C for 1h. The p24 content of the supernatant was determined via p24 ELISA. Values represent means  $\pm$  SD. (Work from collaborators in the Münch lab.) **(d)** HIV-1 was incubated at 37°C with or without 10 $\mu$ M CLR01. Aliquots were taken after different time points and analyzed regarding their infectivity using TZM-bl reporter cells. Values were derived from triplicate infection (n = 3) and give relative infection rates compared to the buffer control (100%). (Work from collaborators in the Münch lab.) **(e)** CLR01 destroys retroviral particles. Images obtained by atomic force microscopy (AFM) show single MLV and glycoprotein-deficient HIV particles before and after treatment with 100 $\mu$ M CLR01. Scale bar: 100 nm. (Work from collaborators in the Münch lab.)

### 3.2.8 CLR01 exhibits broad antiviral activity against enveloped viruses

Because of the surprising capability of CLR01 to destroy viral membranes, we sought to explore whether it could act as a general inhibitor of enveloped viruses. To test this idea, human cytomegalovirus (HCMV), herpes simplex virus type 2 (HSV-2), and hepatitis C virus (HCV) were treated with CLR01 or CLR03 and then assessed for their ability to infect target cells. Remarkably, CLR01, but not CLR03, reduced infection rates of all three analyzed enveloped viruses (Figure 3.9a-c). By contrast, CLR01 did not inhibit infection by the non-enveloped human adenovirus type 5 (HAdV5) (Figure 3.9d). Thus, the tweezer is a broad-spectrum inhibitor of enveloped viruses, including viruses that can be sexually transmitted such as HIV-1, HSV-2 and HCV.

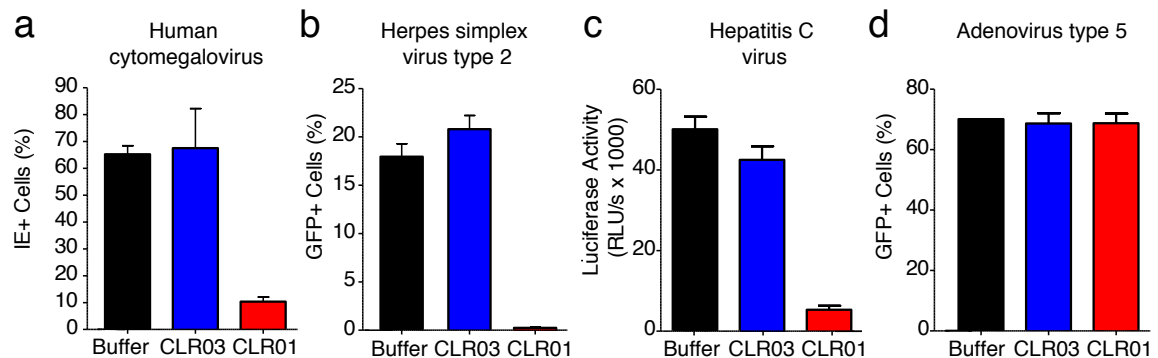


**Figure 3.9 CLR01 is a broad-spectrum inhibitor of enveloped viruses.** **(a)** Human cytomegalovirus was incubated with PBS, 100 $\mu$ M CLR03, or 100 $\mu$ M CLR01. Afterwards, HFF cells were infected and immediate early (IE) antigen positive cells were counted 1 d post infection as a measure for infectivity. Values are means  $\pm$  SD (n = 3). (Work from collaborators in the Münch lab.) **(b)** Herpes simplex virus type 2 comprising a GFP reporter gene was treated with

PBS, 100 $\mu$ M CLR03 or 100 $\mu$ M CLR01 and added to Vero cells. GFP-positive cells were counted using flow cytometry 2d post infection. Values represent means  $\pm$  SD (n = 3). (Work from collaborators in the Münch lab.) (c) A luciferase encoding hepatitis C virus was treated with 150 $\mu$ M CLR01 or 150 $\mu$ M CLR03 and used for infection of Huh-7.5 reporter cells. Infection was measured 3d post infection. Values represent means  $\pm$  SEM (n = 3). (Work from collaborators in the Münch lab.) (d) A GFP-reporter adenovirus type 5 was added to A549 cells after treatment with 158 $\mu$ M CLR01 or 158 $\mu$ M CLR03. GFP positive cells were counted using flow cytometry 1d post infection. Values represent means  $\pm$  SD (n = 3). (Work from collaborators in the Münch lab.)

### **3.2.9 CLR01 disrupts membranes enriched in lipid-raft domains**

The result that CLR01 destroys retroviral particles with IC<sub>50</sub> values between 10-20 $\mu$ M by compromising virion integrity was unexpected, especially because the tweezer does not affect cell viability at these concentrations [152, 155]. Despite the fact that viral envelopes are typically derived from portions of the host cell membrane, there are surprisingly dissimilarities in membrane composition between HIV and plasma membranes. For instance, viral membranes differ from cellular membranes in that they are 2-3-fold enriched in specific lipids such as sphingomyelin and cholesterol, which can form microdomains termed lipid rafts [210-213]. In addition, phosphatidylcholine and phosphatidylethanolamine, which are the major phospholipids comprising mammalian membranes, are depleted in viral membranes by a factor of 2.7 and 2.1, respectively [211]. Because of these disparities, it has been suggested that HIV particles display a more rigid membrane structure, and HIV budding occurs from specialized membrane subdomains [214], which is also proposed for influenza virus [215]. Hence, we hypothesized that CLR01 might more severely disrupt membranes with lipid-raft domains.

To test this hypothesis, preliminary studies were conducted using overly simplified model membranes whose composition was representative of viral or cell membranes. First, dye loaded giant unilamellar vesicles (GUV) were generated that consisted of either 1,2-dioleoyl-*sn*-glycero-3-phosphocholine (DOPC) to recapitulate a bilayer devoid of lipid rafts, or a mixture of DOPC, sphingomyelin and cholesterol (DOPC/SM/Chol) to more closely resemble a lipid raft-rich viral membrane. Strikingly, CLR01 permeabilized the model viral membrane within 5-10min while having no effect on the DOPC membrane, even after 60min of incubation (work from

collaborators in the Winter lab). These results were confirmed by AFM at higher spatial resolution. CLR01 treatment of a DOPC membrane that was deposited on mica surface did not affect bilayer stability, and the tweezer was homogeneously distributed on the scan area. By contrast, the DOPC/SM/Chol raft mixture appeared as coexisting liquid-disordered ( $l_d$ ) and liquid-ordered ( $l_o$ ) domains, and CLR01 addition induced changes in phase coexistence and decreased height differences between both phases (work from collaborators in the Winter lab). After 60min, distinct  $l_d$  and  $l_o$  domains were no longer visible, and CLR01 was homogeneously distributed in the remaining fluid phase. Thus, these initial studies highlight the dissimilarities in CLR01's effects on model membranes and suggest that CLR01 selectively disrupts heterogeneous lipid-raft enriched membranes. While this work is preliminary, we aim to further explore these effects and elucidate a mechanism to better understand CLR01's membrane permeabilizing activity in the future.

### **3.2.10 CLR01 antagonizes the infection enhancing property of human semen**

CLR01 binds exposed lysine and arginine residues in amyloid fibrils. These interactions might be hindered in the presence of bulk protein or conditions resembling those in seminal fluid. To address this issue, lyophilized PAP248-286 was dissolved in an artificial semen simulant (AS) [174, 216] containing 50mg/ml bovine serum albumin and agitated until fibril formation was complete. These PAP248-286(AS) fibrils were then diluted in AS and incubated with CLR01. A reduction in ThT fluorescence intensity to 43% of the initial value was detected (Figure 3.10a). This finding confirms that CLR01 maintains its disaggregating activity in a complex solution resembling seminal fluid, suggesting that CLR01 effectively targets SEVI fibrils in a complex mixture with competing lysine residues.

Next, we tested whether the molecular tweezer inhibited semen-mediated infection enhancement. Seminal plasma, which was obtained from pooled semen of ten donors, was treated with CLR01 or CLR03. Thereafter, a CCR5-tropic lab-adapted virus or a transmitted/founder virus were incubated with 10% of these solutions followed by infection of TZM-bl cells. As previously

observed [51, 108, 175, 204], seminal plasma markedly enhanced infection of both viruses by 10- or 8-fold, respectively (Figure 3.10b). CLR01 decreased viral infectivity in a concentration dependent manner, while CLR03 had no impact on semen-mediated infection enhancement. Remarkably, at a CLR01 concentration of 31 $\mu$ M, the enhancing effect of semen was completely abolished. Thus, CLR01 prevents HIV infection in the presence of semen.

Finally, we sought to determine whether the predominant mode of action of CLR01 was via its anti-amyloid activity or its direct anti-viral effect. To test this, seminal amyloid fibrils were incubated with a concentration of CLR01 that was sufficient to partially disassemble the fibrils. These solutions were subsequently diluted to reduce the concentration of CLR01 such that CLR01 could no longer exert a direct anti-viral effect against HIV (Figure 3.10c, left panel). This set-up allows us to solely examine the infectivity-promoting property of fibrils that were subject to CLR01 treatment, and we found that CLR01-treated fibrils retained their ability to boost HIV infectivity (Figure 3.10c, right panel). However, it should be stated that there are several caveats to this experiment. For instance, it is unclear what happens to fibrils in response to the dilution step. It is plausible that CLR01 may dissociate from fibrils and that fibrils could reform once CLR01 is unbound. Nonetheless, based on these results, we conclude that the primary mechanism for CLR01 activity is through its direct effect on the virus and any anti-amyloid activity plays a secondary role.

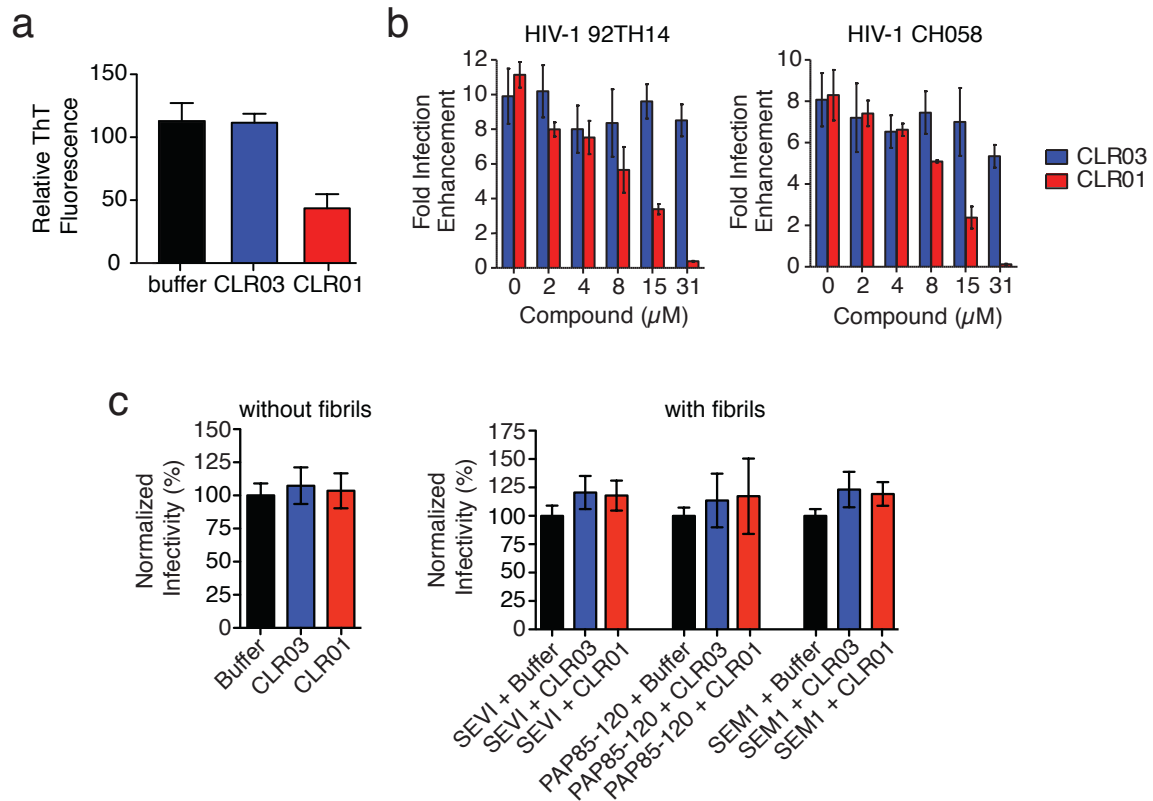


**Figure 3.10 CLRO1 diminishes the infection enhancing property of semen.** (a) SEVI fibrils were formed in an artificial semen simulant (AS) [216]. SEVI(AS) fibrils were then diluted to 20 $\mu$ M in AS and treated with 20 $\mu$ M CLR01 or CLR03, or with buffer for 2h. Fibril integrity was assessed using ThT fluorescence. Values represent means  $\pm$  SEM (n = 4). (b) CLRO1 abrogates semen-mediated enhancement of HIV infection. Seminal plasma (10%) or medium containing CLR01 or CLR03 was mixed with R5-tropic HIV-1 or transmitter/founder HIV-1 CH058. After 10min, TZM-bl cells were infected and infectivity was measured 3 days post infection. Shown are the n-fold increased infection rates obtained for semen-treated virus relative to those of medium-treated virus. Values represent means  $\pm$  SD (n = 4). (Work from collaborators in the Munch lab.) (c) SEVI, PAP85-120, or SEM1(45-107) fibrils (20 $\mu$ M) were treated with 100 $\mu$ M CLR01 or CLR03, or buffer for 3h. Samples were subsequently diluted by a factor of 5, and infectivity was assessed in TZM-bl cells and expressed as normalized infectivity to buffer-treated fibril samples. Values represent means  $\pm$  SEM (n = 3). HIV-1 CH058 virions (100 infectious units) were used.

### 3.3 Discussion

Despite the development of numerous different classes of microbicides, none have proven safe and effective at HIV prevention. The failure of microbicide candidates in previous clinical trials has been attributed to lack of adherence, adverse effects and a greatly diminished antiviral efficacy in the presence of semen. This bodily fluid is not only the main vector for HIV transmission but also

contains amyloid fibrils that markedly increase viral infectivity [179]. Thus, future endeavors should aim to focus on combination products that simultaneously target HIV and the host factors that are exploited by the virus to facilitate its transmission [179]. Here, we report that CLR01, a lysine-specific molecular tweezer, not only counteracts the infection-enhancing activity of seminal amyloids and semen, but also directly destroys HIV virions (Figure 3.11). The minimal *in vivo* toxicity and the combined anti-viral and anti-amyloid activities make this compound a highly promising microbicide candidate.

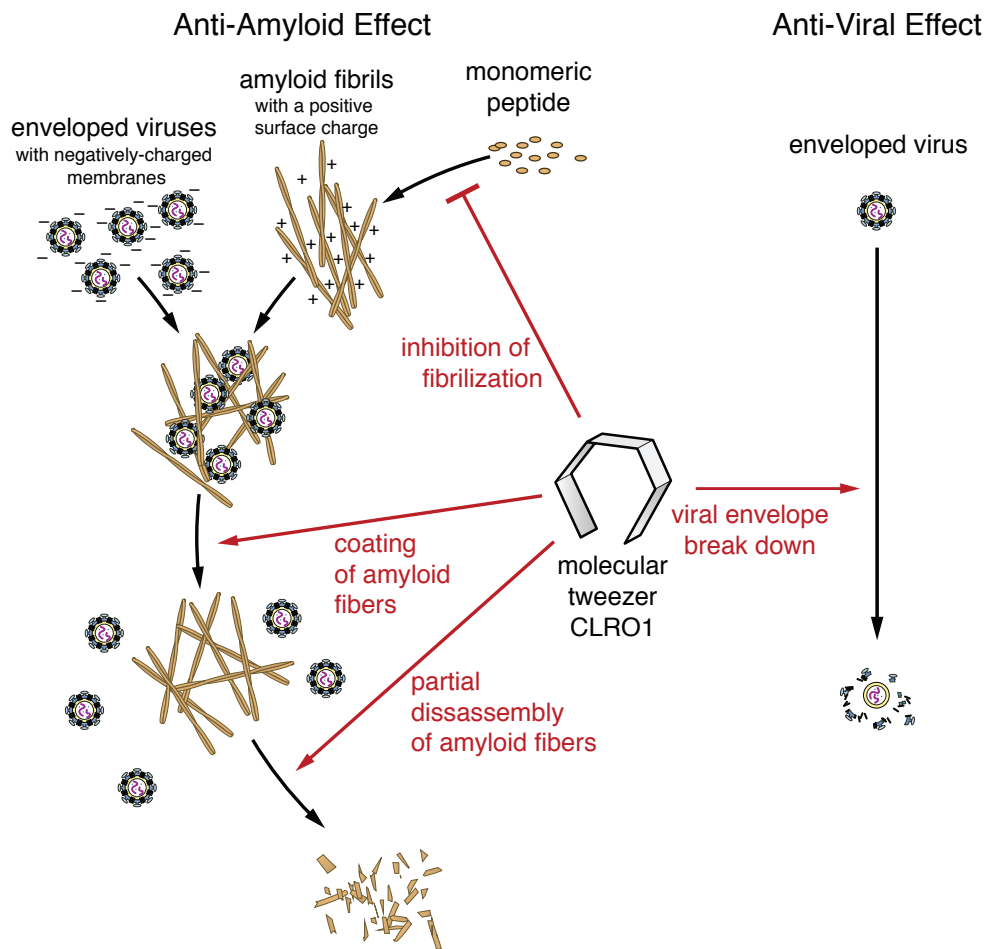


**Figure 3.11 Schematic overview of the anti-amyloid and anti-viral effects of CLR01.**

It was surprising that the tweezer not only affected the formation and function of seminal amyloids but also displayed a broad and direct antiviral activity against HIV and other enveloped viruses (Figure 3.11). Since the CLR03 control, which has a similar negative charge as CLR01 [152], was entirely ineffective at blocking viral infection, a purely polyanion-like mechanism that prevents the interaction of virions and cells by increasing charge repulsion [217, 218] could be excluded. Instead, our results demonstrate that CLR01 selectively disrupts membranes containing elevated levels of sphingomyelin and cholesterol. Envelopes of HIV-1, herpes viruses and HCV differ from the cellular plasma membrane as they are more highly enriched in these and other lipids [211, 212, 219, 220]. We investigated whether the tweezer might recognize the charged lipid head groups but found via NMR shift experiments that this was not the case. However, experiments on various phase boundaries strongly indicated that the tweezer could migrate into lipid bilayers due to its amphiphilic character. A pronounced destabilizing effect may be triggered if this happens at the edge of lipid rafts that are enriched in virion membranes. Importantly, HSV-2, HCMV and HCV can also be transmitted via sexual intercourse [221-223]. Thus, a CLR01-based microbicide would not only protect from HIV-1 acquisition but also from other major human pathogens.

CLR01 binding to lysine residues could potentially disrupt normal protein function leading to toxicity or side effects. However, CLR01 showed no signs of cytotoxicity in this study and has previously been safely employed in multiple cell and animal models [152, 154, 155, 157]. For instance, zebrafish treated with CLR01 showed suppressed  $\alpha$ -synuclein aggregation in neurons with no signs of toxicity [154]. In a mouse model of Alzheimer's disease, transgenic mice given CLR01 showed a decrease in brain amyloid- $\beta$  aggregates with no apparent toxicity or adverse effects [155].

Unlike previous microbicide candidates that block HIV infection by a single mechanism, a CLR01-based formulation would interfere with various essential steps in sexual HIV transmission (Fig. 3.11). On a minute time frame, the tweezer destroys infectious HIV particles that are present in



semen, prevents the formation of amyloid/virus complexes by neutralization of the fibril surface charge, and also displaces pre-bound virions from fibrils. On a longer time frame (hours), CLR01 not only prevents the formation of infection-enhancing seminal amyloids upon ejaculation but also remodels fibrils that are already abundant in semen after ejaculation or formed during semen liquefaction. Given the timeframe of these effects, we suggest that the primary mechanism of CLR01 action is via its direct effect on the virus, and that the anti-amyloid effects, although potent, play a secondary role. Regardless, these combined anti-viral and anti-amyloid activities and the encouraging safety data make CLR01 a highly promising broad-spectrum microbicide against HIV-1 and other sexually transmitted viruses.

## **CHAPTER 4: EPIGALLOCATECHIN-3-GALLATE RAPIDLY ERADICATES PAP85-120, SEM1(45-107), AND SEM2(49-107) SEMINAL AMYLOID FIBRILS**

### **4.1 Introduction**

Human immunodeficiency virus (HIV), which causes acquired immunodeficiency syndrome (AIDS), remains one of the most pressing global health challenges. The global HIV/AIDS prevalence rate is 0.8% and the majority of infections are transmitted heterosexually [169]. Semen harbors amyloid fibrils that potently enhance HIV infectivity in vitro [17, 57, 58]. Specifically, proteolytic fragments of prostatic acid phosphatase (PAP248-286 and PAP85-120), semenogelin 1 (SEM1), and semenogelin 2 (SEM2) form fibrils that boost infectivity by electrostatically facilitating viral attachment to target cells [17, 57, 58, 68]. This enhancement of infection can be as large as several orders of magnitude and is independent of viral genotype and coreceptor tropism as well as the virus producer and target cell type [224]. Remarkably, the stimulatory effect of SEVI fibrils is greatest at low virus concentration, similar to the conditions observed in mucosal transmission of HIV, where relatively few virions traverse the mucosal barrier and initiate infection [20]. Devising a method to rapidly dissolve seminal amyloid fibrils would provide a novel and urgently needed preventative, microbicidal strategy for reducing HIV infection via sexual transmission [179].

We sought small molecules that might disrupt seminal amyloid, as seminal fluid contains various proteases that could threaten the integrity of protein-based agents [225]. However, small molecules that disrupt the highly stable, self-templating amyloid form remain rare [226]. One notable exception is epigallocatechin-3-gallate (EGCG), the major catechin from green tea, which exerts a wide range of antioxidant, anti-cancer, anti-aging, and anti-viral effects, while also exhibiting cardioprotective and neuroprotective properties [227-230]. Interestingly, EGCG can potently inhibit the amyloidogenesis of various polypeptides and can also disassemble a wide range of preformed amyloid fibrils [116, 160-162, 231, 232]. Moreover, EGCG has been shown

to: inhibit formation of PAP248-286 fibrils termed SEVI (Semen derived Enhancer of Viral Infection) via interaction with charged side chains [109]; dose-dependently deconstruct preformed SEVI fibrils [108]; and reduce both SEVI- and semen-mediated enhancement of HIV infection [67, 108]. Importantly, EGCG (0.4mM) was found to have an inhibitory effect on 41 out of 47 individual semen samples with a median inhibition of infection of ~70.6% [67].

Here, we investigated the effect of EGCG on other seminal amyloid conformers formed by PAP85-120, SEM1(45-107), and SEM2(49-107). Because numerous proteolytic peptide fragments of SEM1 and SEM2 can assemble into amyloid fibrils that promote HIV infection, we focused on the SEM1(45-107) and SEM2(49-107) fragments as representative samples. We found that EGCG eradicates PAP85-120, SEM1(45-107), and SEM2(49-107) fibrils, and this deconstruction of amyloid occurs on a drastically more rapid time scale than has been observed with SEVI fibrils. Our findings establish EGCG as the first small molecule shown to eliminate all four classes of seminal amyloid.

## **4.2 Results**

### **4.2.1 EGCG slowly disassembles SEVI fibrils**

The small molecule epigallocatechin-gallate (EGCG), a potent antioxidant found in green tea, has previously been shown to dose-dependently disassemble SEVI fibrils over 24-48 h [108]. We confirmed this gradual disassembly, as a drastic decrease in ThT fluorescence intensity was not observed until SEVI fibrils were treated with a ten-fold excess of EGCG for 24 h (Figure 4.1a). TEM verified that fibrils were still the predominant species present after a 2h treatment with EGCG (Figure 4.1b). Furthermore, we found that SEVI fibrils pre-treated with EGCG for 6h could still effectively 'seed' the fibrillization of monomeric PAP248-286 (Figure 4.1c). Thus, EGCG is unable to eliminate self-templating activity or remodel SEVI into a non-amyloid form on this timescale (Figure 4.1c). After a longer 24h treatment, however, a striking change in morphology

was observed by TEM, where significantly smaller structures were observed in place of fibrils (Figure 4.1b). Thus, we confirm previous observations that EGCG remodels SEVI fibrils [108].

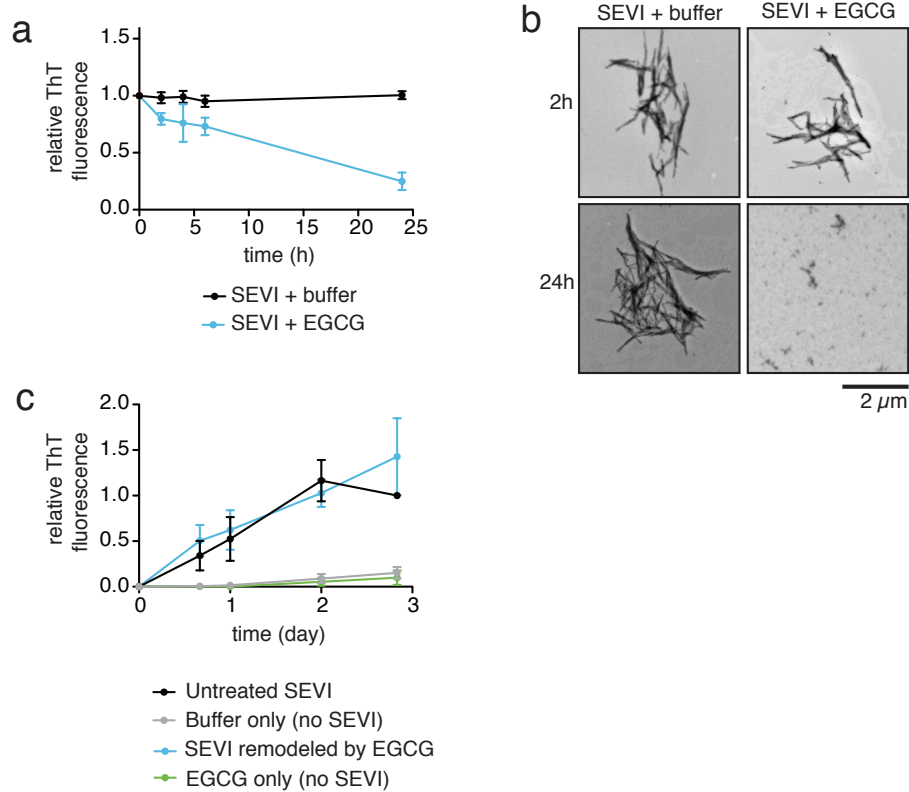


**Figure 4.1 EGCG slowly remodels SEVI fibrils into non-amyloid structures.** (a) Preformed SEVI fibrils (20μM) were incubated with buffer (untreated) or EGCG (200μM) for 0-24 h. Fibril integrity was assessed by ThT fluorescence. Values represent means ± s.e.m. (n=4). (b) Transmission electron micrographs of SEVI fibrils incubated with buffer (untreated) or EGCG for 2h or 24h. (c) SEVI fibrils (20μM) were incubated with buffer (untreated) or EGCG (200μM) for 6h, and the resulting products were used to seed soluble PAP248-286 (1mM, 0.1% fibril seed) fibrillization. Buffer conditions lacking fibril seed were included. Fibril assembly was monitored by ThT fluorescence. Values represent means ± s.e.m. (n=4).

#### 4.2.2 EGCG rapidly eliminates PAP85-120 fibrils

Next, we explored the effect of EGCG on other amyloid fibrils present in semen. Since a multitude of seminal amyloid fibrils have been discovered, it would be advantageous to develop agents that possess broad anti-amyloid activity against a range of amyloid conformers in order to effectively

antagonize amyloid-mediated HIV infectivity enhancement [179]. Hence, we investigated whether EGCG could disrupt PAP85-120, SEM1(45-107), and SEM2(49-107) fibrils.

Using a ten-fold excess of EGCG, we found that the ThT fluorescence intensity of PAP85-120 fibrils decreased to ~55% of the initial value immediately after the addition of EGCG (Figure 4.2a). Several studies have shown that EGCG does not interfere with ThT fluorescence by some non-specific mechanism [116, 160, 161, 232]. Thus, we attribute this rapid decay of ThT fluorescence to rapid fibril remodeling, which has also been observed with EGCG and amylin fibrils [160, 232]. A further reduction of ThT fluorescence to ~27% was seen after 2h of treatment with EGCG, and after 6h, the ThT fluorescence intensity dropped by ~95%. The disassembly of PAP85-120 by EGCG occurred significantly more rapidly than that observed with SEVI fibrils, which were largely intact after 6h (Figure 4.1a). Analysis of PAP85-120 fibrils treated with EGCG for 6h by TEM showed predominately small, non-fibrillar species, as well as a few short fibrils (Figure 4.2b). Thus, EGCG rapidly eliminates PAP85-120 fibrils.

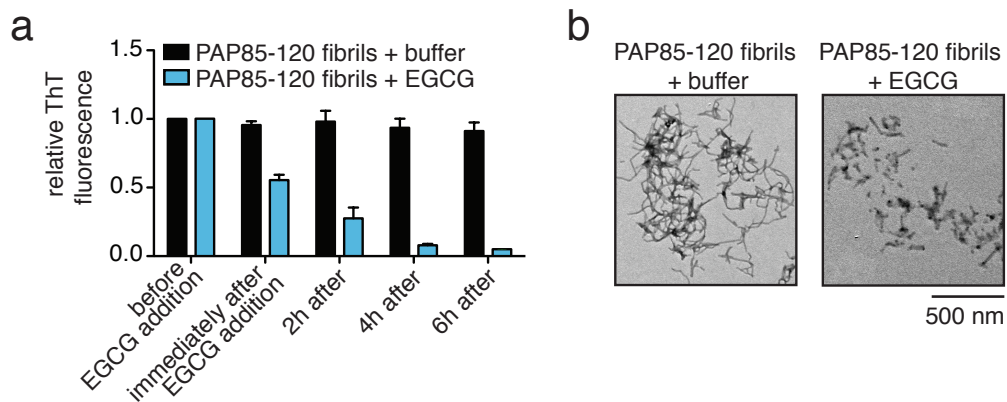


**Figure 4.2 EGCG rapidly disassembles PAP85-120 amyloid fibrils.** (a) PAP85-120 fibrils (20 $\mu$ M) were incubated with buffer (untreated) or EGCG (200 $\mu$ M) for 0-6h. Fibril integrity was assessed by measuring ThT fluorescence intensity. Values represent means  $\pm$  s.e.m. (n=3). (Work of Rebecca Hammond, Shorter lab.) (b) Transmission electron micrographs of PAP85-120 fibrils incubated with buffer (untreated) or EGCG for 6 h. (Work of Rebecca Hammond, Shorter lab.)

### **4.2.3 EGCG rapidly eliminates SEM1(45-107) and SEM2(49-107) fibrils**

Next, we tested whether EGCG could also remodel SEM1(45-107) and SEM2(49-107) fibrils. The ThT fluorescence intensity decayed drastically to ~25% of the initial value for SEM1(45-107) and ~30% for SEM2(49-107) immediately following the addition of a ten-fold excess of EGCG (Figure 4.3a,b). Only a minor additional decline in ThT intensity to ~18% of the initial value was observed for SEM1(45-107) fibrils after 24h of incubation with EGCG (Figure 4.3a). After 6h, EGCG reduced ThT fluorescence of SEM2(49-107) fibrils to ~20% of the initial value (Figure 4.3b). This rapid disintegration of SEM1(45-107) and SEM2(49-107) fibrils by EGCG was unexpected and strongly suggests that EGCG disrupts critical contacts that are required for SEM1(45-107) and SEM2(49-107) fibril stability. Examination by TEM revealed that EGCG-remodeled SEM1(45-107) and SEM2(49-107) products were also very small non-fibrillar structures, illustrating the efficiency and completeness of the disaggregation (Figure 4.3c,d). Thus, EGCG rapidly eliminates SEM1(45-107) and SEM2(49-107) fibrils.

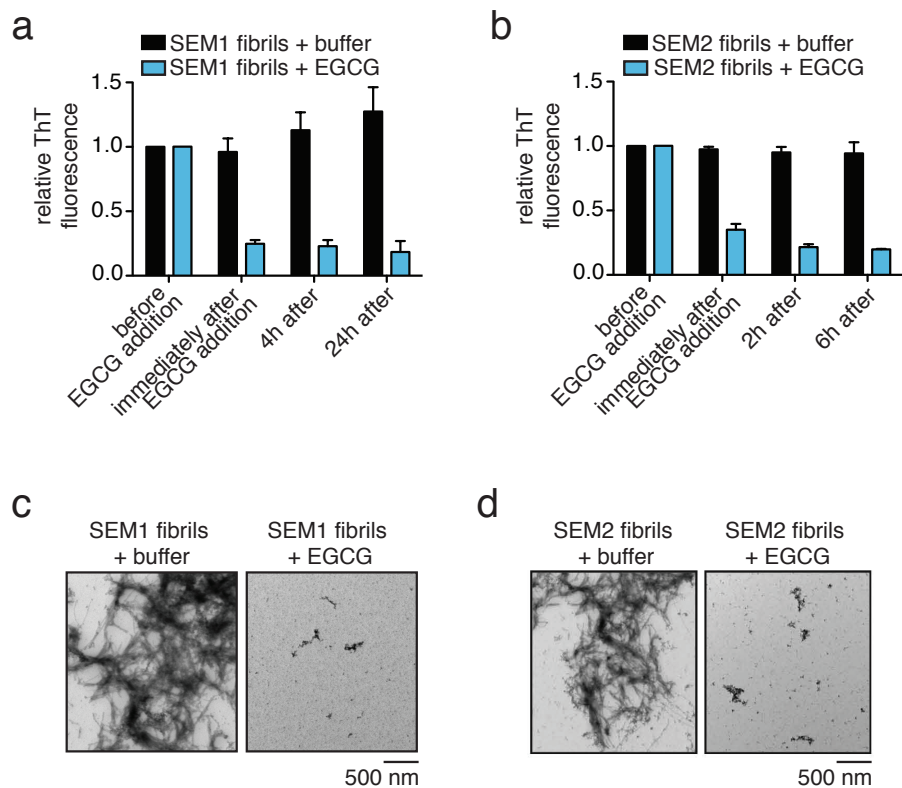


**Figure 4.3 EGCG rapidly eliminates SEM1(45-107) and SEM2(49-107) fibrils.** (a) SEM1(45-107) fibrils (20 $\mu$ M) were incubated with buffer (untreated) or EGCG (200 $\mu$ M) for 0-24h. Fibril integrity was assessed by measuring ThT fluorescence intensity. Values represent means  $\pm$  s.e.m. (n=3). (Work of Rebecca Hammond, Shorter lab.) (b) SEM2(49-107) fibrils (20 $\mu$ M) were incubated with buffer (untreated) or EGCG (200 $\mu$ M) for 0-6h. Fibril integrity was assessed by measuring ThT fluorescence intensity. Values represent means  $\pm$  s.e.m. (n=3). (Work of Rebecca Hammond, Shorter lab.) (c, d) Transmission electron micrographs of SEM1(45-107) fibrils (c) or SEM2(49-107) fibrils (d) incubated with buffer (untreated) or EGCG for 2h. (Work of Rebecca Hammond, Shorter lab.)

#### 4.2.4 EGCG inhibits HIV infectivity in cell culture

EGCG is the first agent that has been found to disrupt the amyloid architecture of all four classes of seminal amyloids that have been identified (SEVI, PAP85-120, SEM1, and SEM2). Since previous work reported that EGCG counteracts the viral infection enhancing activity of SEVI [108], we next sought to determine whether the products of PAP85-120, SEM1(45-107) and SEM2(49-107) fibril remodeling by EGCG also had a reduced capacity to boost HIV infectivity. However, our analysis was confounded, since EGCG on its own exhibited a marked anti-viral

effect against three different HIV strains that were tested (Figure 4.4). At a concentration of only 0.25 $\mu$ M EGCG, viral infectivity was reduced to ~61%, ~35%, and ~11% of the control condition against the HIV-1 viral strains BL2, BaL, and 89.6, respectively (Figure 4.4). When the EGCG concentration was increased to 1.25 $\mu$ M or higher, the infectivity of all three strains was essentially abolished. None of the EGCG concentrations tested were toxic to cells (data not shown). The anti-HIV effect of EGCG has been previously described and is proposed to occur through a variety of diverse mechanisms [233]. This direct anti-viral property in combination with the ability of EGCG to remodel SEVI, PAP85-120, SEM1(45-107) and SEM2(49-107) seminal amyloids highlight the potential for the use of EGCG in a preventative HIV microbicide with dual mechanisms of action.

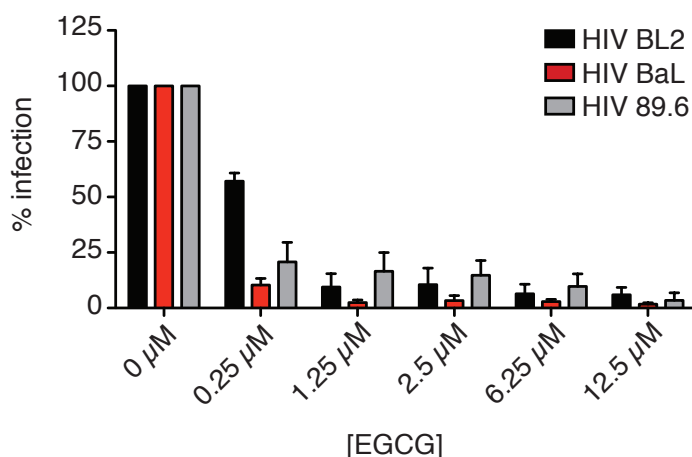


**Figure 4.4 EGCG inhibits HIV infectivity in cell culture.** TZM-bl cells were infected with three HIV-1 strains (BL2, BaL, and 89.6) in the presence of the indicated concentrations of EGCG, which represent the final concentrations in cell culture. Infectivity was monitored by measuring luciferase activity in the cell cultures (in RLU). Background activities derived from uninfected cells were subtracted. Values represent means  $\pm$  s.e.m. (n=3).

#### 4.3 Discussion

Here, we show that in addition to disaggregating SEVI fibrils [108], EGCG can dismantle PAP85-120, SEM1(45-107), and SEM2(49-107) fibrils rapidly and completely. EGCG is the first reported



agent that can remodel all four classes of seminal amyloid identified to date. PAP85-120, SEM1(45-107), and SEM2(49-107) fibrils were remodeled by EGCG more rapidly than SEVI fibrils, indicating that the cross- $\beta$  contacts that maintain PAP85-120, SEM1(45-107), and SEM2(49-107) fibrils are more susceptible to disruption by EGCG. Because we also observed complete inhibition of three HIV strains by micromolar concentrations of EGCG in our experimental paradigm, we were unable to investigate the infectivity-enhancing potential of the disassembled products.

Preliminary experiments have been conducted to further characterize EGCG-remodeled products. These studies have suggested that it is unlikely that EGCG is solubilizing seminal amyloid into peptide monomers, but is instead inducing a conformational conversion of seminal amyloid into highly SDS-resistant structures. Similar results have been observed previously, and in fact, EGCG was found to remodel  $\alpha$ -synuclein fibrils, A $\beta$ 42 fibrils, and A $\beta$ 42 oligomers causing a considerable increase in the amount of SDS-stable structures [161]. Additional experiments examining the nature of EGCG-remodeled seminal amyloid products are ongoing.

EGCG has also been shown to inhibit the infection-enhancing properties of both SEVI and semen [67, 108]. In a minority of individual semen samples, however, this enhancement was resistant to EGCG treatment, and reasons for this variability remain to be further elucidated. In this regard, it is interesting to note that EGCG can exhibit differential ability to remodel distinct yeast Sup35 prion strains [116, 119, 234]. By analogy, it is plausible that seminal peptides might also be capable of assembling into EGCG-resistant amyloid polymorphs in a minority of individuals. It therefore becomes important to elucidate small molecule combinations that disrupt all seminal amyloid strains [116, 119, 234].

Finally, EGCG exhibits pronounced antiretroviral effects in the absence of seminal amyloid and affects a multitude of steps in the HIV replication cycle. Specifically, EGCG inhibits cell entry by

obstructing the attachment of viral gp120 to CD4 T cells [235, 236], and viral replication through inhibition of Tat-induced LTR transactivation [237]. EGCG has also been proposed to function as an allosteric reverse transcriptase inhibitor [238] and an integrase inhibitor [239]. Interestingly, EGCG also exerts anti-viral effects on both herpes simplex virus (HSV) [240] and Hepatitis C virus (HCV) [241]. In each of these cases, EGCG is believed to interact with either HSV or HCV glycoproteins, thus inhibiting cell entry by the virus. The combined anti-amyloid and anti-viral effects of EGCG make it a promising candidate for use in a vaginal microbicide with diverse modes of action.

## CHAPTER 5: CONCLUSIONS AND FUTURE DIRECTIONS

### 5.1 Conclusions

In this thesis, we have deciphered several strategies to counteract amyloid-mediated enhancement of HIV infection. In Chapter 1, we explored the use of a protein disaggregase from yeast, Hsp104, to antagonize seminal amyloid. We characterized three predominant modes of action of Hsp104 that inhibited seminal amyloid activity: 1) Hsp104 remodeled SEVI and PAP85-120 fibrils into non-amyloid aggregates, 2) Hsp104 and enzymatically inactive Hsp104 scaffolds induced the clustering of seminal amyloid into larger species, and 3) Hsp104 was modified to interact with a bacterial peptidase resulting in degradation of seminal amyloid substrates. In Chapter 2, we establish that a small molecule lysine-specific “molecular tweezer,” CLR01, partially remodeled seminal amyloid and abrogated the ability of seminal amyloid and semen to boost HIV infection. Surprisingly, CLR01 also directly inhibited infection by HIV and other enveloped viruses by selectively disrupting the integrity of enveloped virions, although the exact mechanism behind this effect remains to be further elucidated. Finally, in Chapter 3, we demonstrated that the compound epigallocatechin gallate (EGCG) is the first small molecule to eradicate all four classes of seminal amyloid, and we confirmed that EGCG also has direct anti-HIV activity.

Our results that CLR01 and EGCG both displayed direct anti-viral activity against HIV made it difficult to ascertain the effects of remodeled seminal amyloid fibrils on HIV infection enhancement. However, there are certainly advantages to small molecules that possess both anti-amyloid and anti-viral activities, as they can directly antagonize virions and also counteract the host-derived factors that play a role in viral transmission. Such dual-functioning compounds could present as promising microbicide components to prevent HIV transmission. Nevertheless, our work with Hsp104 has conclusively demonstrated that strategies aimed at targeting and

inhibiting seminal amyloid are practicable and valuable approaches for reducing HIV transmission.

Despite the development of numerous different classes of microbicides, none have proven effective at HIV prevention in clinical trials. The failure of these compounds raised questions about what factors could impact microbicide efficacy and highlighted our incomplete understanding of the complexities that occur during sexual transmission. One important factor that has contributed to microbicide inefficiency is reduction of antiviral activity in the presence of semen [242]. Preclinical models do not typically accurately replicate what occurs during heterosexual transmission, where semen and female genital tract secretions could potentially modulate microbicide efficacy. In fact, seminal proteins were found to interfere with the antiviral activity of PRO 2000 and cellulose sulfate by competitively inhibiting binding of microbicide compounds to the viral envelope [243-245]. In addition, other polyanion microbicide candidates including carrageenan, cellulose acetate phthalate, poly(naphthalene sulfonate), and polystyrene sulfonate, were all found to have considerably reduced HIV inhibitory activity in the presence of seminal plasma [94]. These instances emphasize the significance of testing potential microbicides under conditions reflective of sexual transmission. Importantly, EGCG abrogates semen-mediated enhancement of virus infection [246], and we have shown that CLR01 also markedly reduces the infectivity promoting property of semen and targets amyloid fibrils in a solution resembling seminal fluid. These experiments highlight the utility and potential efficacy of these agents as candidate microbicides. In the future, it will also be crucial to conduct similar studies with Hsp104 to examine whether Hsp104 can counteract seminal amyloid in the presence of semen.

## **5.2 Future Directions**

In Chapter 2, we find that seminal amyloid fibrils must be disseminated to retain their HIV infection promoting capability, and Hsp104 can reduce amyloid mediated infection enhancement

by clustering fibrils into larger assemblies. A key future experiment would be to pinpoint short, specific regions within the Hsp104 sequence that mediate clumping of seminal amyloid fibrils. Using this novel approach, we can design peptide-based inhibitors to block seminal amyloid functionality. With these principles in mind, we could also conduct a small molecule screen to identify compounds that function similarly to induce the formation of larger seminal amyloid aggregates. A small molecule that can counteract seminal amyloid in this way may be a more feasible option for a microbicide candidate than a large biologic like Hsp104 or even a small peptide, since semen contains an abundance of seminal proteases that could interfere with their stability.

In this thesis, we have identified several methods to remodel, disassemble, and even degrade seminal amyloid fibrils. In the future, it will be interesting to combine sequential strategies to further enhance amyloid clearance. For example, we could remodel seminal amyloid using the small molecules CLR01 or EGCG, and then subsequently subject the remodeled products to the HAP-ClpP proteolytic system. By incorporating an initial step to partially disassemble the amyloid substrate, we could potentially enhance amyloid degradation and clearance with HAP-ClpP, and therefore preclude amyloid from reforming. This strategy could also be developed for intractable amyloids involved in other human diseases as well.

An important next step in reinforcing the potential utility of Hsp104, CLR01, and EGCG as topical microbicides will be to assess the inflammatory potential of these agents and ensure that they do not induce pro-inflammatory responses or disruption of the vaginal epithelium, as these adverse reactions could actually increase HIV infection. It is also crucial to think about the use of these agents in terms of how they fit into a natural biological setting. For example, if these compounds/proteins are to be used as a component of a vaginal microbicide, we must consider their efficacy in the setting of the vaginal extracellular matrix. Fibronectin has been identified as a natural and consistent interaction partner of seminal amyloid fibrils, and it even synergistically

increases the infectivity enhancing property of seminal amyloid [247]. Thus, it will important to decipher how effective Hsp104, CLR01, and EGCG are at targeting seminal amyloid fibrils that are bound to natural interaction partners.

Another key future goal in the continuation of this research project is to pre-clinically test Hsp104, CLR01, and EGCG for microbicide safety and efficacy. However, one of the major limitations in microbicide development is the lack of an animal model that recapitulates the principal features of HIV infection in humans. Humanized mouse and nonhuman primate models could be used to test the efficacy of our anti-amyloid (and anti-viral) agents as potential microbicides. However, there are still many limitations to such experiments, and because seminal amyloid has not been identified in other species, these models would not accurately replicate the physiological context of human sexual virus transmission.

## CHAPTER 6: MATERIALS AND METHODS

### 6.1 Small molecules and seminal plasma

EGCG was obtained from Sigma-Aldrich and stock solutions of 10mM were freshly prepared daily in assay buffer (25mM HEPES, 150mM KOAc, 10mM Mg(OAc)<sub>2</sub>, pH 7.4). CLR01 and CLR03 were generated as described previously [151], and 10mM stock solutions were prepared in Gibco Ultrapure water and frozen at -20°C. Poly-L-lysine hydrobromide (molecular weight 4,000-15,000 by viscosity) was purchased from Sigma-Aldrich and stock solutions of 10mM were prepared in assay buffer and frozen at -20°C. Seminal plasma represents the cell-free fraction of pooled human semen centrifuged at 20,000g for 30min at 4°C. The artificial semen simulant was prepared as described previously [216].

### 6.2 Peptides and amyloid formation

Lyophilized peptides were reconstituted and assembled into fibrils as described [17, 57, 58]. Synthetic peptides PAP248-286 (SEVI), PAP248-286(Ala), PAP85-120, and SEM1(45-107) or (49-107) were purchased from Keck Biotechnology Resource Laboratory (Yale University, New Haven, CT) or Celtek peptides. Synthetic PAP85-120(Ala) was obtained from Bachem.

**PAP248-286:** Briefly, lyophilized PAP248-286 (1-2mg) was dissolved in 100µL of PBS and passaged through a 0.2µm filter. The concentration of a 1:10 diluted sample was determined by measuring absorbance at 280nm on a Nanodrop spectrophotometer using an extinction coefficient of 2980M<sup>-1</sup>cm<sup>-1</sup>. The concentration was then adjusted with PBS to result in a 100µL aliquot of a 1mM peptide solution, which was then agitated at 37°C and 1400rpm (Eppendorf Thermomixer) for ~72h. All subsequent SEVI fibrils were assembled by adding 1% preformed fibril seed to soluble PAP248-286 solutions and agitating at 37°C and 1400rpm overnight.

**PAP85-120:** Lyophilized PAP85-120 (1-2mg) was first dissolved in 100µL of 1,1,1,3,3,3-hexafluoro-2-propanol (HFIP) to remove preformed aggregates. HFIP was removed by drying in a speed vacuum for 30min. The resulting film was dissolved in Gibco UltraPure water and

passed through a 0.2 $\mu$ m filter. The concentration of a 1:10 diluted sample was determined by measuring absorbance at 280nm on a Nanodrop spectrophotometer using an extinction coefficient of 4470M<sup>-1</sup>cm<sup>-1</sup>. The concentration was then adjusted with Gibco UltraPure water to result in a 100 $\mu$ L aliquot of a 1 mM peptide solution, which was then agitated at 37°C and 1400rpm for 24-48h.

**SEM1 and SEM2 peptides:** Lyophilized SEM1(45-107) or SEM2(49-107) (~1mg) were dissolved in either 100 $\mu$ L of PBS or 0.123M sodium phosphate buffer and passed through a 0.2 $\mu$ m filter. The concentration of a 1:10 diluted sample was determined by measuring absorbance at 280nm on a Nanodrop spectrophotometer using an extinction coefficient of either 5960M<sup>-1</sup>cm<sup>-1</sup> (SEM1) or 8480M<sup>-1</sup>cm<sup>-1</sup> (SEM2). The concentration was then adjusted to result in a 100 $\mu$ L aliquot of a 0.5mM peptide solution, which was then agitated at 37°C and 1400rpm for 7 days.

**PAP248-286(Ala):** Lyophilized PAP248-286(Ala) (1.5mg) was dissolved in 500 $\mu$ L of PBS. The solution was heated at 99°C for 5min to improve solubility and was subsequently passed through a 0.2 $\mu$ m filter to remove insoluble material. The concentration was determined by measuring absorbance at 280nm on a Nanodrop spectrophotometer using an extinction coefficient of 2980M<sup>-1</sup>cm<sup>-1</sup>. The concentration was then adjusted with PBS to result in a 100 $\mu$ L aliquot of a 100 $\mu$ M peptide solution, which was then agitated at 37°C and 1400rpm for 24h.

**PAP85-120(Ala):** Lyophilized PAP85-120(Ala) (1mg) was dissolved in 100 $\mu$ L of Gibco UltraPure water and passed through a 0.2 $\mu$ m filter to remove insoluble material. The concentration was determined by measuring absorbance at 280nm on a Nanodrop spectrophotometer using an extinction coefficient of 4470M<sup>-1</sup>cm<sup>-1</sup>. The concentration was then adjusted with Gibco UltraPure water to result in a 100 $\mu$ L aliquot of a 100 $\mu$ M peptide solution, which was then agitated at 37°C and 1400rpm for 24h.

### 6.3 Protein expression and purification

**Untagged Hsp104 variants:** Hsp104 variants were generated using QuikChange Lightning Site-Directed Mutagenesis (Agilent). Untagged Hsp104 variants in a pNOTAG vector (WT, HAP,



DWB, and A503V) were overexpressed in BL21(DE3)-RIL *E. coli* cells and induced with 1mM IPTG overnight at 15°C. Untagged Hsp104 variants were purified using Affi-Gel Blue (Bio-Rad) followed by Resource Q anion-exchange chromatography as described [183]. Briefly, cells were harvested via centrifugation (4000rpm, 20min, 4°C) and resuspended in lysis buffer (50mM Tris pH 8, 10mM MgCl<sub>2</sub>, 2.5% glycerol, 2mM β-mercaptoethanol, 5μM pepstatin A, complete protease inhibitor cocktail (1 EDTA-free tablet per 50mL (Roche))). Cells were lysed by sonication, and cell debris was removed via centrifugation (16,000rpm, 20min, 4°C). A 50% slurry of Affi Blue (Bio-Rad) equilibrated in lysis buffer was added to the supernatant and samples were rotated for 4h at 4°C. The beads were washed 3 times with wash buffer (50mM Tris pH 8, 10mM MgCl<sub>2</sub>, 2.5% glycerol, 2mM β-mercaptoethanol, 100mM KCl) and collected after each wash by centrifugation (2000rpm, 2min, 4°C). The protein was eluted from the Affi-Blue resin by incubating with elution buffer (50mM Tris pH 8, 10mM MgCl<sub>2</sub>, 2.5% glycerol, 2mM β-mercaptoethanol, 1M KCl) for 30 minutes. Following elution, the protein was buffer exchanged into Buffer Q (20mM Tris pH 8, 0.5mM EDTA, 5mM MgCl<sub>2</sub>, 50mM NaCl) using centrifugal filter units (Amicon). The protein was further purified via Resource Q anion exchange chromatography using a gradient of buffer Q+ (20mM Tris pH 8, 0.5mM EDTA, 5mM MgCl<sub>2</sub>, 1M NaCl). Hsp104 typically elutes around 31-34% Buffer Q+. Hsp104-containing fractions were collected, buffer exchanged into Hsp104 storage buffer (40mM HEPES pH 7.4, 150mM KCl, 20mM MgCl<sub>2</sub>, 10% glycerol, 1mM DTT), snap frozen, and stored at -80°C.

**His-tagged proteins:** His-tagged proteins (ClpP, ClpB, GFP, Hsp104<sup>1-548</sup>, and Hsp104<sup>773-908</sup>) were purified using Ni Sepharose 6 Fast Flow (GE Life Sciences) following standard procedures. See Table 1 for overexpression, induction, and storage conditions for each his-tagged protein. The reported concentrations of Hsp104 or ClpB refer to the hexamer and ClpP to the 14-mer unless otherwise indicated. Hsp70, Hsp40, DnaK, DnaJ, and GrpE were from Enzo Life Sciences.

**Table 1: Expression, induction, and storage conditions for purification of his-tagged proteins**

His-tagged protein	Cells used for expression	Induction conditions	Storage buffer
<b>ClpP</b>	BL21(DE3)	1mM IPTG for 3.5h at 37°C	20mM Tris pH 7.5, 100mM KCl, 0.1mM EDTA, 10% glycerol, 5mM DTT
<b>ClpB</b>	M15	1mM IPTG overnight at 15°C	40mM HEPES pH 7.4, 150mM KCl, 20mM MgCl <sub>2</sub> , 10% glycerol, 1mM DTT
<b>GFP</b>	BL21-RIL	1mM IPTG for 4h at 30°C	20mM Tris pH 7.5, 100mM KCl, 0.1mM EDTA, 10% glycerol, 20mM MgCl <sub>2</sub> , 5mM DTT
<b>Hsp104<sup>1-548</sup> or Hsp104<sup>773-908</sup></b>	BL21-RIL	1mM IPTG overnight at 15°C	40mM HEPES pH 7.4, 150mM KCl, 20mM MgCl <sub>2</sub> , 10% glycerol, 1mM DTT

#### 6.4 Inhibition of amyloid fibrillization with CLR01

Each reconstituted peptide was incubated with equimolar CLR01 or CLR03 in a volume of 100µL and agitated at 37°C at 1400rpm. At various time points, 1µL aliquots were removed and added to 200µL of 25µM ThT in PBS. Changes in fluorescence (excitation: 440 nm, emission: 482 nm, gain: 100) were measured using a Tecan Safire2 microplate reader. To determine IC<sub>50</sub> values for dose-response relationships, the data was analyzed using GraphPad Prism software. A nonlinear regression analysis (log(inhibitor) vs. response (three parameters)) was used and fitted with the least squares (ordinary) fit.

#### 6.5 Sedimentation analysis

To assess the extent of fibril assembly or disassembly using sedimentation analysis, fibril samples (20µM fibrils, 100µL volume) were centrifuged for 10min at 13,200rpm. The supernatant was carefully removed and transferred to a new tube, and the pellet was redissolved in an equal volume (100µL) of buffer. Then, 50µL of 3X sample buffer (6% SDS, 187.5mM Tris, 30% glycerol, 10% β-mercaptoethanol, 0.05% bromophenol blue, pH 6.8) was added to the supernatant and pellet fractions. Samples were analyzed by SDS-PAGE using 10-20% Tris-Tricine peptide gels

and XT Tricine running buffer (Bio-Rad) and visualized by coomassie staining. A gradient of soluble peptide controls were also run on the gels. Densitometry (using Image J software) was used to quantify the percent of protein in the pellet fractions by comparing to a standard curve created from the soluble peptide controls.

### **6.6 Fibril disaggregation assays**

Hsp104 or the indicated variant (3 $\mu$ M), CLR01 or CLR03 (200 $\mu$ M), or EGCG (200 $\mu$ M) were diluted into assay buffer (25mM HEPES-KOH, 150mM KOAc, 10mM Mg(OAc)<sub>2</sub>, 1mM DTT, pH 7.4) in the presence of ATP (5mM) and an ATP regeneration system (0.1mM ATP, 0.02mg/ml creatine kinase, 10mM creatine phosphate) at a final volume of 75 $\mu$ L. SEVI, PAP85-120 or SEM1(45-107) fibrils (20 $\mu$ M based on peptide monomer concentrations) were added last and samples were incubated at 37°C for the duration of the experiments. Buffer control samples were included which contained all components except that buffer was substituted for fibrils. At various timepoints, 5 $\mu$ L aliquots were removed and added to a 96-well plate containing 55 $\mu$ L of 25 $\mu$ M ThT diluted in assay buffer. Changes in fluorescence intensity (excitation: 440nm, 5nm bandwidth; emission: 482nm, 10nm bandwidth; gain 160) were measured using a Tecan Safire<sup>2</sup> microplate reader. For data analysis, buffer control measurements were subtracted and ThT values were normalized to measurements at the 0h timepoint. To determine EC<sub>50</sub> values for dose-response relationships, the data was analyzed using GraphPad Prism software. A nonlinear regression analysis (log(inhibitor) vs. response (three parameters)) was used and fitted with the least squares (ordinary) fit.

### **6.7 Fibril degradation assays**

For degradation experiments, fibrils (20 $\mu$ M based on peptide monomer concentrations) were incubated with HAP (3 $\mu$ M) and ClpP (4.5 $\mu$ M) and diluted into assay buffer in the presence of ATP (5mM) and an ATP regeneration system (described above) at a final volume of 100 $\mu$ L. Samples

were incubated at 37°C for the duration of the experiments. At given time points, 10µL aliquots were removed and added to 3X sample buffer. Samples were analyzed by SDS-PAGE using 10-20% Tris-Tricine peptide gels and XT Tricine running buffer (Bio-Rad). Gels were visualized by silver staining (Invitrogen).

### **6.8 Transmission electron microscopy**

Aliquots (10µL) were removed from the assembly and disassembly reactions, spotted on Formvar carbon-coated grids for 10min (EM Sciences), stained with 2% uranyl acetate for 5min, and washed with water for 30sec. Samples were visualized using a Jeol-1010 transmission electron microscope.

### **6.9 Filter trap assays**

Reaction aliquots (50µL) were removed at various time points and centrifuged in pre-rinsed Microcon centrifugal filter devices (Amicon) for 25min at 14000rcf. The retentate was redissolved in 50µL of LRB and 25µL of 3X sample buffer, and 25µL of 3X sample buffer was also added to the filtrate. Filtrate and retentate contents were analyzed by SDS-PAGE using 10-20% Tris-Tricine peptide gels and XT Tricine running buffer (Bio-Rad). Gels were visualized by silver staining (Invitrogen).

### **6.10 Turbidity assays**

Hsp104 variants (at the indicated concentrations) were diluted into assay buffer in the presence of ATP (5mM) and an ATP regeneration system (described above) at a total volume of 75µL in eppendorf tubes. Fibrils (20µM based on peptide monomer concentrations) were added last and samples were transferred to 96-well plates. Turbidity was measured as absorbance at 395nm at room temperature on a Tecan Safire<sup>2</sup> microplate reader.

### **6.11 Dynamic light scattering**

SEVI fibrils (20 $\mu$ M based on peptide monomer concentrations) were incubated for ~5min with the indicated proteins (1.8 $\mu$ M monomeric concentration) and diluted into assay buffer in the presence of ATP (5mM). Samples were immediately transferred into disposable cuvettes (Eppendorf) and light scattering at 658nm was measured using a DynaPro NanoStar Dynamic Light Scattering instrument (Wyatt Technology). Dynamic light scattering (DLS) measurements of hydrodynamic radius ( $R_h$ ) were made at room temperature. Samples were measured using an acquisition time of 10 seconds for 10 consecutive measurements. Particle translational diffusion coefficients were calculated from decay curves of autocorrelation of light scattering data and converted to hydrodynamic radius ( $R_h$ ) with the Stokes-Einstein equation. Histograms of mass versus  $R_h$  were calculated using a Regularization algorithm with Dynamics V7 software.

### **6.12 Zeta potential** (Work from collaborators in the Münch lab)

PAP248-286, PAP85-120 and SEM1(49-107) fibrils were treated with a ten-fold excess of CLR01 or CLR03. After centrifugation at 14,000rpm for 10min, the pellets were resuspended in 1mM KCl. Zeta potential was measured using the Zeta Nanosizer (Malvern Instruments, UK).

### **6.13 Confocal microscopy** (Work from collaborators in the Münch lab)

Fibrils (200 $\mu$ g/ml in PBS) were stained with Proteostat Amyloid Plaque Detection Kit (Enzo Life Sciences, Plymouth Meeting, PA). Fibrils were then treated with 20-fold excess CLR01 or CLR03 and mixed 1:2 with MLV-gag-YFP virions. Samples were transferred to  $\mu$ -slides VI0.4 (Ibidi, Munich, Germany) and imaged with a Zeiss LSM confocal microscope.

### **6.14 Circular dichroism spectroscopy**

To remove any PAP248-286 monomers or oligomers that did not assemble completely into amyloid fibrils, SEVI fibrils were first pelleted at 13,200rpm for 10min. The supernatant was

removed and the resulting pellet was resuspended in an equal volume (same volume as supernatant removed) of PBS. The concentration of the supernatant was determined by measuring absorbance at 280nm on a Nanodrop spectrophotometer. The supernatant concentration was then subtracted from the original fibril sample concentration to establish the new concentration of the pelleted fibrils.

Fibrils (50 $\mu$ M) were incubated with buffer, CLR01, or CLR03 (500 $\mu$ M) in a final volume of 200 $\mu$ L in PBS. Samples were incubated at 2h at 37°C. CD spectra were then collected on an AVIV Model 410 Circular Dichroism Spectrometer using a 15sec averaging time. Mean residue ellipticity (MRE) was calculated using the equation  $MRE = \theta / (10lcN)$  where  $\theta$  is the measured ellipticity in millidegrees,  $l$  is the pathlength in cm,  $c$  is the molar protein concentration, and  $N$  is the number of residues.

#### **6.15 Cell culture and HIV infectivity experiments using Hsp104**

TZM-bl cells were maintained in DMEM medium supplemented with 10% fetal bovine serum and 1% L-glutamine. The day before infection, 10<sup>4</sup> TZM-bl cells/well were seeded in a volume of 200 $\mu$ L in a 96-well collagen-coated microplate. Prior to infection, seminal amyloid fibrils were incubated with Hsp104 (or variants) in a sterile reaction tube for 3h at 37°C at a volume of 50 $\mu$ L. After 3h, each 50 $\mu$ L sample was diluted with 50 $\mu$ L of DMEM. Next, 82.5 $\mu$ L of the resulting mixture was diluted with 82.5 $\mu$ L of HIV-1, and samples were allowed to pre-incubate with the virus for 10min at room temperature. After the pre-incubation was complete, the media was removed from the 96-well plate, and the virus/protein mixtures were immediately added in triplicate (50 $\mu$ L per well) to TZM-bl cells and further incubated for 3h at 37°C and 5% CO<sub>2</sub>. The virus/protein mixtures were then removed and replaced with 200 $\mu$ L of complete media. Luciferase activity was assessed 3 days post-infection using a Luciferase Assay System (Promega), and luminescence was measured on a MLX Microtiter Plate Luminometer (Dynex Technologies). The background luminescence from buffer control samples was subtracted and values were normalized to

untreated fibril samples. HIV-1 strains used included BL2 (R5-tropic primary isolate; 130 infectious units; 0.90ng p24) and 89.6 (dual tropic; 1000 infectious units, 0.92ng p24). Statistical analyses were performed in GraphPad Prism using a one-way ANOVA and the Dunnett post-test, comparing all conditions to the untreated fibril control.

### **6.16 Effect of tweezer on amyloid and semen-mediated enhancement of HIV infection**

(Work from collaborators in the Münch lab)

The reporter cell line TZM-bl was obtained through the NIH ARRRP and cultured in DMEM medium supplemented with 120µg/ml penicillin, 120µg/ml streptomycin, 350µg/ml glutamine and 10% inactivated fetal calf serum (FCS). This cell line is stably transfected with an LTR-lacZ cassette and expresses CD4, CXCR4 and CCR5. Upon infection with HIV-1, the viral protein Tat is expressed which transactivates the long terminal repeat (LTR) resulting in the generation of β-galactosidase molecules.

Virus stocks of X4-tropic HIV-1 NL4-3, R5-tropic HIV-1 NL4-3 92TH014 derivative, and of the transmitter/founder viruses THRO.c and CH058.c (kindly provided by B. Hahn) were generated by transient transfection of 293T cells as described [51]. After transfection and overnight incubation, the transfection mixture was replaced with 2ml DMEM medium supplemented with 120µg/ml penicillin, 120µg/ml streptomycin, 350µg/ml glutamine, and 2% inactivated FCS. After 40h, the culture supernatant was collected and centrifuged for 3min at 330g to remove cell debris. Virus stocks were analyzed by p24 antigen ELISA and stored at -80 °C.

To assess the effect of CLR01 and CLR03 on amyloid-mediated enhancement of HIV-1 infection, 10<sup>4</sup> TZM-bl cells in 180µl medium were seeded in 96-well flat-bottom plates the day before infection. 200µg/ml fibrils (44µM SEVI, 45µM PAP85-120 fibrils, 30µM SEM1(49-107) fibrils) were treated with a 20-fold molar excess of CLR01 or CLR03 for 10min at room temperature, serially diluted 5-fold and then added to an R5-tropic HIV-1 NL4-3 92TH014 (0.5ng/ml p24 antigen). After

5min, 20µl of these mixtures were added to TZM-bl cells and infection rates were determined 3 days post infection by detecting β-galactosidase activity in cellular lysates using the Tropix Gal-Screen kit (Applied Biosystems) and the Orion microplate luminometer (Berthold). All values represent reporter gene activities (relative light units per second; RLU/s) derived from triplicate infections minus background activities derived from uninfected cells.

To assess the effect of CLR01 and CLR03 on semen-mediated enhancement of HIV-1 infection, 10<sup>4</sup> TZM-bl cells were seeded in 280µl medium in 96-well flat-bottom plates the day before infection. Seminal plasma (20%) was treated with different concentrations of CLR01 or CLR03 (highest 925µM) for 10min at RT and then mixed with R5-tropic HIV-1 NL4-3 and CH058 (0.5ng/ml p24 antigen). After 5min, 20µl of these mixtures were added to 280µl TZM-bl cells. To minimize cytotoxic effects mediated by seminal plasma, the inoculums were replaced 2h later with fresh medium. Infection rates were determined as described above.

### **6.17 Antiviral activity of CLR01 on HIV-1, HCMV, HSV-2, HCV and adenovirus infection**

(Work from collaborators in the Münch lab)

**HIV-1:** In the virus treatment assay, R5- and X4-tropic HIV-1 NL4-3, and HIV-1 transmitter/founder viruses CH058 and THRO were titrated with CLR01 or CLR03 (0-150µM). After incubation for 10min at 37°C, 20µl of these mixtures were added to 10<sup>4</sup> TZM-bl cells seeded one day prior in 180µl medium. For the cell-treatment assay, DMEM instead of virus was titrated with CLR01 or CLR03, incubated, and added to TZM-bl cells analogous to the virus treatment protocol. After a 2h incubation at 37°C, old medium was replaced by fresh medium and cells were infected with the different HIV-1 strains. β-galactosidase activity was measured 3 days post infection. IC<sub>50</sub> values were calculated with PRISM software.

**Human cytomegalovirus (HCMV):** Human foreskin fibroblasts (HFFs) were maintained in minimal essential medium (MEM, Invitrogen, Germany) supplemented with 10% fetal calf serum (Invitrogen), 2mM L-glutamine (Biochrom AG, Germany), 100U of penicillin and 100µg of



streptomycin (Gibco/BRL) per ml, and 1 x non-essential amino acids (Biochrom AG). Production of HCMV stock virus was a derivative of strain TB40-BAC4 [248], and all HCMV infection experiments were performed on HFF under serum-free conditions. To evaluate the inhibitory effect of compounds on virus entry, HCMV virus, corresponding to a multiplicity of infection of approximately 1 plaque forming units, was pre-incubated with PBS, 100 $\mu$ M CLR03, or 100 $\mu$ M CLR01 for 30, 60, or 120min, respectively, at 37°C in serum-free MEM. The virus/compound mixtures were then incubated for 16h with HFFs ( $1.7 \times 10^4$ /well) in a 96-well plate that was seeded one day prior to infection and washed twice with PBS before adding the mixtures. To determine infection rates, virus/compound mixtures were first removed by washing twice with PBS followed by fixation with ice-cold methanol for 10min. HCMV infected cells were visualized by indirect immunofluorescence staining for HCMV immediate-early (IE) antigen employing Mab13 (Argene) and cell nuclei staining by using 4',6-diamidin-2-phenylindol (DAPI, Roche). HCMV infection rates for each compound were determined from images taken with the 10 $\times$ -objective lens and the fluorescence microscope Axio-Observer.Z1 (Zeiss) by counting numbers of IE-positive cells. Maximum inhibition of HCMV infection by CLR01 was found already after 30min of incubation. The mean infection rate and standard deviation included the results from the different incubation times.

**Herpes simplex virus type 2 (HSV-2):** HSV-2 comprising a GFP reporter gene was treated with PBS, 100 $\mu$ M CLR03, or 100 $\mu$ M CLR01 and added to Vero cells. GFP-positive cells were counted using flow cytometry two days post infection.

**Hepatitis C virus (HCV):** HCV in-vitro transcripts were generated and transfected using electroporation as described recently [249]. Harvested virus was then precipitated using PEG800 as described previously [250] and resuspended in 10mM HEPES, 150mM NaCl. Huh-7.5 cells stably expressing firefly luciferase were seeded at a density of  $2 \times 10^4$  cells per well of a 96-well plate 24 h prior to inoculation. CLR01 and CLR03 were diluted in 10mM HEPES, 150mM NaCl and incubated with Renilla luciferase reporter virus particles (JcR-2a) [251, 252] for 5min at 37°C. Cells were inoculated with JcR2-2a HCV in the presence of CLR01 or CLR03 for 72h at 37°C,

washed with PBS, and lysed with 50  $\mu$ l passive lysis buffer (Promega, Mannheim, Germany). To measure cytotoxicity, lysates were assayed for firefly luciferase activity using luciferin (200 $\mu$ M luciferin, 25mM glycylglycine, pH 8) in a plate luminometer (Lumat LB9507). For infectivity readout, lysates were assayed for Renilla luminescence using 1 $\mu$ M coelenterazin (P.J.K., Kleinblittersdorf, Germany) in the same luminometer.

**Human adenovirus type 5 (HAdV5):** The E1-deleted replication-deficient human adenovirus type 5-based vector containing a HCMV promoter-controlled EGFP expression cassette was produced on N52.E6 cells [253], purified by one discontinuous and one continuous CsCl density gradient and subsequent size-exclusion chromatography (disposable PD-10, Amersham). The physical particle titer was determined by particle lysis and OD260 and confirmed by slot-blotting [254]. To assess effects of CLR01 and CLR03 on the ability of the vector to transduce cells, the vector was titrated with 0-100 $\mu$ M CLR01 or CLR03 and incubated 10min at 37°C in 50mM HEPES, 150mM NaCl, pH 7.4. One day prior to infection, 10<sup>5</sup> A549 cells per well were seeded in a 24-well format. Cells were infected with 200MOI of the pretreated virus. EGFP expression was analyzed using a Beckman-Coulter Gallios flow cytometer 1 day post transduction.

#### **6.18 p24 release assay** (Work from collaborators in the Münch lab)

HIV-1 NL4-3 92TH014 was incubated for 10min at 37°C with PBS, 100 $\mu$ M CLR03 or 100 $\mu$ M CLR01 and centrifuged at 20,000g and 4°C for 1h. The p24 content of the supernatant and pellet was determined using an in house p24-antigen ELISA.

#### **6.19 Atomic force microscopy of virions** (Work from members of the Münch lab)

Virus solutions (20 $\mu$ L) were deposited on Aminopropyl-modified glass cover slips (AP-Glass) and incubated for 1h at RT. After removing excess liquid, the deposited virus particles were treated with 40 $\mu$ L of 100 $\mu$ M CLR01 or CLR03 and incubated for 10min at RT. The samples were rinsed

with PBS and imaged in PBS on a Nanowizard 3 AFM (JPK) in Quantitative Imaging mode using silicon nitride cantilevers with a spring constant of 0.03N/m (Bruker).

## **6.20 Analysis of cellular toxicity**

**CLR01 and CLR03:** (Work from collaborators in the Münch lab) The effect of CLR01 and CLR03 on the metabolic activity of TZM-bl cells was analyzed using the 3-(4,5-dimethylthiazol-2-yl)-2,5-diphenyltetrazolium bromide (MTT) assay. After 3 days of incubation, 20µl of 5mg/ml MTT (Sigma #M2003) solution was added to the cells. After 4h the cell-free supernatant was discarded and formazan crystals were dissolved in 100µl DMSO:Ethanol (1:2). Absorption was detected at 490nm and corrected by the background absorption at 650nm.

**Hsp104:** Cell viability of TZM-bl cells treated with Hsp104 or variants was also measured using the MTT reduction assay. TZM-bl cells ( $10^4$  cells/well) were treated as described in the HIV infectivity assays, except with DMEM replacing virus at each step. Protein/DMEM mixtures were removed after 3h and replaced with 200µL of complete media. Plates were incubated overnight at 37°C. The next day, an MTT stock (50mg of MTT dissolved in 10mL of PBS) was mixed in a 1:1 ratio with DMEM to result in the MTT reagent. Media was removed from all wells on the 96-well plate and replaced with 125µL of fresh media. MTT reagent (25µL) was added to each well and incubated at 37°C for 3-4h. Formazan crystals were dissolved in 150µL of 0.1N HCl in isopropanol with 10% Triton X-100. MTT reduction was assessed the by detection of absorbance at 570nm (630nm reference wavelength) on a MRX Revelation Microplate Reader (Dynex Technologies).

## **6.21 Dosing the anti-viral effect of EGCG**

TZM-bl cells were maintained in DMEM medium supplemented with 10% fetal bovine serine and 1% L-glutamine. The day before infection,  $10^4$  TZM-bl cells/well were seeded in a volume of 200µL in a 96-well collagen-coated microplate. To dose the inhibition of HIV infectivity by EGCG,

EGCG was freshly dissolved in assay buffer and dilutions of various concentrations were prepared. These EGCG solutions (50 $\mu$ L) were first added to 50 $\mu$ L of DMEM. Next, 82.5 $\mu$ L of the resulting mixture was allowed to preincubate with 82.5 $\mu$ L of HIV at room temperature for 10min. When the preincubation was complete, media was removed from the 96-well plate, and the EGCG/virus mixtures were immediately added in triplicate (50 $\mu$ L per well) to TZM-bl cells. After 3h at 37°C, mixtures were removed and replaced with 200 $\mu$ L of complete media. Luciferase activity was determined at 3 days post infection using a MLX Microtiter Plate Luminometer. HIV-1 aliquots were obtained from the Center for AIDS Research at the University of Pennsylvania. HIV strains used included BL2 (R5-tropic; 130 infectious units; 0.90 ng p24), BaL (R5-tropic; 75 infectious units; 0.42 ng p24), and 89.6 (dual-tropic; 1000 infectious units, 0.92 ng p24).

## CHAPTER 7: BIBLIOGRAPHY

1. Ascher, M.S., et al., *Aetiology of AIDS*. Lancet, 1993. **341**(8854): p. 1223.
2. Schechter, M.T., et al., *Aetiology of AIDS*. Lancet, 1993. **341**(8854): p. 1222-3.
3. Weiss, R.A., *How does HIV cause AIDS?* Science, 1993. **260**(5112): p. 1273-9.
4. Weiss, R.A. and H.W. Jaffe, *Duesberg, HIV and AIDS*. Nature, 1990. **345**(6277): p. 659-60.
5. UNAIDS, *2013 UNAIDS Report on the global AIDS epidemic*. 2013: p. 1-116.
6. UNAIDS, *2010 UNAIDS Report on the global AIDS epidemic*. 2010: p. 1-359.
7. Royce, R.A., et al., *Sexual transmission of HIV*. N Engl J Med, 1997. **336**(15): p. 1072-8.
8. Gray, R.H., et al., *Probability of HIV-1 transmission per coital act in monogamous, heterosexual, HIV-1-discordant couples in Rakai, Uganda*. Lancet, 2001. **357**(9263): p. 1149-53.
9. Pilcher, C.D., et al., *Brief but efficient: acute HIV infection and the sexual transmission of HIV*. J Infect Dis, 2004. **189**(10): p. 1785-92.
10. Dimitrov, D.S., et al., *Quantitation of human immunodeficiency virus type 1 infection kinetics*. J Virol, 1993. **67**(4): p. 2182-90.
11. Ruser, P., et al., *Quantification of infectious HIV-1 plasma viral load using a boosted in vitro infection protocol*. Virology, 2004. **326**(1): p. 113-29.
12. Chuck, A.S., M.F. Clarke, and B.O. Palsson, *Retroviral infection is limited by Brownian motion*. Hum Gen Ther, 1996. **7**: p. 1527-1534.
13. Eckert, D.M. and P.S. Kim, *Mechanisms of viral membrane fusion and its inhibition*. Annu Rev Biochem, 2001. **70**: p. 777-810.
14. Orloff, G.M., et al., *Penetration of CD4 T cells by HIV-1. The CD4 receptor does not internalize with HIV, and CD4-related signal transduction events are not required for entry*. J Immunol, 1991. **146**: p. 2578-87.
15. Galvin, S.R. and M.S. Cohen, *The role of sexually transmitted diseases in HIV transmission*. Nat Rev Microbiol, 2004. **2**(1): p. 33-42.
16. Kim, K.A., et al., *Semen-mediated enhancement of HIV infection is donor-dependent and correlates with the levels of SEVI*. Retrovirology, 2010. **7**: p. 55.
17. Munch, J., et al., *Semen-derived amyloid fibrils drastically enhance HIV infection*. Cell, 2007. **131**(6): p. 1059-71.
18. Olsen, J.S., et al., *Amyloid binding small molecules efficiently block SEVI and semen mediated enhancement of HIV-1 infection*. J Biol Chem, 2010. **285**: p. 35488 -35496.
19. Roan, N.R. and W.C. Greene, *A seminal finding for understanding HIV transmission*. Cell, 2007. **131**(6): p. 1044-6.
20. Roan, N.R., et al., *The cationic properties of SEVI underlie its ability to enhance human immunodeficiency virus infection*. J Virol, 2009. **83**(1): p. 73-80.
21. Ronnberg, L., et al., *Clomiphene citrate administration to normogonadotropic subfertile men: blood hormone changes and activation of acid phosphatase in seminal fluid*. Int J Androl, 1981. **4**(3): p. 372-8.
22. Munch, J., et al., *Effect of semen and seminal amyloid on vaginal transmission of simian immunodeficiency virus*. Retrovirology, 2013. **10**: p. 148.
23. Wurm, M., et al., *The influence of semen-derived enhancer of virus infection on the efficiency of retroviral gene transfer*. J Gene Med, 2010. **12**(2): p. 137-46.
24. Tang, Q., N.R. Roan, and Y. Yamamura, *Seminal plasma and semen amyloids enhance cytomegalovirus infection in cell culture*. J Virol, 2013. **87**(23): p. 12583-91.
25. Caughey, B. and P.T. Lansbury, *Protofibrils, pores, fibrils, and neurodegeneration: separating the responsible protein aggregates from the innocent bystanders*. Annu Rev Neurosci, 2003. **26**: p. 267-98.
26. Morimoto, R.I., *Stress, aging, and neurodegenerative disease*. N Engl J Med, 2006. **355**(21): p. 2254-5.

27. Skovronsky, D.M., V.M. Lee, and J.Q. Trojanowski, *Neurodegenerative diseases: new concepts of pathogenesis and their therapeutic implications*. *Annu Rev Pathol*, 2006. **1**: p. 151-70.
28. Cushman, M., et al., *Prion-like disorders: blurring the divide between transmissibility and infectivity*. *J Cell Sci*, 2010. **123**(Pt 8): p. 1191-201.
29. Dobson, C.M., *Protein folding and misfolding*. *Nature*, 2003. **426**(6968): p. 884-90.
30. Fandrich, M., M.A. Fletcher, and C.M. Dobson, *Amyloid fibrils from muscle myoglobin*. *Nature*, 2001. **410**(6825): p. 165-6.
31. Fowler, D.M., et al., *Functional amyloid formation within mammalian tissue*. *PLoS Biol*, 2006. **4**(1): p. e6.
32. Fowler, D.M., et al., *Functional amyloid--from bacteria to humans*. *Trends Biochem Sci*, 2007. **32**(5): p. 217-24.
33. Si, K., et al., *Aplysia CPEB can form prion-like multimers in sensory neurons that contribute to long-term facilitation*. *Cell*, 2010. **140**: p. 421-435.
34. Watt, B., et al., *N-terminal domains elicit formation of functional Pmel17 amyloid fibrils*. *J Biol Chem*, 2009. **284**(51): p. 35543-55.
35. Shorter, J. and S. Lindquist, *Prions as adaptive conduits of memory and inheritance*. *Nat Rev Genet*, 2005. **6**(6): p. 435-50.
36. True, H.L. and S.L. Lindquist, *A yeast prion provides a mechanism for genetic variation and phenotypic diversity*. *Nature*, 2000. **407**(6803): p. 477-83.
37. Halfmann, R., et al., *Prions are a common mechanism for phenotypic inheritance in wild yeasts*. *Nature*, 2012. **482**(7385): p. 363-8.
38. Suzuki, G., N. Shimazu, and M. Tanaka, *A yeast prion, Mod5, promotes acquired drug resistance and cell survival under environmental stress*. *Science*, 2012. **336**(6079): p. 355-9.
39. Barnhart, M.M. and M.R. Chapman, *Curli biogenesis and function*. *Annu Rev Microbiol.*, 2006. **60**: p. 131-47.
40. Eanes, E.D. and G.G. Glenner, *X-ray diffraction studies on amyloid filaments*. *J Histochem Cytochem*, 1968. **16**(11): p. 673-7.
41. Nelson, R. and D. Eisenberg, *Structural Models of Amyloid Like Fibrils*. *Adv Protein Chem*, 2006. **73**: p. 235-282.
42. Sunde, M. and C. Blake, *The structure of amyloid fibrils by electron microscopy and X-ray diffraction*. *Adv Protein Chem*, 1997. **50**: p. 123-59.
43. Roan, N.R., et al., *Aminoquinoline surfen inhibits the action of SEVI (semen-derived enhancer of viral infection)*. *J Biol Chem*, 2010. **285**(3): p. 1861-9.
44. Arcasoy, S.M., et al., *Polycations increase the efficiency of adenovirus-mediated gene transfer to epithelial and endothelial cells in vitro*. *Gene Ther*, 1997. **4**(1): p. 32-8.
45. Davis, H.E., J.R. Morgan, and M.L. Yarmush, *Polybrene increases retrovirus gene transfer efficiency by enhancing receptor-independent virus adsorption on target cell membranes*. *Biophys Chem*, 2002. **97**(2-3): p. 159-72.
46. Brender, J.R., et al., *The amyloidogenic SEVI precursor, PAP248-286, is highly unfolded in solution despite an underlying helical tendency*. *Biochim Biophys Acta*, 2011. **1808**(4): p. 1161-9.
47. Nanga, R.P.R., et al., *NMR Structure in a Membrane Environment Reveals Putative Amyloidogenic Regions of the SEVI Precursor Peptide PAP248- 286*. *J. Am. Chem. Soc*, 2009. **131**: p. 17972-17979.
48. Sievers, S.A., et al., *Structure-based design of non-natural amino-acid inhibitors of amyloid fibril formation*. *Nature*, 2011. **475**(7354): p. 96-100.
49. Tompa, P., *Structural disorder in amyloid fibrils: its implication in dynamic interactions of proteins*. *FEBS J*, 2009. **276**(19): p. 5406-15.
50. Elias, A.K., et al., *SEVI, the semen enhancer of HIV infection along with fragments from its central region, form amyloid fibrils that are toxic to neuronal cells*. *Biochim Biophys Acta*, 2014. **1844**(9): p. 1591-8.

51. Münch, J., et al., *Semen-derived amyloid fibrils drastically enhance HIV infection*. Cell, 2007. **131**: p. 1059-71.
52. Tan, S., et al., *Peptides derived from HIV-1 gp120 co-receptor binding domain form amyloid fibrils and enhance HIV-1 infection*. FEBS Lett, 2014. **588**(9): p. 1515-22.
53. Zhang, L., et al., *A novel modified peptide derived from membrane-proximal external region of human immunodeficiency virus type 1 envelope significantly enhances retrovirus infection*. J Pept Sci, 2014. **20**(1): p. 46-54.
54. Munch, J., et al., *Discovery of modulators of HIV-1 infection from the human peptidome*. Nat Rev Microbiol, 2014. **12**(10): p. 715-22.
55. Yolamanova, M., et al., *Peptide nanofibrils boost retroviral gene transfer and provide a rapid means for concentrating viruses*. Nat Nanotechnol, 2013. **8**(2): p. 130-6.
56. Wojtowicz, W.M., et al., *Stimulation of enveloped virus infection by beta-amyloid fibrils*. J Biol Chem., 2002. **277**(38): p. 35019-24.
57. Arnold, F., et al., *Naturally occurring fragments from two distinct regions of the prostatic acid phosphatase form amyloidogenic enhancers of HIV infection*. J Virol, 2012. **86**(2): p. 1244-9.
58. Roan, N.R., et al., *Peptides released by physiological cleavage of semen coagulum proteins form amyloids that enhance HIV infection*. Cell Host Microbe, 2011. **10**(6): p. 541-50.
59. de Lamirande, E., *Semenogelin, the main protein of the human semen coagulum, regulates sperm function*. Semin Thromb Hemost, 2007. **33**(1): p. 60-8.
60. Robert, M. and C. Gagnon, *Semenogelin I: a coagulum forming, multifunctional seminal vesicle protein*. Cell Mol Life Sci., 1999. **55**(6-7): p. 944-60.
61. Robert, M. and C. Gagnon, *Purification and characterization of the active precursor of a human sperm motility inhibitor secreted by the seminal vesicles: identity with semenogelin*. Biol Reprod, 1996. **55**(4): p. 813-21.
62. Robert, M., et al., *Characterization of prostate-specific antigen proteolytic activity on its major physiological substrate, the sperm motility inhibitor precursor/semenogelin I*. Biochemistry, 1997. **36**(13): p. 3811-9.
63. Olsen, J.S., et al., *Seminal plasma accelerates SEVI fibril formation by the PAP[248-286] peptide*. J Biol Chem, 2012: p. 1-17.
64. Hartjen, P., et al., *Assessment of the range of the HIV-1 infectivity enhancing effect of individual human semen specimen and the range of inhibition by EGCG*. AIDS research and therapy, 2012. **9**: p. 2.
65. Martellini, J.A., et al., *HIV-1 enhancing effect of prostatic acid phosphatase peptides is reduced in human seminal plasma*. PLoS One, 2011. **6**(1): p. e16285.
66. Easterhoff, D., et al., *Fluorescence detection of cationic amyloid fibrils in human semen*. Bioorg Med Chem Lett, 2013. **23**(18): p. 5199-202.
67. Hartjen, P., et al., *Assessment of the range of the HIV-1 infectivity enhancing effect of individual human semen specimen and the range of inhibition by EGCG*. AIDS Res Ther, 2012. **9**(1): p. 2.
68. Usmani, S.M., et al., *Direct visualization of HIV-enhancing endogenous amyloid fibrils in human semen*. Nat Commun, 2014. **5**: p. 3508.
69. Roan, N.R., et al., *Liquefaction of semen generates and later degrades a conserved semenogelin peptide that enhances HIV infection*. J Virol, 2014. **88**(13): p. 7221-34.
70. Hu, J., M.B. Gardner, and C.J. Miller, *Simian immunodeficiency virus rapidly penetrates the cervicovaginal mucosa after intravaginal inoculation and infects intraepithelial dendritic cells*. J Virol, 2000. **74**(13): p. 6087-95.
71. Doncel, G.F., *Exploiting common targets in human fertilization and HIV infection: development of novel contraceptive microbicides*. Hum Reprod Update, 2006. **12**(2): p. 103-17.
72. Doncel, G. and C. Mauck, *Vaginal microbicides: a novel approach to preventing sexual transmission of HIV*. Curr HIV/AIDS Rep, 2004. **1**(1): p. 25-32.

73. Jones, R., *Interaction of zona pellucida glycoproteins, sulphated carbohydrates and synthetic polymers with proacrosin, the putative egg-binding protein from mammalian spermatozoa*. Development, 1991. **111**(4): p. 1155-63.
74. Oehninger, S., et al., *Nature of the inhibitory effect of complex saccharide moieties on the tight binding of human spermatozoa to the human zona pellucida*. Fertil Steril, 1991. **55**: p. 165-169.
75. Cohen, F.S. and G.B. Melikyan, *The Energetics of Membrane Fusion from Binding, through Hemifusion, Pore Formation, and Pore Enlargement*. J Membr Biol, 2004. **199**(1): p. 1-14.
76. Evans, J.P. and H.M. Florman, *The state of the union: the cell biology of fertilization*. Nat Cell Biol, 2002. **4 Suppl**: p. s57-63.
77. Herbein, G., et al., *Macrophage signaling in HIV-1 infection*. Retrovirology, 2010. **7**: p. 34.
78. Salicioni, A.M., et al., *Signalling pathways involved in sperm capacitation*. Soc Reprod Fertil Suppl, 2007. **65**: p. 245-59.
79. Liu, Z. and R.H. Foote, *Bull sperm motility and membrane integrity in media varying in osmolality*. J Dairy Sci, 1998. **81**(7): p. 1868-73.
80. Bjartell, A., et al., *Distribution and Tissue Expression of Semenogelin I and II in Man as Demonstrated by In Situ Hybridization and Immunocytochemistry*. J Androl, 1996. **17**: p. 17-26.
81. Herr, J.C., et al., *Characterization of a monoclonal antibody to a conserved epitope on human seminal vesicle-specific peptides: a novel probe/marker system for semen identification*. Biol Reprod, 1986. **35**(3): p. 773-84.
82. Easterhoff, D., et al., *Semen-derived enhancer of viral infection (SEVI) binds bacteria, enhances bacterial phagocytosis by macrophages, and can protect against vaginal infection by a sexually transmitted bacterial pathogen*. Antimicrob Agents Chemother, 2013. **57**(6): p. 2443-50.
83. Bourgeon, F., et al., *Involvement of semenogelin-derived peptides in the antibacterial activity of human seminal plasma*. Biol Reprod, 2004. **70**(3): p. 768-74.
84. Edstrom, A.M., et al., *The major bactericidal activity of human seminal plasma is zinc-dependent and derived from fragmentation of the semenogelins*. J Immunol, 2008. **181**(5): p. 3413-21.
85. Cutler, B. and J. Justman, *Vaginal microbicides and the prevention of HIV transmission*. Lancet Infect Dis, 2008. **8**(11): p. 685-97.
86. Klasse, P.J., R. Shattock, and J.P. Moore, *Antiretroviral drug-based microbicides to prevent HIV-1 sexual transmission*. Annu Rev Med, 2008. **59**: p. 455-71.
87. Garg, A.B., J. Nuttall, and J. Romano, *The future of HIV microbicides: challenges and opportunities*. Antivir Chem Chemother, 2009. **19**(4): p. 143-50.
88. Clavel, F. and A.J. Hance, *HIV drug resistance*. N Engl J Med, 2004. **350**(10): p. 1023-35.
89. Callahan, L.N., et al., *Dextran Sulfate Blocks Antibody Binding to the Principal Neutralizing Domain of Human Immunodeficiency Virus Type 1 without Interfering with gp120-CD4 Interactions*. J Virol, 1991. **65**: p. 1543-1550.
90. Rider, C.C., *The potential for heparin and its derivatives in the therapy and prevention of HIV-1 infection*. Glycoconj J, 1997. **14**(5): p. 639-42.
91. Witvrouw, M. and E. De Clercq, *Sulfated polysaccharides extracted from sea algae as potential antiviral drugs*. Gen Pharmacol, 1997. **29**: p. 497-511.
92. Luscher-Mattli, M., *Polyanions--a lost chance in the fight against HIV and other virus diseases?* Antivir Chem Chemother, 2000. **11**(4): p. 249-59.
93. van de Wijgert, J.H. and R.J. Shattock, *Vaginal microbicides: moving ahead after an unexpected setback*. Aids, 2007. **21**(18): p. 2369-76.
94. Neurath, A.R., N. Strick, and Y.Y. Li, *Role of seminal plasma in the anti-HIV-1 activity of candidate microbicides*. BMC Infect Dis, 2006. **6**: p. 150.
95. Tan, S., et al., *Polyanionic candidate microbicides accelerate the formation of semen-derived amyloid fibrils to enhance HIV-1 infection*. PLoS One, 2013. **8**(3): p. e59777.



96. Lanza, T.J., et al., *Substituted 4,6-diaminoquinolines as inhibitors of C5a receptor binding*. J Med Chem, 1992. **35**: p. 252-8.
97. Schuksz, M., et al., *Surfen, a small molecule antagonist of heparan sulfate*. Proc Natl Acad Sci U S A, 2008. **105**(35): p. 13075-80.
98. Capule, C.C., et al., *Oligovalent amyloid-binding agents reduce SEVI-mediated enhancement of HIV-1 infection*. J Am Chem Soc, 2012. **134**(2): p. 905-8.
99. Sawaya, M.R., et al., *Atomic structures of amyloid cross-beta spines reveal varied steric zippers*. Nature, 2007. **447**(7143): p. 453-7.
100. Goldschmidt, L., et al., *Identifying the amyloyme, proteins capable of forming amyloid-like fibrils*. Proceedings of the National Academy of Sciences of the United States of America, 2010. **107**: p. 3487-92.
101. Scheibel, T., et al., *Conducting nanowires built by controlled self-assembly of amyloid fibers and selective metal deposition*. Proc Natl Acad Sci U S A, 2003. **100**(8): p. 4527-32.
102. Smith, J.F., et al., *Characterization of the nanoscale properties of individual amyloid fibrils*. Proc Natl Acad Sci U S A, 2006. **103**(43): p. 15806-11.
103. Shorter, J., *Hsp104: a weapon to combat diverse neurodegenerative disorders*. Neurosignals, 2008. **16**(1): p. 63-74.
104. Roberts, B.E. and J. Shorter, *Escaping amyloid fate*. Nat Struct Mol Biol., 2008. **15**(6): p. 544-6.
105. Ehrnhoefer, D.E., et al., *EGCG redirects amyloidogenic polypeptides into unstructured, off-pathway oligomers*. Nat Struct Mol Biol., 2008. **15**(6): p. 558-66.
106. Ehrnhoefer, D.E., et al., *Green tea (-)-epigallocatechin-gallate modulates early events in huntingtin misfolding and reduces toxicity in Huntington's disease models*. Hum Mol Genet., 2006. **15**(18): p. 2743-51.
107. Masuda, M., et al., *Small molecule inhibitors of alpha-synuclein filament assembly*. Biochemistry, 2006. **45**(19): p. 6085-94.
108. Hauber, I., et al., *The main green tea polyphenol epigallocatechin-3-gallate counteracts semen-mediated enhancement of HIV infection*. Proc Natl Acad Sci U S A, 2009. **106**(22): p. 9033-8.
109. Popovych, N., et al., *Site specific interaction of the polyphenol EGCG with the SEVI amyloid precursor peptide PAP(248-286)*. J Phys Chem B, 2012. **116**(11): p. 3650-8.
110. Zhu, Q.Y., et al., *Stability of Green Tea Catechins*. J Agric Food Chem, 1997. **45**: p. 4624-4628.
111. Goldsbury, C.S., et al., *Polymorphic fibrillar assembly of human amylin*. J Struct Biol, 1997. **119**(1): p. 17-27.
112. Petkova, A.T., et al., *Self-propagating, molecular-level polymorphism in Alzheimer's beta-amyloid fibrils*. Science, 2005. **307**(5707): p. 262-5.
113. Tanaka, M., et al., *Conformational variations in an infectious protein determine prion strain differences*. Nature, 2004. **428**(6980): p. 323-8.
114. Wiltzius, J.J., et al., *Molecular mechanisms for protein-encoded inheritance*. Nat Struct Mol Biol., 2009. **16**(9): p. 973-8.
115. Goldschmidt, L., et al., *Identifying the amyloyme, proteins capable of forming amyloid-like fibrils*. Proc Natl Acad Sci U S A, 2010. **107**(8): p. 3487-92.
116. Roberts, B.E., et al., *A synergistic small-molecule combination directly eradicates diverse prion strain structures*. Nat Chem Biol, 2009. **5**(12): p. 936-46.
117. Shorter, J., *Emergence and natural selection of drug-resistant prions*. Mol Biosyst., 2010. **6**(7): p. 1115-30.
118. Hartjen, P., et al., *Assessment of the range of the HIV-1 infectivity enhancing effect of individual human semen specimen and the range of inhibition by EGCG*. AIDS Res Ther., 2012. **9**(1): p. 2.
119. Duennwald, M.L. and J. Shorter, *Countering amyloid polymorphism and drug resistance with minimal drug cocktails*. Prion, 2010. **4**(4): p. 244-51.

120. Wang, H., et al., *Direct and selective elimination of specific prions and amyloids by 4,5-dianilinophthalimide and analogs*. Proc Natl Acad Sci U S A, 2008. **105**(20): p. 7159-64.
121. Weissmann, C., *Mutation and selection of prions*. PLoS Pathog, 2012. **8**(3): p. e1002582.
122. Parsell, D.A., et al., *Protein disaggregation mediated by heat-shock protein Hsp104*. Nature, 1994. **372**(6505): p. 475-8.
123. Sanchez, Y. and S.L. Lindquist, *HSP104 required for induced thermotolerance*. Science, 1990. **248**(4959): p. 1112-5.
124. Sanchez, Y., et al., *Hsp104 is required for tolerance to many forms of stress*. EMBO J, 1992. **11**(6): p. 2357-64.
125. Glover, J.R. and S. Lindquist, *Hsp104, Hsp70, and Hsp40: a novel chaperone system that rescues previously aggregated proteins*. Cell, 1998. **94**(1): p. 73-82.
126. Weibezahn, J., B. Bukau, and A. Mogk, *Unscrambling an egg: protein disaggregation by AAA+ proteins*. Microb Cell Fact, 2004. **3**(1): p. 1.
127. Liu, Y.H., et al., *Heat shock protein 104 inhibited the fibrillization of prion peptide 106-126 and disassembled prion peptide 106-126 fibrils in vitro*. Int J Biochem Cell Biol, 2011. **43**(5): p. 768-74.
128. Lo Bianco, C., et al., *Hsp104 antagonizes alpha-synuclein aggregation and reduces dopaminergic degeneration in a rat model of Parkinson disease*. J Clin Invest, 2008. **118**(9): p. 3087-97.
129. Shorter, J. and S. Lindquist, *Hsp104, Hsp70 and Hsp40 interplay regulates formation, growth and elimination of Sup35 prions*. EMBO J, 2008. **27**(20): p. 2712-24.
130. Sweeny, E.A. and J. Shorter, *Prion proteostasis: Hsp104 meets its supporting cast*. Prion, 2008. **2**(4): p. 135-40.
131. Doyle, S.M. and S. Wickner, *Hsp104 and ClpB: protein disaggregating machines*. Trends Biochem Sci, 2009. **34**(1): p. 40-8.
132. Wendler, P., et al., *Atypical AAA+ subunit packing creates an expanded cavity for disaggregation by the protein-remodeling factor Hsp104*. Cell, 2007. **131**(7): p. 1366-77.
133. Bosl, B., V. Grimminger, and S. Walter, *Substrate binding to the molecular chaperone Hsp104 and its regulation by nucleotides*. J Biol Chem, 2005. **280**(46): p. 38170-6.
134. Hanson, P.I. and S.W. Whiteheart, *AAA+ proteins: have engine, will work*. Nat Rev Mol Cell Biol, 2005. **6**(7): p. 519-29.
135. Lum, R., M. Niggemann, and J.R. Glover, *Peptide and protein binding in the axial channel of Hsp104. Insights into the mechanism of protein unfolding*. J Biol Chem, 2008. **283**(44): p. 30139-50.
136. Lum, R., et al., *Evidence for an unfolding/threading mechanism for protein disaggregation by Saccharomyces cerevisiae Hsp104*. J Biol Chem, 2004. **279**(28): p. 29139-46.
137. Wendler, P., et al., *Motor mechanism for protein threading through Hsp104*. Mol Cell, 2009. **34**(1): p. 81-92.
138. Cashikar, A.G., et al., *Defining a pathway of communication from the C-terminal peptide binding domain to the N-terminal ATPase domain in a AAA protein*. Mol Cell, 2002. **9**(4): p. 751-60.
139. Li, L. and S. Lindquist, *Creating a protein-based element of inheritance*. Science, 2000. **287**(5453): p. 661-4.
140. Sauer, R.T., et al., *Sculpting the proteome with AAA(+) proteases and disassembly machines*. Cell, 2004. **119**(1): p. 9-18.
141. Shorter, J. and S. Lindquist, *Navigating the ClpB channel to solution*. Nat Struct Mol Biol, 2005. **12**(1): p. 4-6.
142. Tessarz, P., A. Mogk, and B. Bukau, *Substrate threading through the central pore of the Hsp104 chaperone as a common mechanism for protein disaggregation and prion propagation*. Mol Microbiol, 2008. **68**(1): p. 87-97.
143. Yu, A.Y. and W.A. Houry, *ClpP: a distinctive family of cylindrical energy-dependent serine proteases*. FEBS Lett, 2007. **581**(19): p. 3749-57.
144. Choi, K.H. and S. Licht, *Control of peptide product sizes by the energy-dependent protease ClpAP*. Biochemistry, 2005. **44**(42): p. 13921-31.

145. Dandoy-Dron, F., et al., *Infection by ME7 prion is not modified in transgenic mice expressing the yeast chaperone Hsp104 in neurons*. *Neurosci Lett*, 2006. **405**(3): p. 181-5.
146. Vacher, C., L. Garcia-Oroz, and D.C. Rubinsztein, *Overexpression of yeast hsp104 reduces polyglutamine aggregation and prolongs survival of a transgenic mouse model of Huntington's disease*. *Hum Mol Genet*, 2005. **14**(22): p. 3425-33.
147. Vashist, S., M. Cushman, and J. Shorter, *Applying Hsp104 to protein-misfolding disorders*. *Biochem Cell Biol*, 2010. **88**(1): p. 1-13.
148. Mosser, D.D., S. Ho, and J.R. Glover, *Saccharomyces cerevisiae Hsp104 enhances the chaperone capacity of human cells and inhibits heat stress-induced proapoptotic signaling*. *Biochemistry*, 2004. **43**(25): p. 8107-15.
149. Schaupp, A., et al., *Processing of proteins by the molecular chaperone Hsp104*. *J Mol Biol*, 2007. **370**(4): p. 674-86.
150. Carmichael, J., et al., *Bacterial and yeast chaperones reduce both aggregate formation and cell death in mammalian cell models of Huntington's disease*. *Proc Natl Acad Sci U S A*, 2000. **97**(17): p. 9701-5.
151. Fokkens, M., T. Schrader, and F.G. Klärner, *A molecular tweezer for lysine and arginine*. *J Am Chem Soc*, 2005. **127**(41): p. 14415-21.
152. Sinha, S., et al., *Lysine-specific molecular tweezers are broad-spectrum inhibitors of assembly and toxicity of amyloid proteins*. *J Am Chem Soc*, 2011. **133**(42): p. 16958-69.
153. Acharya, S., et al., *Molecular basis for preventing alpha-synuclein aggregation by a molecular tweezer*. *J Biol Chem*, 2014. **289**(15): p. 10727-37.
154. Prabhudesai, S., et al., *A novel "molecular tweezer" inhibitor of alpha-synuclein neurotoxicity in vitro and in vivo*. *Neurotherapeutics*, 2012. **9**(2): p. 464-76.
155. Attar, A., et al., *Protection of primary neurons and mouse brain from Alzheimer's pathology by molecular tweezers*. *Brain*, 2012. **135**(Pt 12): p. 3735-48.
156. Ferreira, N., et al., *Molecular tweezers targeting transthyretin amyloidosis*. *Neurotherapeutics*, 2014. **11**(2): p. 450-61.
157. Attar, A., et al., *Safety and pharmacological characterization of the molecular tweezer CLR01 - a broad-spectrum inhibitor of amyloid proteins' toxicity*. *BMC Pharmacol Toxicol*, 2014. **15**(1): p. 23.
158. Talbiersky, P., et al., *Molecular clip and tweezer introduce new mechanisms of enzyme inhibition*. *J Am Chem Soc*, 2008. **130**(30): p. 9824-8.
159. Mak, J.C., *Potential role of green tea catechins in various disease therapies: progress and promise*. *Clin Exp Pharmacol Physiol*, 2012. **39**(3): p. 265-73.
160. Meng, F., et al., *The flavanol (-)-epigallocatechin 3-gallate inhibits amyloid formation by islet amyloid polypeptide, disaggregates amyloid fibrils, and protects cultured cells against IAPP-induced toxicity*. *Biochemistry*, 2010. **49**(37): p. 8127-33.
161. Bieschke, J., et al., *EGCG remodels mature alpha-synuclein and amyloid-beta fibrils and reduces cellular toxicity*. *Proc Natl Acad Sci U S A*, 2010. **107**(17): p. 7710-5.
162. Ferreira, N., M.J. Saraiva, and M.R. Almeida, *Natural polyphenols inhibit different steps of the process of transthyretin (TTR) amyloid fibril formation*. *FEBS Lett*, 2011. **585**(15): p. 2424-30.
163. Bastianetto, S., et al., *Neuroprotective effects of green and black teas and their catechin gallate esters against beta-amyloid-induced toxicity*. *Eur J Neurosci*, 2006. **23**(1): p. 55-64.
164. Ehrnhoefer, D.E., et al., *Green tea (-)-epigallocatechin-gallate modulates early events in huntingtin misfolding and reduces toxicity in Huntington's disease models*. *Hum Mol Genet*, 2006. **15**(18): p. 2743-51.
165. Palhano, F.L., et al., *Toward the molecular mechanism(s) by which EGCG treatment remodels mature amyloid fibrils*. *J Am Chem Soc*, 2013. **135**(20): p. 7503-10.
166. Das, A.T. and B. Berkhout, *HIV-1 evolution: frustrating therapies, but disclosing molecular mechanisms*. *Philos Trans R Soc Lond B Biol Sci*, 2010. **365**(1548): p. 1965-73.

167. Iwasa, Y., F. Michor, and M.A. Nowak, *Evolutionary dynamics of escape from biomedical intervention*. Proc Biol Sci, 2003. **270**(1533): p. 2573-8.
168. Iwasa, Y., F. Michor, and M.A. Nowak, *Evolutionary dynamics of invasion and escape*. J Theor Biol, 2004. **226**(2): p. 205-14.
169. UNAIDS, *World AIDS Day Report 2011*. 2011: p. 1-48.
170. Gray, R.H., et al., *Probability of HIV-1 transmission per coital act in monogamous, heterosexual, HIV-1-discordant couples in Rakai, Uganda*. Lancet, 2001. **357**: p. 1149-53.
171. Pilcher, C.D., et al., *Brief but efficient: acute HIV infection and the sexual transmission of HIV*. The Journal of infectious diseases, 2004. **189**: p. 1785-92.
172. Arnold, F., et al., *Naturally Occurring Fragments from Two Distinct Regions of the Prostatic Acid Phosphatase Form Amyloidogenic Enhancers of HIV Infection*. Journal of virology, 2012. **86**: p. 1244-9.
173. Roan, Nadia R., et al., *Peptides Released by Physiological Cleavage of Semen Coagulum Proteins Form Amyloids that Enhance HIV Infection*. Cell Host & Microbe, 2011. **10**: p. 541-550.
174. Olsen, J.S., et al., *Seminal plasma accelerates SEVI fibril formation by the PAP[248-286] peptide*. The Journal of biological chemistry, 2012: p. 1-17.
175. Roan, N.R., et al., *The cationic properties of SEVI underlie its ability to enhance human immunodeficiency virus infection*. Journal of virology, 2009. **83**: p. 73-80.
176. Eisenberg, D. and M. Jucker, *The amyloid state of proteins in human diseases*. Cell, 2012. **148**(6): p. 1188-203.
177. Knowles, T.P., M. Vendruscolo, and C.M. Dobson, *The amyloid state and its association with protein misfolding diseases*. Nat Rev Mol Cell Biol, 2014. **15**(6): p. 384-96.
178. Knowles, T.P., et al., *Role of intermolecular forces in defining material properties of protein nanofibrils*. Science, 2007. **318**(5858): p. 1900-3.
179. Castellano, L.M. and J. Shorter, *The surprising role of amyloid fibrils in HIV infection*. Biology, 2012. **1**(1): p. 58-80.
180. Desantis, M.E. and J. Shorter, *The elusive middle domain of Hsp104 and ClpB: location and function*. Biochim Biophys Acta, 2012. **1823**(1): p. 29-39.
181. Shorter, J. and S. Lindquist, *Hsp104 catalyzes formation and elimination of self-replicating Sup35 prion conformers*. Science, 2004. **304**(5678): p. 1793-7.
182. DeSantis, M.E., et al., *Operational plasticity enables hsp104 to disaggregate diverse amyloid and nonamyloid clients*. Cell, 2012. **151**(4): p. 778-93.
183. Jackrel, M.E., et al., *Potentiated hsp104 variants antagonize diverse proteotoxic misfolding events*. Cell, 2014. **156**(1-2): p. 170-82.
184. Shorter, J. and S. Lindquist, *Destruction or potentiation of different prions catalyzed by similar Hsp104 remodeling activities*. Mol Cell, 2006. **23**(3): p. 425-38.
185. Alberti, S., et al., *A systematic survey identifies prions and illuminates sequence features of prionogenic proteins*. Cell, 2009. **137**(1): p. 146-58.
186. Cushman-Nick, M., N.M. Bonini, and J. Shorter, *Hsp104 suppresses polyglutamine-induced degeneration post onset in a drosophila MJD/SCA3 model*. PLoS Genet, 2013. **9**(9): p. e1003781.
187. Kim, Y., et al., *Characterization and Hsp104-induced artificial clearance of familial ALS-related SOD1 aggregates*. Biochem Biophys Res Commun, 2013. **434**(3): p. 521-6.
188. Satyal, S.H., et al., *Polyglutamine aggregates alter protein folding homeostasis in Caenorhabditis elegans*. Proc Natl Acad Sci U S A, 2000. **97**(11): p. 5750-5.
189. DeSantis, M.E. and J. Shorter, *Hsp104 drives "protein-only" positive selection of Sup35 prion strains encoding strong [PSI(+)]*. Chem Biol, 2012. **19**(11): p. 1400-10.
190. Shorter, J., *The mammalian disaggregase machinery: Hsp110 synergizes with Hsp70 and Hsp40 to catalyze protein disaggregation and reactivation in a cell-free system*. PLoS One, 2011. **6**(10): p. e26319.

191. Reidy, M., M. Miot, and D.C. Masison, *Prokaryotic chaperones support yeast prions and thermotolerance and define disaggregation machinery interactions*. Genetics, 2012. **192**(1): p. 185-93.
192. Ye, Z., et al., *Mechanism of fibril formation by a 39-residue peptide (PAPf39) from human prostatic acidic phosphatase*. Biochemistry, 2009. **48**(48): p. 11582-91.
193. Oguchi, Y., et al., *A tightly regulated molecular toggle controls AAA+ disaggregase*. Nat Struct Mol Biol, 2012. **19**(12): p. 1338-46.
194. Mannini, B., et al., *Molecular mechanisms used by chaperones to reduce the toxicity of aberrant protein oligomers*. Proc Natl Acad Sci U S A, 2012. **109**(31): p. 12479-84.
195. Narayanan, S., et al., *Importance of low-oligomeric-weight species for prion propagation in the yeast prion system Sup35/Hsp104*. Proc Natl Acad Sci U S A, 2003. **100**(16): p. 9286-91.
196. Hattendorf, D.A., *Multiple Allosteric Signaling Events in the Hsp104 ATP Hydrolysis Cycle Revealed by Mutagenesis of Conserved AAA Active Site Residues*. 2001: University of Chicago, Department of Biochemistry and Molecular Biology.
197. Thompson, M.W., S.K. Singh, and M.R. Maurizi, *Processive degradation of proteins by the ATP-dependent Clp protease from Escherichia coli. Requirement for the multiple array of active sites in ClpP but not ATP hydrolysis*. J Biol Chem, 1994. **269**(27): p. 18209-15.
198. Wang, J., J.A. Hartling, and J.M. Flanagan, *The structure of ClpP at 2.3 Å resolution suggests a model for ATP-dependent proteolysis*. Cell, 1997. **91**(4): p. 447-56.
199. Kaganovich, D., R. Kopito, and J. Frydman, *Misfolded proteins partition between two distinct quality control compartments*. Nature, 2008. **454**(7208): p. 1088-95.
200. Spokoini, R., et al., *Confinement to organelle-associated inclusion structures mediates asymmetric inheritance of aggregated protein in budding yeast*. Cell Rep, 2012. **2**(4): p. 738-47.
201. Escusa-Toret, S., W.I. Vonk, and J. Frydman, *Spatial sequestration of misfolded proteins by a dynamic chaperone pathway enhances cellular fitness during stress*. Nat Cell Biol, 2013. **15**(10): p. 1231-43.
202. Sontag, E.M., W.I. Vonk, and J. Frydman, *Sorting out the trash: the spatial nature of eukaryotic protein quality control*. Curr Opin Cell Biol, 2014. **26**: p. 139-46.
203. Cohen, E., et al., *Opposing activities protect against age-onset proteotoxicity*. Science, 2006. **313**(5793): p. 1604-10.
204. Kim, K.-A., et al., *Semen-mediated enhancement of HIV infection is donor-dependent and correlates with the levels of SEVI*. Retrovirology, 2010. **7**: p. 1-12.
205. Sinha, S., et al., *Comparison of three amyloid assembly inhibitors: the sugar scyllo-inositol, the polyphenol epigallocatechin gallate, and the molecular tweezer CLR01*. ACS Chem Neurosci, 2012. **3**(6): p. 451-8.
206. Dutt, S., et al., *Molecular tweezers with varying anions: a comparative study*. J Org Chem, 2013. **78**(13): p. 6721-34.
207. Bier, D., et al., *Molecular tweezers modulate 14-3-3 protein-protein interactions*. Nat Chem, 2013. **5**(3): p. 234-9.
208. Nelson, R., et al., *Structure of the cross-beta spine of amyloid-like fibrils*. Nature, 2005. **435**(7043): p. 773-8.
209. French, K.C. and G.I. Makhatadze, *Core sequence of PAPf39 amyloid fibrils and mechanism of pH-dependent fibril formation: the role of monomer conformation*. Biochemistry, 2012. **51**(51): p. 10127-36.
210. Aloia, R.C., et al., *Lipid composition and fluidity of the human immunodeficiency virus*. Proc Natl Acad Sci U S A, 1988. **85**(3): p. 900-4.
211. Brugger, B., et al., *The HIV lipidome: a raft with an unusual composition*. Proc Natl Acad Sci U S A, 2006. **103**(8): p. 2641-6.
212. Chan, R., et al., *Retroviruses human immunodeficiency virus and murine leukemia virus are enriched in phosphoinositides*. J Virol, 2008. **82**(22): p. 11228-38.

213. Gerl, M.J., et al., *Quantitative analysis of the lipidomes of the influenza virus envelope and MDCK cell apical membrane*. J. Cell Biol., 2012. **196**(2): p. 213-21.
214. Lorizate, M., et al., *Comparative lipidomics analysis of HIV-1 particles and their producer cell membrane in different cell lines*. Cell Microbiol, 2013. **15**(2): p. 292-304.
215. Gerl, M.J., et al., *Quantitative analysis of the lipidomes of the influenza virus envelope and MDCK cell apical membrane*. J Cell Biol, 2012. **196**(2): p. 213-21.
216. Owen, D.H. and D.F. Katz, *A review of the physical and chemical properties of human semen and the formulation of a semen simulant*. J Androl, 2005. **26**(4): p. 459-69.
217. Neurath, A.R., N. Strick, and Y.Y. Li, *Anti-HIV-1 activity of anionic polymers: a comparative study of candidate microbicides*. BMC Infect Dis, 2002. **2**: p. 27.
218. Weber, J., et al., *The development of vaginal microbicides for the prevention of HIV transmission*. PLoS Med, 2005. **2**(5): p. e142.
219. Merz, A., et al., *Biochemical and morphological properties of hepatitis C virus particles and determination of their lipidome*. J Biol Chem, 2011. **286**(4): p. 3018-32.
220. van Genderen, I.L., et al., *The phospholipid composition of extracellular herpes simplex virions differs from that of host cell nuclei*. Virology, 1994. **200**(2): p. 831-6.
221. Handsfield, H.H., et al., *Cytomegalovirus infection in sex partners: evidence for sexual transmission*. J Infect Dis, 1985. **151**(2): p. 344-8.
222. Rapp, F., *Sexually transmitted viruses*. Yale J Biol Med, 1989. **62**(2): p. 173-85.
223. Tedder, R.S., et al., *Hepatitis C virus: evidence for sexual transmission*. BMJ, 1991. **302**(6788): p. 1299-302.
224. Kim, K.A., et al., *Semen-mediated enhancement of HIV infection is donor-dependent and correlates with the levels of SEVI*. Retrovirology, 2010. **7**: p. 55.
225. Lundquist, F., *Proteolytic enzymes in human semen*, in *Ciba Foundation Symposium - Mammalian Germ Cells*, G.E.W. Wolstenholme, Editor. 2008, John Wiley & Sons, Ltd., Chichester, UK. .
226. Roberts, B.E. and J. Shorter, *Escaping amyloid fate*. Nat Struct Mol Biol, 2008. **15**(6): p. 544-6.
227. Cabrera, C., R. Artacho, and R. Gimenez, *Beneficial effects of green tea--a review*. J Am Coll Nutr, 2006. **25**(2): p. 79-99.
228. Khurana, S., et al., *Polyphenols: benefits to the cardiovascular system in health and in aging*. Nutrients, 2013. **5**(10): p. 3779-827.
229. Nance, C.L. and W.T. Shearer, *Is green tea good for HIV-1 infection?* J Allergy Clin Immunol, 2003. **112**(5): p. 851-3.
230. Yang, C.S., P. Maliakal, and X. Meng, *Inhibition of carcinogenesis by tea*. Annu Rev Pharmacol Toxicol, 2002. **42**: p. 25-54.
231. Ehrnhoefer, D.E., et al., *EGCG redirects amyloidogenic polypeptides into unstructured, off-pathway oligomers*. Nat Struct Mol Biol, 2008. **15**(6): p. 558-66.
232. Cao, P. and D.P. Raleigh, *Analysis of the inhibition and remodeling of islet amyloid polypeptide amyloid fibers by flavanols*. Biochemistry, 2012. **51**(13): p. 2670-83.
233. Steinmann, J., et al., *Anti-infective properties of epigallocatechin-3-gallate (EGCG), a component of green tea*. Br J Pharmacol, 2013. **168**(5): p. 1059-73.
234. Shorter, J., *Emergence and natural selection of drug-resistant prions*. Mol Biosyst, 2010. **6**(7): p. 1115-30.
235. Nance, C.L., E.B. Siwak, and W.T. Shearer, *Preclinical development of the green tea catechin, epigallocatechin gallate, as an HIV-1 therapy*. J Allergy Clin Immunol, 2009. **123**(2): p. 459-65.
236. Kawai, K., et al., *Epigallocatechin gallate, the main component of tea polyphenol, binds to CD4 and interferes with gp120 binding*. J Allergy Clin Immunol, 2003. **112**(5): p. 951-7.
237. Zhang, H.S., et al., *EGCG inhibits Tat-induced LTR transactivation: role of Nrf2, AKT, AMPK signaling pathway*. Life Sci, 2012. **90**(19-20): p. 747-54.
238. Li, S., T. Hattori, and E.N. Kodama, *Epigallocatechin gallate inhibits the HIV reverse transcription step*. Antivir Chem Chemother, 2011. **21**(6): p. 239-43.

239. Jiang, F., et al., *The evaluation of catechins that contain a galloyl moiety as potential HIV-1 integrase inhibitors*. Clin Immunol, 2010. **137**(3): p. 347-56.
240. Isaacs, C.E., et al., *Epigallocatechin gallate inactivates clinical isolates of herpes simplex virus*. Antimicrob Agents Chemother, 2008. **52**(3): p. 962-70.
241. Ciesek, S., et al., *The green tea polyphenol, epigallocatechin-3-gallate, inhibits hepatitis C virus entry*. Hepatology, 2011. **54**(6): p. 1947-55.
242. Friend, D.R. and P.F. Kiser, *Assessment of topical microbicides to prevent HIV-1 transmission: concepts, testing, lessons learned*. Antiviral Res, 2013. **99**(3): p. 391-400.
243. Herold, B.C., et al., *Female genital tract secretions and semen impact the development of microbicides for the prevention of HIV and other sexually transmitted infections*. Am J Reprod Immunol, 2011. **65**(3): p. 325-33.
244. Keller, M.J., et al., *Postcoital bioavailability and antiviral activity of 0.5% PRO 2000 gel: implications for future microbicide clinical trials*. PLoS One, 2010. **5**(1): p. e8781.
245. Patel, S., et al., *Seminal plasma reduces the effectiveness of topical polyanionic microbicides*. J Infect Dis, 2007. **196**(9): p. 1394-402.
246. Hauber, I., et al., *The main green tea polyphenol epigallocatechin-3-gallate counteracts semen-mediated enhancement of HIV infection*. Proceedings of the National Academy of Sciences of the United States of America, 2009. **106**: p. 9033-8.
247. Roan, N.R., et al., *Interaction of fibronectin with semen amyloids synergistically enhances HIV infection*. J Infect Dis, 2014. **210**(7): p. 1062-6.
248. Sinzger, C., et al., *Cloning and sequencing of a highly productive, endotheliotropic virus strain derived from human cytomegalovirus TB40/E*. J Gen Virol, 2008. **89**(Pt 2): p. 359-68.
249. Koutsoudakis, G., et al., *Characterization of the early steps of hepatitis C virus infection by using luciferase reporter viruses*. J Virol, 2006. **80**(11): p. 5308-20.
250. Lindenbach, B.D., et al., *Complete replication of hepatitis C virus in cell culture*. Science, 2005. **309**(5734): p. 623-6.
251. Haid, S., et al., *A plant-derived flavonoid inhibits entry of all HCV genotypes into human hepatocytes*. Gastroenterology, 2012. **143**(1): p. 213-22 e5.
252. Reiss, S., et al., *Recruitment and activation of a lipid kinase by hepatitis C virus NS5A is essential for integrity of the membranous replication compartment*. Cell Host Microbe, 2011. **9**(1): p. 32-45.
253. Schiedner, G., S. Hertel, and S. Kochanek, *Efficient transformation of primary human amniocytes by E1 functions of Ad5: Generation of new cell lines for adenoviral vector production*. Human Gene Therapy, 2000. **11**(15): p. 2105-2116.
254. Kreppel, F., et al., *A DNA-based method to assay total and infectious particle contents and helper virus contamination in high-capacity adenoviral vector preparations*. Hum Gene Ther, 2002. **13**(10): p. 1151-6.